Thomas Hüpf

Density Determination of Liquid Metals

DISSERTATION

zur Erlangung des akademischen Grades
Doktor der technischen Wissenschaften

Doktoratsstudium der technischen Wissenschaften
Technische Physik

Technische Universität Graz

Betreuer:
A.o. Univ.-Prof. Dipl.-Ing. Dr.techn. Gernot Pottlacher
Institut für Experimentalphysik

Graz, August 2010

Deutsche Fassung:
Beschluss der Curricula-Kommission für Bachelor-, Master- und Diplomstudien vom 10.11.2008
Genehmigung des Senates am 1.12.2008

EIDESSTATTLICHE ERKLÄRUNG

Ich erkläre an Eides statt, dass ich die vorliegende Arbeit selbstständig verfasst, andere als die angegebenen Quellen/Hilfsmittel nicht benutzt, und die den benutzten Quellen wörtlich und inhaltlich entnommene Stellen als solche kenntlich gemacht habe.

Graz, am 23.7.2010 ..... Thomas Kügl
(Unterschrift)

Englische Fassung:

STATUTORY DECLARATION

I declare that I have authored this thesis independently, that I have not used other than the declared sources / resources, and that I have explicitly marked all material which has been quoted either literally or by content from the used sources.

2010.7.23 ..... Thomas Kügl
date (signature)

Abstract (English)

Fast pulse-heating is an established experimental method. It was used during this work to obtain thermophysical properties of electrically conducting samples as a function of temperature. Especially the liquid state of metals can be investigated using this technique. Measurement results were published in international peer-reviewed journals. Twelve publications were edited to form a cumulative PhD thesis. They are depicted as printed or as they were submitted.

The listed papers describe the scientific process which includes the following steps: A *target-oriented material-selection* was done in coordination with the project partners at DLR in Cologne as preparation for their experiments onboard the international space station ISS. *Manufacturing of the samples* is a fundamental task, because wire-shaped specimens are preferred for investigations with the pulse-heating apparatus. *Measurements* are actually the most pleasant task for the experimenter. They are followed by the *evaluation of results*. The final steps include the *preparation for publication* and participation at conferences.

Thermal expansion is one of the obtained quantities. It can be converted into density as a function of temperature. Density is more present in the scientific community and more data are available in the literature. Knowledge about thermal expansion is necessary to get the specific electrical resistivity since it includes the geometry of the sample. Explanatory text was added to describe the details of the expansion measurements. This part of the thesis includes investigations that did not conclude in favorable results (e.g. because of contradictions which could not be resolved). However, the additional information is even more attractive to the natural scientist, because it does not present the reader with a fait accompli as publications might do.

Abstract (Deutsch)

Schnelles Pulsheizen ist eine etablierte experimentelle Methode. Sie wurde in dieser Arbeit dazu benutzt, thermophysikalische Daten von elektrisch leitenden Proben als Funktion der Temperatur zu erhalten. Insbesondere die flüssige Phase kann mit dieser Technik untersucht werden. Die Messergebnisse wurden in internationalen, referierten Zeitschriften publiziert. Eine Auswahl von zwölf Publikationen bildet diese kumulative Dissertation. Die Beiträge sind so dargestellt, wie sie gedruckt oder eingereicht wurden.

Die angeführten Papiere dokumentieren den wissenschaftlichen Prozess, der aus folgenden Schritten besteht: In Absprache mit Partnern an der DLR in Köln wurde eine *zielgerichtete Materialauswahl* getroffen als Vorbereitung für deren Experimente an Bord der internationalen Raumstation ISS. Eine wesentliche Aufgabe ist die *Probenherstellung*, da als Proben zur Untersuchung in der Pulsheizapparatur runde Drähte bevorzugt werden. *Messungen* an sich sind für den Experimentator die erbaulichste Arbeit. Danach folgt die *Auswertung der Ergebnisse*. Die letzten Schritte sind die *Aufbereitung zur Publikation* und die Teilnahme an Konferenzen.

Eine der erhaltenen Größen ist die thermische Expansion. Sie kann in Dichte als Funktion der Temperatur umgerechnet werden. Die Dichte ist in der wissenschaftlichen Gemeinschaft präsenter und es gibt dazu auch mehr verfügbare Daten in der Literatur. Kenntnis über die Expansion ist notwendig um den spezifischen elektrischen Widerstand zu erhalten, der ja die Geometrie der Probe berücksichtigt. Den Publikationen wurde ergänzender Text vorangestellt, der genauer auf die Expansionsmessung eingeht. Dieser Teil der Arbeit enthält diejenigen Versuche, die zu keinem befriedigenden Ergebnis geführt haben (beispielsweise aufgrund von Widersprüchen, die nicht aufgelöst werden konnten). Dennoch ist gerade dieser Teil von besonderem Interesse für den Naturwissenschaftler, da der Leser nicht vor vollendete Tatsachen gestellt wird, wie das durch die Publikationen möglicherweise der Fall ist.

Preface

A major part of the work I have done during my PhD is best represented by the publications. They are depicted as published or as they were submitted for publication. Each paper is annotated concerning the content and the teamwork of authors.

I have added explanatory text to guide the reader through the scientific process. On the one hand it specifies the context for the publications and on the other hand it describes the investigations which did not result in a favorable conclusion. Additionally, this text should be a letter of reference to my successors at the lab.

Contents

Gratitude

Special thanks go to my doctoral advisor Prof. Gernot Pottlacher. He advanced my education by much more than just the guidance surrounding laboratory work. I was sent to conferences all around the world, I did a lot of paper work ranging from publications to proposals, I cooperated with partners from other laboratories, and I was permitted to supervise practical courses. During all that he always appreciated my autonomous work which gave me extraordinary freedom in all aspects.

Working on the PhD would not have been half as enjoyable without my colleagues Claus Cagran, Harald Reschab, and Boris Wilthan. Besides all the joking they gave me straightforward support whenever I asked for it.

I want to thank Prof. Ernst as representative of the Institute of Experimental Physics. I received friendly cooperation from all the professors, the girls in the office, from the machine shop, and the electronics group.

Dr. Erhard Kaschnitz and Dr. Georg Lohöfer were competent and accommodating whenever we got in contact with each other.

Prof. Ortrud Posedu from the University of Arts always valued my work in the natural sciences. She is diplomatic and broadminded regarding these sometimes conflicting interests of mine.

My parents were consistently proud of me during all stages of my PhD. Sure, this is their job, but nonetheless it feels good.

1 Principles of fast pulse-heating

Pulse-heating is a dynamic method. The measurements are not carried out in static conditions but during a heating process. The high heating rate (10^8 K/s) is the key-feature of this technique. It is achieved by applying a high voltage (up to 10 kV) to an electrically conducting sample. Because of its resistivity, the sample heats up rapidly. Heating continues until the end of the liquid phase, where at the transition to the gasphase, the so-called wireexplosion takes place.

Advantages

- Some metals oxidize quickly when exposed to air at high temperatures. This changes the properties of the surface. In such a case the results no longer correspond to the pure metal but to a mixture of metal and oxide. The process of oxidation or any chemical reaction with the surrounding atmosphere is strongly inhibited when the experimental duration is short. The typical duration of the pulse-heating process is 50 μs.

- When investigating liquid metals, usually some kind of container is necessary. But again, reactions with walls, which additionally have to have a higher melting point than the sample, can change the properties of the investigated metal. In pulse-heating experiments, no crucible is necessary. The sample maintains its position even in the liquid phase because in 50 μs no divergence or disturbance due to gravity is relevant.

- Heat transfer from sample to environment is strongly inhibited. It is therefore easy to calculate the amount of input energy.

Disadvantages

- The data recording system has to be fast. Today, this is no longer a problem, but years ago this difficulty could only be managed through the astute implementation of available equipment (see chapter expansion measurement).

- All properties are usually stated under the assumption of thermodynamic equilibrium. This might be abandoned during pulse-heating. Nevertheless, the obtained results are in agreement with results obtained in static conditions. This has to be kept in mind separately for every thermodynamic property. E.g. when measuring alloys, one has to be aware that the diffusion of particles is strongly inhibited and hence, the concentration of the alloy between the solidus and liquidus temperature is different from the concentration in thermodynamic equilibrium at that temperature.

1.1 Obtained results

The following quantities are measured simultaneously: temperature, current, voltage drop, and thermal expansion. Temperature is measured by means of pyrometry. A pyrometer detects the surface radiation that is emitted at a certain wavelength (650 nm or 1570 nm). The current through the sample is measured with an induction coil. Voltage drop is measured with two knife edge contacts directly placed on the sample. These quantities are called 'electrical data' to point out the difference from the thermal expansion, which we measure optically: a specially designed CCD camera delivers images of the expanding wire (see [1]).

The paper [2] describes measurements on rhodium. It serves as a paradigm for the standard approach when investigating pure metals; including introduction, description of formulas, polynomial and graphical data presentations, discussion and comparison, and uncertainty considerations. More details about the uncertainty can be found in [3].

In the discussion section of [2], rhodium was set in context with the other so-called 'platinum metals': palladium, iridium, and platinum. They were measured under the same experimental conditions by predecessors at the lab. As this approach of comparison is generally very instructive and as the workgroup has done a lot of measurements on pure metals (almost all elements which are suitable for pulse-heating have so far been investigated), the author started to write a compilation.

2 Creation of a compilation

At the workgroup of subsecond thermophysics, the following pure metals were investigated under pulse-heating conditions (ordered alphabetically with respect to spoken words): Co, Cu, Au, Hf, Ir, Fe, Mo, Ni, Nb, Pd, Pt, Re, Rh, Ag, Ta, Ti, W, V, and Zr.

These 19 elements fulfill the requirements for being investigated by pulse-heating: the melting point is high enough to enable pyrometric temperature measurement and the samples are available in the shape of a wire (preferably round, but rectangular wires are practicable, too). Data are also available for In, Pb, and Zn where no pyrometric measurements were possible.

The quantities which are summarized in this compilation are: volume expansion, specific enthalpy and electrical resistivity as a function of temperature. As the results are obtained in quite homogenous conditions (same laboratory, same method, etc.) and cover a large temperature range, such a compilation gives a unique possibility to start systematic investigations (e.g.: comparing all elements of one group/period in the periodic system of the elements, comparing the so called platinum metals, etc.). This was done in three publications [4 - 6] and one poster [7].

The compilation is the last point in pure metals investigations. But partners and sponsors are mainly interested in results on alloys. With highly alloyed materials it is hard to trace back the properties to each single constituent (often more than 10). They are designed by trial and error with the help of empirical know-how. Thus, from a scientific point of view, it is better to start the investigation with binary alloys and compare their properties to the pure ingredients. Two publications are dedicated to this systematic approach: [8] and [9]. A poster [10] analyzes the methodology of investigations on binary alloys.

In the compilation of pure elements something is noticable: in the liquid state the electrical resistivity of Hf, Mo, Re, Ta, Ti, and W, calculated from what was called 'electrical data', decreases with increasing temperature (also mentioned in [4]). This would be a non-physical behavior. Increased thermal movements of the atoms lead to increased scattering of electrons and consequently the resistivity has to be higher. It is evident that the change of the sample diameter, due to thermal expansion, has to be taken into account.

$$\rho = \frac{U \cdot r^2 \cdot \pi}{I \cdot l}, \tag{1}$$

ρ: electrical resistivity, U: voltage drop, I: current, r: radius of sample at room temperature, l: length.

When the actual radius of the sample is inserted in the formula instead of r at room temperature, the resistivity no longer decreases with increasing temperature (consequently the nomenclature is ρ_{IG}: resistivity with initial geometry and ρ: resistivity). Hence, the simultaneous measurement of the diameter, called 'optical measurement', is a crucial point and much more than just a byproduct. Without knowledge of thermal expansion, the obtained resistivity with initial geometry is just an artifact, hardly comparable to the results of any other measurement technique. New measurements on Ir, Ni, Pd, Pt, Ag, Ti, V, and Zr were added to the compilation [11]. The expansion measurement is worth being described in more detail:

3 Expansion measurement

The paper [1] gives an excellent review of expansion measurements under pulse-heating conditions. Different methods around the globe as well as the 'stages of development' at the TU Graz are described.

At the TU Graz the thermal expansion is calculated from an optical measurement of the wire-diameter. As the wire is clamped on both ends, expansion in an axial direction can lead to bending. This can be seen in the extraordinary picture in figure 1. The disturbing behavior is inhibited by increasing the heating-rate. When the heating-rate is high enough, the wire does not bend in any direction.

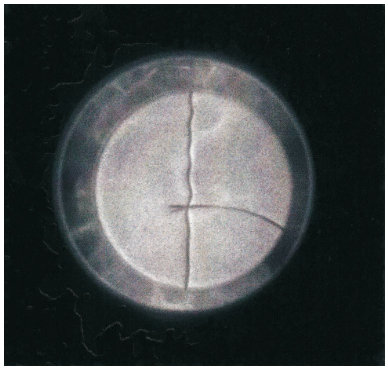

Figure 1: Picture of wire in pulse-heating experiment. The wire is bending because of too slow heating (see paper [1]). Picture by Dr. Claus Cagran.

This raises new questiones: where does the volume go which is associated with axial expansion? Figure 2 shows the configuration. Picture c indicates the volume of the expanded wire (exaggerated). The axial expansion would be inside the clamps which is mechanically impossible. Now, two situations are possible. They are displayed in figure 3.

Firstly, the wire could get elastically compressed with the radial component of expansion not affected (picture b of figure 3). The relative volume expansion equivalent to static conditions would have to be calculated from the diameter as the cube of the ratio D/D_0 (D: diameter, D_0: diameter at room temperature).

Secondly, the radial expansion of the wire could be enlarged by the amount of axial expansion (picture c in figure 3). Volume expansion in this case would have to be calculated from the square of the ratio D/D_0. This second approach was used in all 'stages of development' at the TU Graz.

The paper [2] contains a comparison of rhodium results of expansion to literature values (see figure 4). The diameter expansion (solid lines) is enlarged. The calculation according to the second approach yields the dashed lines which are in agreement with the literature values.

To be precise, it has to be mentioned that the explanations and scetches above are only an aid to provide easy access. What prevents the sample from expanding in an axial direction is not the clamping. It is the interaction of the particles themselves. On the time-scale of pulse-heating (typically 40 μs), their inertial forces are a relevant factor.

In order to cross-check the expansion results obtained at different stages of development the high pressure setup was put into operation again. In this setup, the discharge-vessel is not filled with nitrogen (which is used by default) but with water. The vessel allows one to apply pressures of up to 5000 bar.

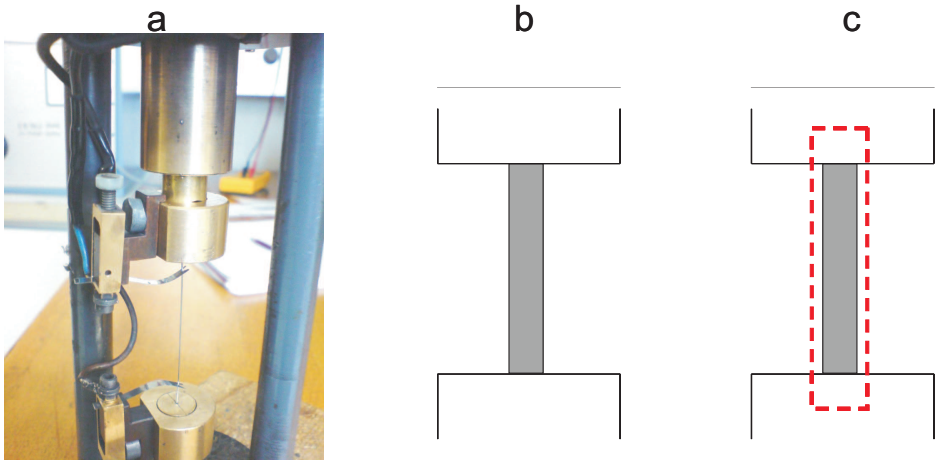

Figure 2: Wire in pulse-heating setup. a: photograph prior to experiment, b: scetch of clamped wire, c: indication of equal expansion in all directions.

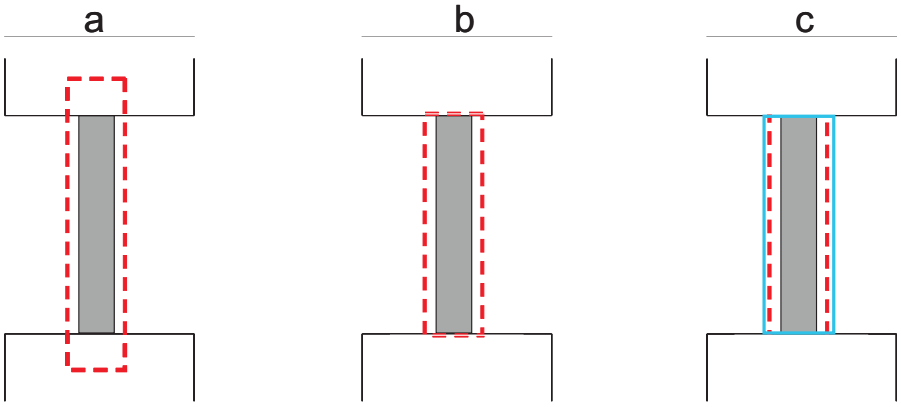

Figure 3: Two possible results. a: impossible expansion into the clamps, b: radial expansion not affected - wire is elastically compressed, c: radial expansion is enlarged - wire expands along the path of least mechanical resistance.

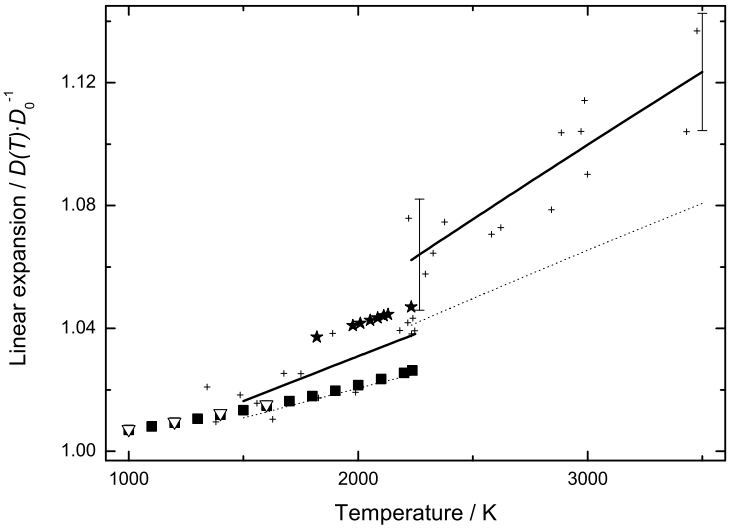

Figure 4: Literature comparison of linear expansion of rhodium (see paper [2]). Small crosses: data-points of diameter measurement, solid lines: linear least squares fits to the data-points, dashed lines: calculation of linear expansion according to case two (enlarged radial expansion), full stars: literature values of Paradis [P.-F. Paradis, T. Ishikawa, S. Yoda, *Int. J. Thermophys.*, **24**, 2008, p. 1121 - 1136.] for supercooled liquid Rh, full squares: literature values of Arblaster [J.W. Arblaster, *Platinum Met. Rev.*, **41**, 1997, p. 184 - 189.], open down triangle: recommended values of Touloukian [Y.S. Touloukian, *Thermophysical Properties of Matter*, vol. 12, *Thermal Expansion*, New York: 1970, IFI/Plenum.].

Surprisingly, the author discovered a discrepancy: the thermal expansion in water at 1000 bar seems to be higher than the expansion in nitrogen at 2.3 bar. This actual situation is described in paper [12]. The possible explanations described there were put to the test as described in the following chapter.

4 Dedicated investigations

For continuative investigations, a material was chosen (Ni80Cr20) which delivered expansion pictures - obtained in the established setup (nitrogen atmosphere, pressure of 2.3 bar) - which from the point of view of the experimenter were not defective at all but could be called beautiful instead. They show low scattering and the value of expansion is sensible. The rule

of thumb - that a metal expands to about 6-8% until it reaches the melting point - is perfectly exemplified.

Straightaway, one would expect that a surrounding atmosphere of water at 1000 bar should not have an effect on the expansion of a metal or if anything, a lower expansion would be estimated. But the evaluation delivers much higher expansion in water at 1000 bar (see circles in figure 5).

Different material

The unexpected behavior was first checked on a different material. Standard material at the lab for testing is niobium. The results are displayed in figure 6. Again, the high pressure measurements (1000 bar) in water deliver more expansion than the measurements in nitrogen at 2.3 bar. The difference is smaller than with Ni80Cr20 but still significant.

Ni80Cr20 is therefore not an exception. Other materials - especially the standard material niobium - show the discrepancy as well. To keep things as simple as possible, further investigations were carried out on Ni80Cr20 only.

Basic considerations

Objects immersed in water appear 1/3 larger than they are. This can be noticed by anyone by just looking into a river. When this topic is raised, the natural scientist has to be on the spot with an explanation: the refractive index of water is higher than the refractive index of air. This leads to the refraction of light at the surface and to the observed phenomenon.

But this is not an explanation for the discrepancy. The stated expansion values are related to the diameter at room temperature (D^2/D_0^2). The relative expansion is not affected by a linear magnification.

Additionally, the usage of relative values makes the measurement insensitive to any differences in imaging, magnification or adjustment of the optical devices. Nevertheless, it was tested whether the backlighting by a conventional photo-flash could cause an error; be it the finite dimension of the light source or possible non-parallel light rays. Instead of the photo-flash the author used a laser as backlighting. Figure 6 displays the results for nitrogen atmosphere (open rectangles). No difference to the photo-flash is observed.

The only things that could cause a difference in the relative expansion results are effects that happen during the heating process only. The diameter at room temperature is measured prior to the heating process. If something changed during heating, then the relation might be affected.

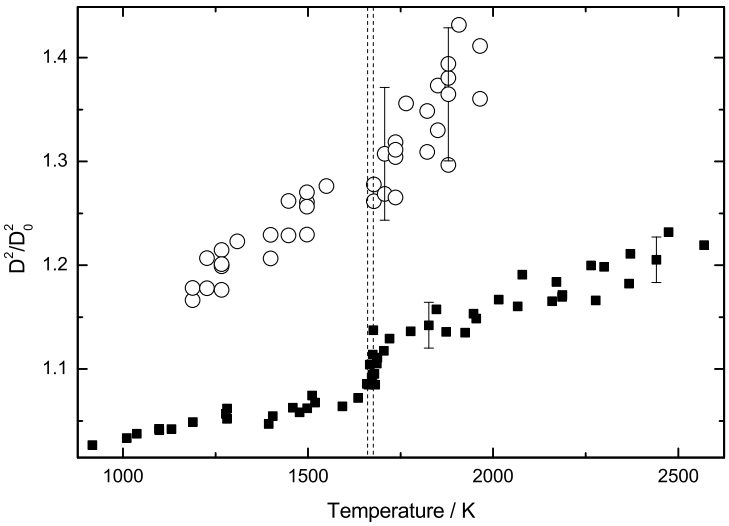

Figure 5: Thermal Expansion of Ni80Cr20 as a function of temperature. D: diameter, D_0: diameter at room temperature, circles: high pressure (water) results, rectangles: low pressure (nitrogen) results; dashed lines: solidus 1661 K and liquidus 1676 K temperature, uncertainty bars indicate relative uncertainties with coverage factor $k = 2$.

Methodological trickiness

The easiest way to find an empirical explanation for any phenomenon is to change only one parameter and monitor its effect. If there is no effect, then this single parameter is not responsible for the phenomenon.

Now, in this situation, one can not change, for example, just the atmosphere without changing the pressure because of the following reason: If the sample is heated in water atmosphere at 1 bar, the water near the hot sample will boil. This will lead to a steam tube. On the pictures the steam tube is not distinguishable from the sample and the record will show the diameter of the steam tube instead of the sample diameter. If the pressure is higher than the critical point of water, there will be no difference between water and steam. Hence, water experiments always have to be operated above the critical point of water.

On the other hand, the apparatus is not able to compress nitrogen to high pressures. Water was chosen as atmosphere for high pressure measurements of up to 5000 bar because it is almost incompressible. This makes the compression much easier and safer. If the vessel breaks, only a small volume

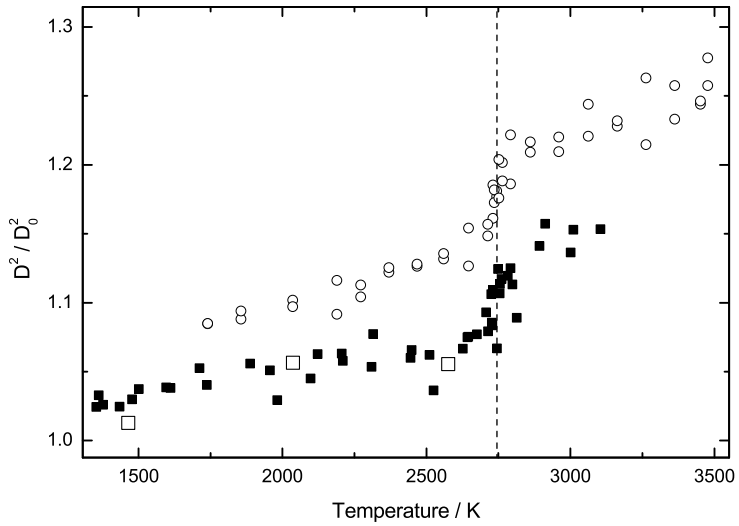

Figure 6: Thermal Expansion of niobium as a function of temperature. D: diameter, D_0: diameter at room temperature, Circles: high pressure (water) results, rectangles: low pressure (nitrogen) results, open rectangles: backlighting provided by a laser instead of the photo-flash; dashed line: melting temperature 2745 K.

of water will be released. If a gas-filled vessel of 5000 bar breaks, the volume of approximately 5000 such vessels is released - a dangerous explosion. In summary: water has to be operated at high pressures; nitrogen can only be operated at low pressures. Hence, one can not stick to just changing one parameter at once. Two must always change: atmosphere and pressure. This the author called methodological trickiness.

4.1 Probe laser

The expanding wire could have an effect on the surrounding atmosphere. This could be a traveling shock-wave or some gradient in the refractive index. Conventional photographs, which were used as detectors before the CCD camera, prove that such shock waves exist (see figure 7) and that they have an influence on the path of light (otherwise they would not be visible). But the heating process at that time was 10 times faster.

The author decided to use a laser as a probe for the path of light (as mentioned above: thermal expansion is measured with an 'optic' device, which is based on the rules of linear optics).

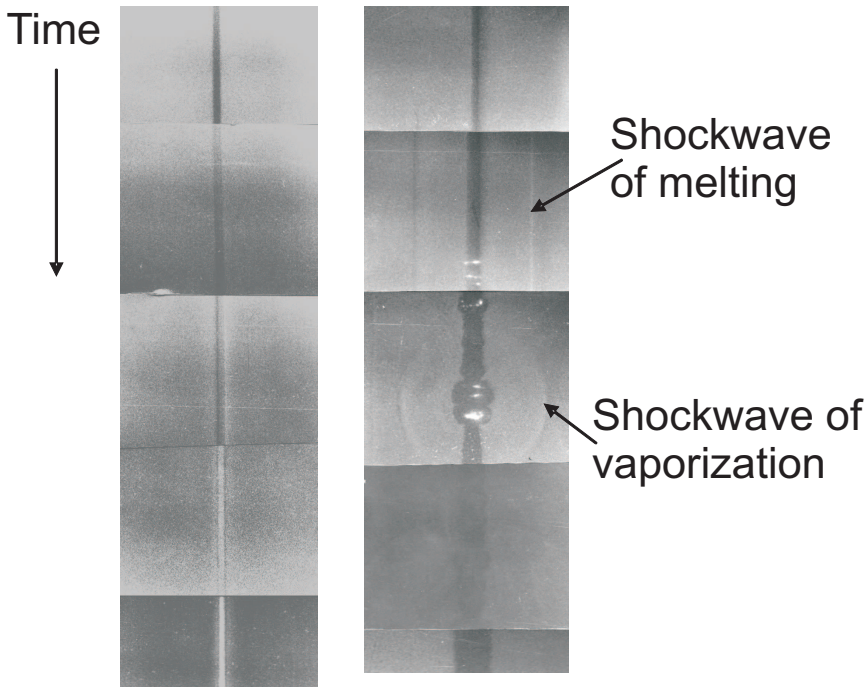

Figure 7: Photographs of the expanding wires from several independent experiments lined up according to experimental time. Left: Ta at 3000 bar (proper result); right: Pb at 1 bar (with irregularities caused by inhomogeneities in the starting material), shock-waves are visible on the photographs. Photographs by Dr. Gernot Pottlacher [Gernot Pottlacher: *Bestimmung thermophysikalischer Daten von Metallen bis in den Überhitzungsbreich der flüssigen Phase*, PhD-Thesis, Graz University of Technology, 1987].

The sketch of this setup can be seen in figure 8. The laser light is passing the sample. During the heating process its location can be monitored on the detector. If some kind of gradient developed, it would lead to a movement of the spot.

Additionally, figure 8 shows a ray of light (solid line) which is passing the atmosphere which has a gradient in the refractive index. The apparent origin (in geometric optics the supposed path of light is a straight line) is somewhere on the dashed line which is a tangent to the solid line on the imaging lense. The sketch shows that the recorded image can be enlarged or reduced depending on the forming of a gradient in the refractive index. The 'probe-laser' allows one to draw conclusions about this effect.

Neither the experiments in water atmosphere and in nitrogen atmosphere showed any movement of the laser spot. This was tested with and without an imaging lens. Figure 9 shows the result from a water experiment. One

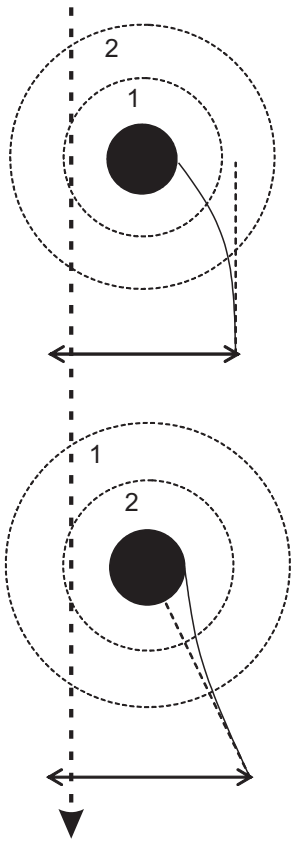

Figure 8: Sketch of geometric circumstances with 'probe-laser'; arrow: laser light passing the sample, upper picture: inner layer of surrounding atmosphere with higher refractive index ($n_1 > n_2$), the image seems to be larger (dashed line); lower picture: inner layer with lower refractive index, the image seems to be smaller (exaggerated drawing).

horizontal picture consists of 8 lines (compare figure 7). The time shift between two pictures is 2.5 μs (time axis from top to bottom). The wire is not visible due to the missing backlighting (dashed lines). The laser-spot does not move in any direction during the heating process.

4.2 Lens effect

The aforementioned effect of a shock-wave or a gradient in the refractive index could be called a lens effect. To be more precise: a cylindrical lens effect. It can not be monitored with a probe laser but there are further possibilities to explore it: the related experimental parameters can be changed and their effect on the evaluated results can be studied. These parameters are the heating-rate and the pressure.

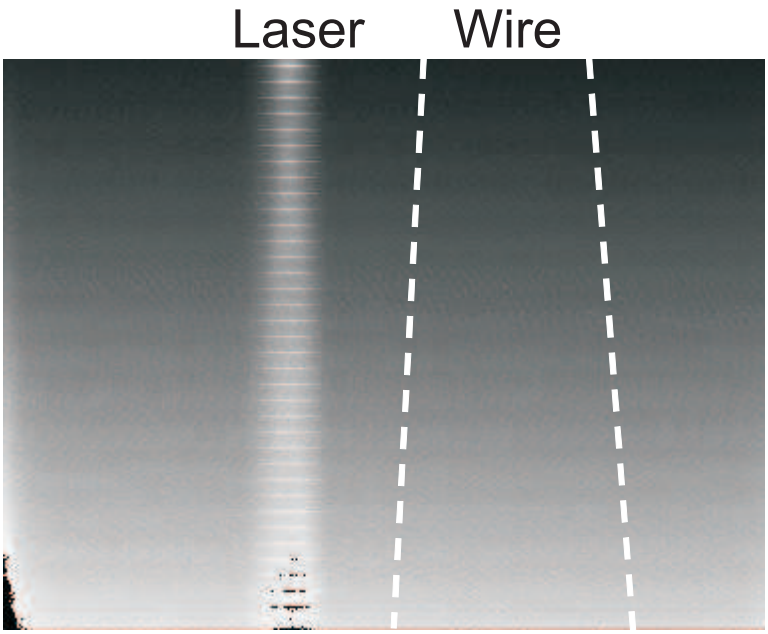

Figure 9: Laser-spot on the detector adjacent to heated wire ('streak image'); time axis from top to bottom, laser is passing the heated sample without being deflected, dashed lines: most likely position of wire (not visible because of missing back-lighting).

Firstly, when the pressure is kept constant a traveling wave will not change its speed. The formation of the 'lens' (of the misleading effect) remains constant. If now the property under investigation (the thermal expansion) is changed, e.g.: by changing the heating rate, this misleading effect will act on it differently. A heating rate dependency of the expansion would be observed.

Secondly, if the speed of sound in the ambient medium is pressure dependent, a pressure dependency of the expansion will be observed. Figure 10 displays the results of experiments in water atmosphere with changed parameters. No pressure dependency and no heating-rate dependency were found. In every adjustment the results obtained in water remain significantly higher than the results obtained in nitrogen. While changing the pressure, no tendency of the curves is observed.

4.3 Detector properties

The detector consists of a multi-channel-plate (MCP), a luminescent phosphor screen and a one-to-one image onto a CCD-array. Only a small part of this array is left open for exposure (8 or 16 lines), the rest is masked. This leads to images as can be seen in figure 11. The purpose of masking is to

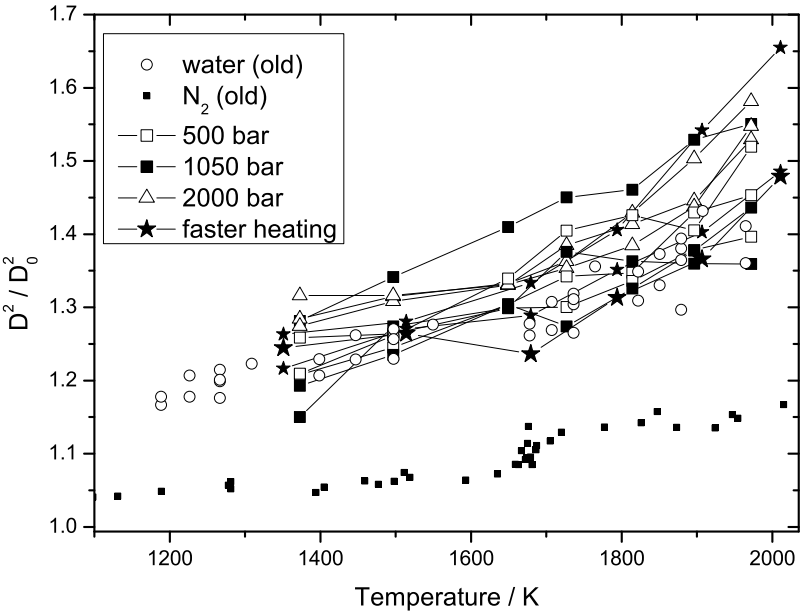

Figure 10: Thermal expansion of Ni80Cr20 while changing 'lens-effect-related' parameters (see text).

get a quick succession of pictures. Usually, the entire chip is read out, which is a slow process. In this setup the information of the exposed lines is just shifted into the masked storage area. Thus, a frame rate of $400000\,\mathrm{s}^{-1}$ is achievable (one picture each $2.5\,\mu$s).

For the evaluation of the diameter, one sequence of pictures is taken prior to the heating process ('cold' picture) and the second sequence is taken during heating ('hot' picture). Consequently the pictures are converted into intensity profiles (dark region: low intensity). Then, each hot picture diameter is ratioed with its corresponding cold picture diameter (see figure 12).

This approach makes the measurement insensitive to imaging effects (e.g.: changed magnification due to usage of water as ambient medium). But it is necessary for other reasons too: When a static picture is recorded (picture of wire prior to the heating process) the obtained diameter is not constant during the sequence of pictures. This effect is related to the summation of charge. A certain amount of dark current is present in every charge-coupled device. Figure 13 displays the data points (cold pictures) of Nb measurements in nitrogen atmosphere (the final results for expansion

Figure 11: CCD shadowgraph pictures (8 lines) of heated sample. a: picture number 2, b: picture number 17 (43 μs later).

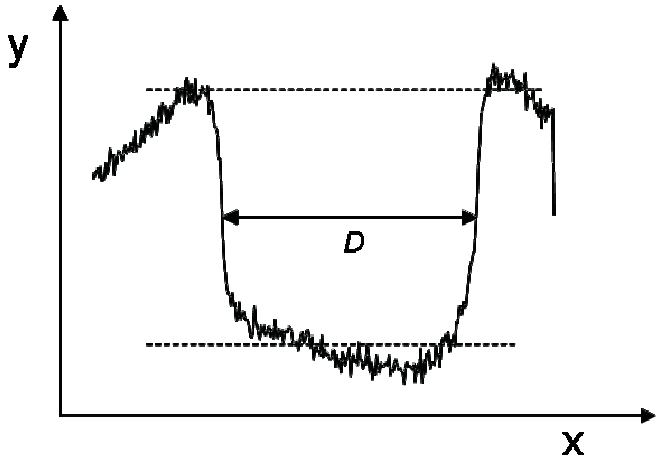

Figure 12: Diameter evaluation from intensity profile.

were already shown in figure 6):

Firstly, the absolute value of the diameter can vary due to differences in the adjustment.
Secondly, pictures were taken with 16 lines left open for exposure, leading to one data point each 5 μs.

Thirdly, although the wire does not change, the evaluation of the diameter from the CCD pictures delivers a decreasing behavior (approx. 2.5 pixels in 40 μs). This could be the effect of charge moving from the region of high intensity (see figure 12) to low intensity which makes the profile more narrow.

Previously, the author related the influence of dark current with the increase of overall intensity (y-axis in figure 12) only. But in the region of a high gradient a movement of charge in x-direction is supposable, too. During the ratioing of hot and cold pictures the effect is canceled out. If the apparent decrease of 'cold diameter' D_0 was more significant in the water experiments, it would lead to the observed results (it would increase the ratio D^2/D_0^2). To be more precise: There would have to be a difference

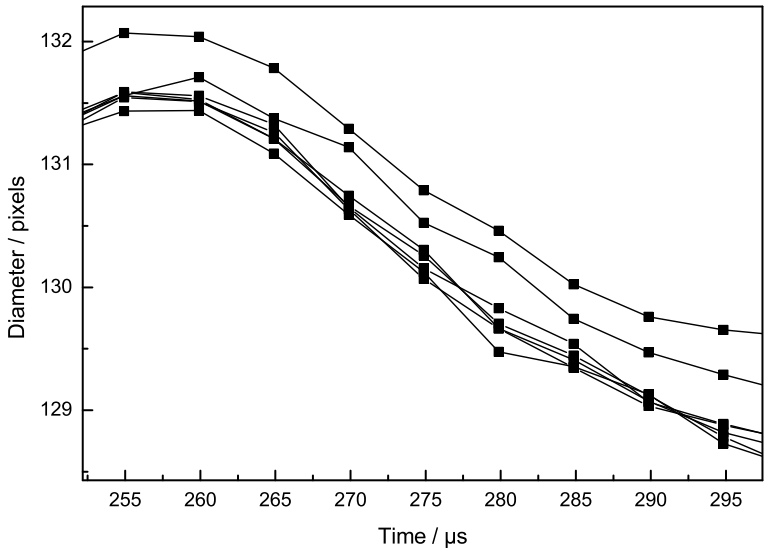

Figure 13: Influence of dark current on static picture: Evaluated diameter from intensity profiles changes during the sequence of pictures although it is constant.

between 'cold' and 'hot' dark current and this difference would have to be dependent on the atmosphere.

1. The only region of charge movement in x-direction is around a gradient. In a 'cold' picture this gradient is static and the moved charges can sum up (thus leading to the decrease in figure 13). In a 'hot' picture this gradient moves due to the expansion of the wire and the moved charges are distributed over a certain area. They can not sum up in the same way. Therefore, a difference between cold and hot dark current is imaginable.

2. Water has two effects on the optical imaging system: On the one hand, the path of light is different due to a difference in the refractive index, and on the other hand, it acts as a filter, because it is not transparent for all wavelengths. This second effect could be responsible for a difference that is dependent on the atmosphere (see figure 14).

To investigate the influence of dark current, new analyses of the CCD-pictures were started: The evaluation of the wire-diameter is based on transverse profiles (see figure 12). An influence of dark current can only be seen in longitudinal profiles (see figure 15). Figure 16 shows two longitudinal profiles which are located as can be seen in figure 15, obtained in water atmosphere.

In the dark region (green line) the dark current leads to a linear increase

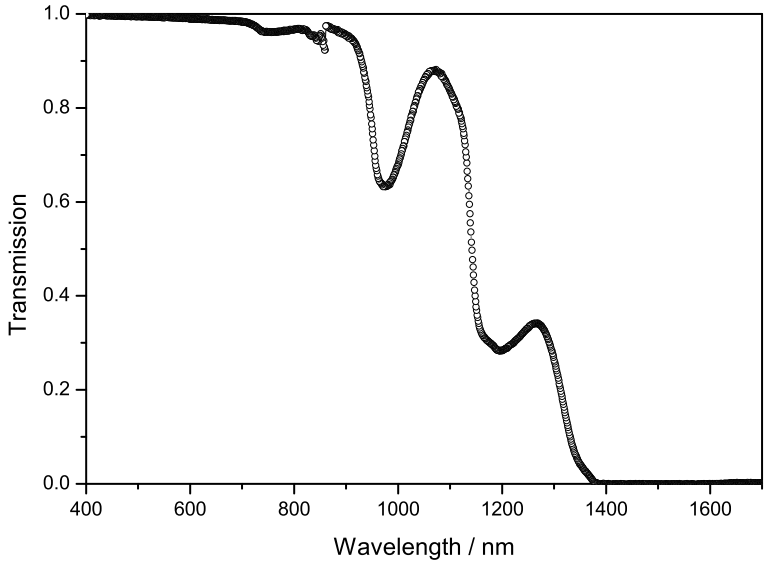

Figure 14: Spectral transmission of water. Graph by courtesy of Dr. Claus Cagran.

of intensity (dashed line in figure 16). Shortly before the transition into the gas phase (end of the experiment) the wire is so hot, that its radiation contribution can be observed (bump on green line). Nevertheless, the intensity trace returns to linear behavior shortly after heating is stopped. In the bright region (red line) the intensity trace finishes at almost the same level but it starts higher, because of backlighting. The trace is no longer linear.

Figure 17 shows two longitudinal profiles obtained in nitrogen atmosphere. Again the light region starts with higher intensity (because of backlighting), but this time the two traces keep their distance. Backlighting acts like an offset; both traces are linear. This is the expected situation. The experiment was stopped earlier; this is why the radiance contribution of the hot wire is not visible.

It is only a speculation that pictures which deliver linear longitudinal profiles are correct whereas pictures with non-linear longitudinal profiles are defective. There are many other reasons for such a contrast: differences in adjustment, magnification, gain of the MCP, saturation effects, etc. Experiments with and without water in the optical path or in the vessel did not reveal a significant trend.

The above mentioned idea, that the filtering effect of water and the consequently different spectral intensity might be the reason for unequal dark current, turned out to be a dead end. The light, which is detected by the

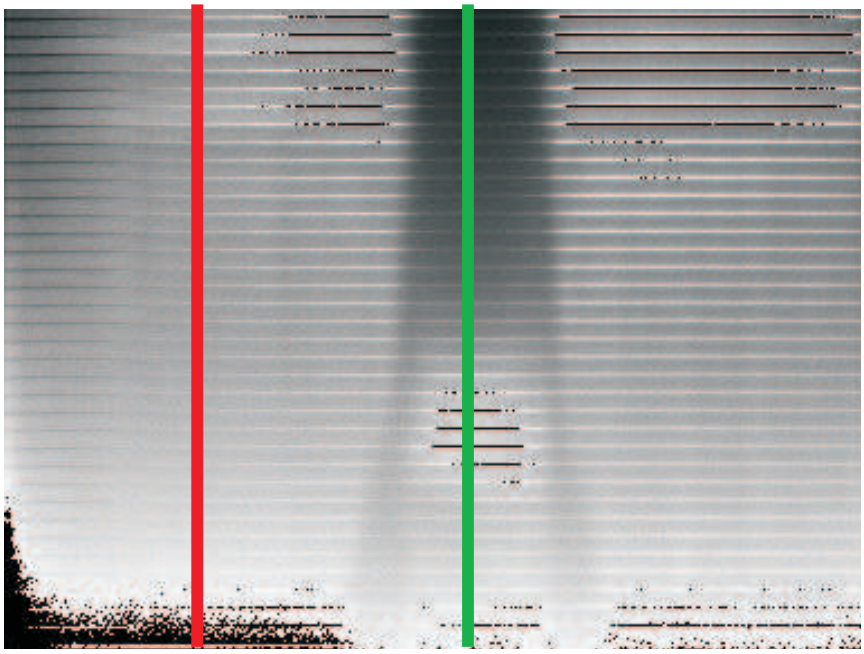

Figure 15: Positions of the longitudinal profiles on the CCD-record for figure 16 (8-lines configuration, surrounding atmosphere is water; red: region with no object, green: region where the radiation of the exploding wire is relevant).

CCD-array comes from the phosphor screen. The spectral distribution is always identical. The only component, which is sensitive to the lights' spectral distribution is the MCP. Figure 18 shows its spectral response characteristics. After the conversion to photo-current only the dimension of 'more or less' remains, no conclusions can be drawn on the wavelengths.

The details discussed in this chapter reveal the need for a reassurance that the setup actually delivers sensible results when being applied to fast pulse-heating.

1. As discussed for figure 16, the influence of self-radiation of the wire can easily be monitored with the help of longitudinal profiles. But what is its influence on the transversal profiles from which the diameter is calculated? Chapter 'self-radiation' is dedicated to this topic.

2. It has to be checked whether the charge-coupled device is able to deliver the expected results in a pre-set configuration with known distances. This is a big difficulty because pulse-heating is a dynamic method and the desired states can not be pre-set. They are only present during the heating process. Nevertheless, the author devised an assembly which can at least prove the irrelevance of dark current: double wire experiments.

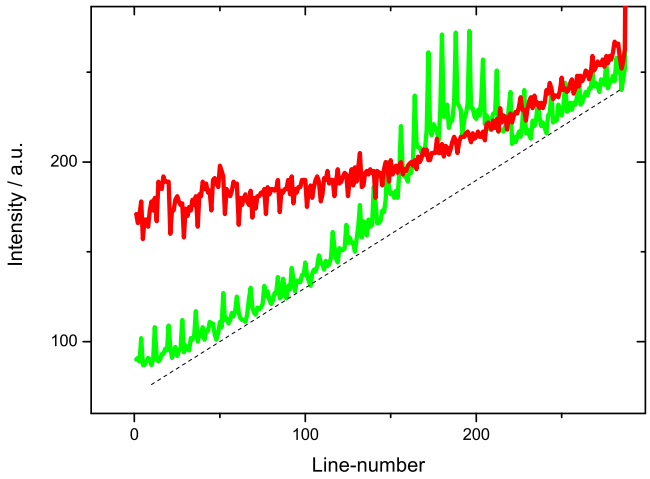

Figure 16: Longitudinal profiles from figure 15 (water atmosphere). Red: region with no object, green: region where the exploding wire influences the recorded intensity.

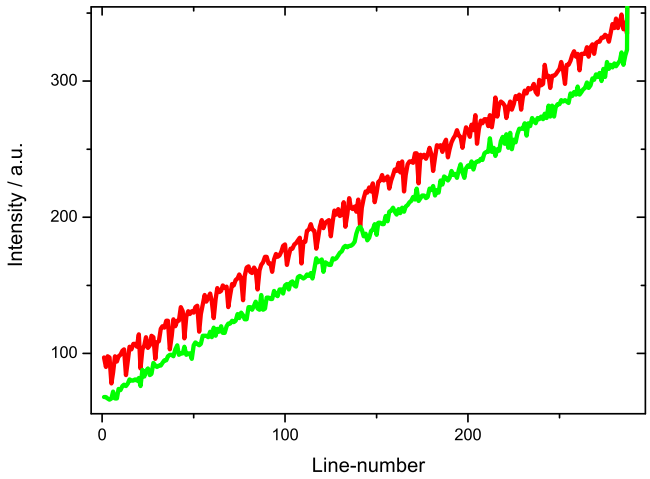

Figure 17: Longitudinal profiles obtained in nitrogen atmosphere. Red: region with no object, green: region where the exploding wire influences the recorded intensity.

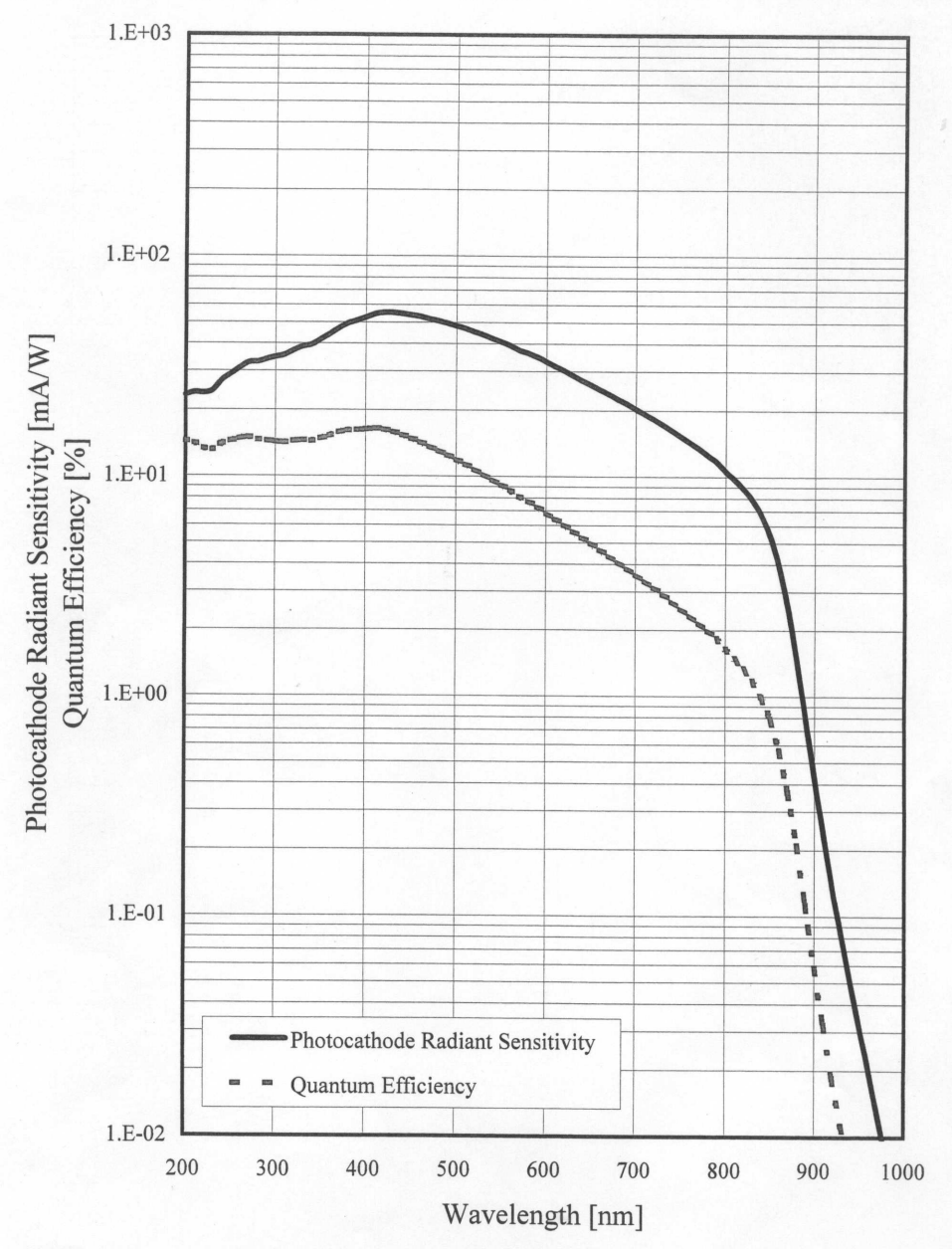

Figure 18: Spectral response characteristics of the multi-channel-plate, scan from the data sheet [Hamamatsu Photonics K.K., Electron Tube Division, V7670U-70-P46].

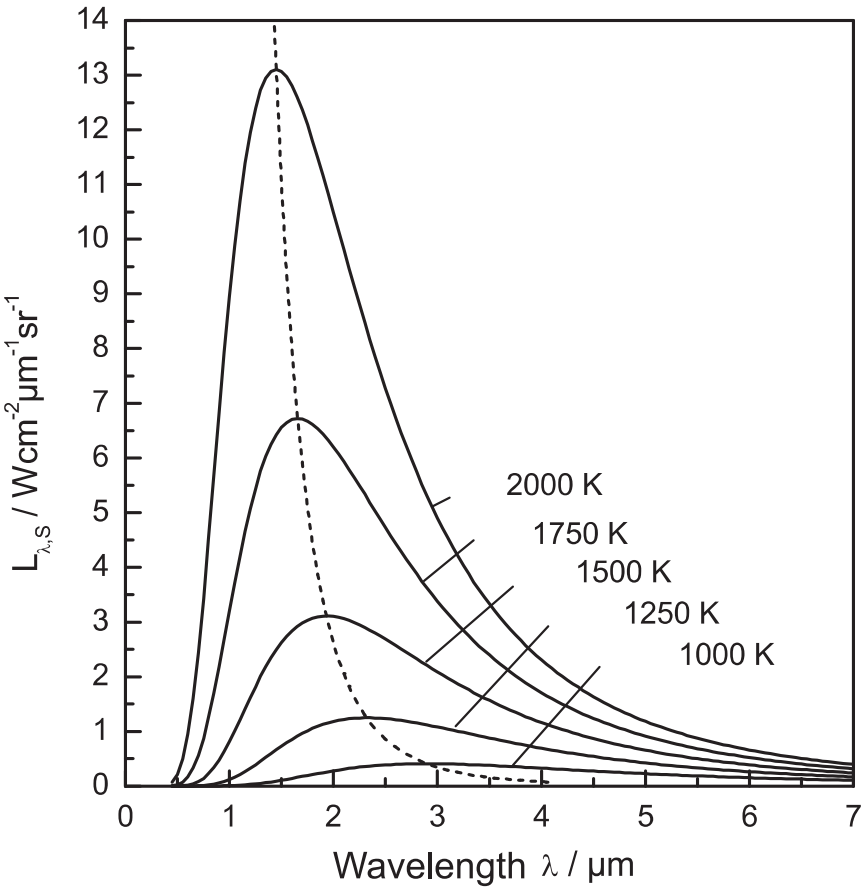

Figure 19: Radiance as a function of wavelength according to Plancks law. Dashed line: maximum of distribution moves to shorter wavelengths with increasing temperature (Wiens displacement law). Graph by Dr. Claus Cagran.

4.4 Self-radiation

According to Plancks law, every surface which has a temperature higher than absolute zero irradiates heat ('radiance' L) via electromagnetic waves. The spectral radiance of the blackbody $L_{\lambda,S}$ is:

$$L_{\lambda,S}(\lambda, T) = \frac{c_1}{\pi\Omega_0} \cdot \lambda^{-5} \cdot (e^{\frac{c_2}{\lambda T}} - 1)^{-1} \tag{2}$$

$c_1 = 3.7415{\cdot}10\text{-}12\,\mathrm{W\ cm^2}$, $c_2 = 1.4388\,\mathrm{cm\ K}$, $\Omega_0 = 1\,\mathrm{sr}$, λ : wavelength, T: temperature.

The spectral distribution changes with temperature (see figure 19).

At high temperatures the intensity which is in the region of visible light is high enough to be detected with the human eye (compare: famous 'red heat').

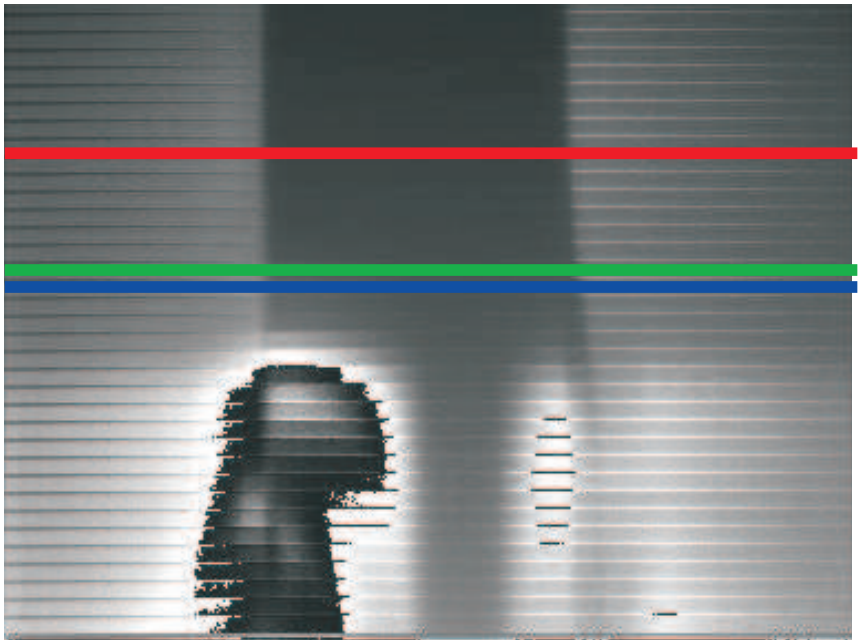

Figure 20: Streak image of heated wire including shielding. Colored lines: location of transversal profiles (see figures 21, 22, and 23).

During fast pulse-heating the emitted light is also detected with the CCD-camera. The result can be seen in figure 15 and 16. It has to be asked whether the radiation, which comes from the wire, has an influence on the expansion evaluation. Thus, experiments with different shielding were performed: a shield was placed in the path of light, close to the MCP. It was adjusted in a way that one section of the wire was blocked out and that the rest of the wire could still execute its influence. Figure 20 displays the result: As long as the intensity of the emitted light from the wire is low, the wire and the shield just seem dark (shadow of backlighting). As soon as the intensity is high enough to be detected, the wire illuminates the whole area except for where the shield is.

The influence on the profiles to be evaluated can be discussed via three pictures: Figure 21 shows a profile which is not affected by self radiation.

According to the Stefan-Boltzmann law, the radiated energy per unit time is proportional to the 4^{th} power of the temperature. That means that the influence of the radiation of the wire is first smaller than the noise and suddenly it increases rapidly. Let's make a rough estimation: suppose the upper limit of the temperature range was 2500 K and suppose there is a CCD picture right at that time. With a heating rate of 10^8 K/s the picture prior to the 'last' picture is obtained at a temperature 250 K lower. This difference leads to a relative difference in radiation of 0.6561. Figure 22 displays the

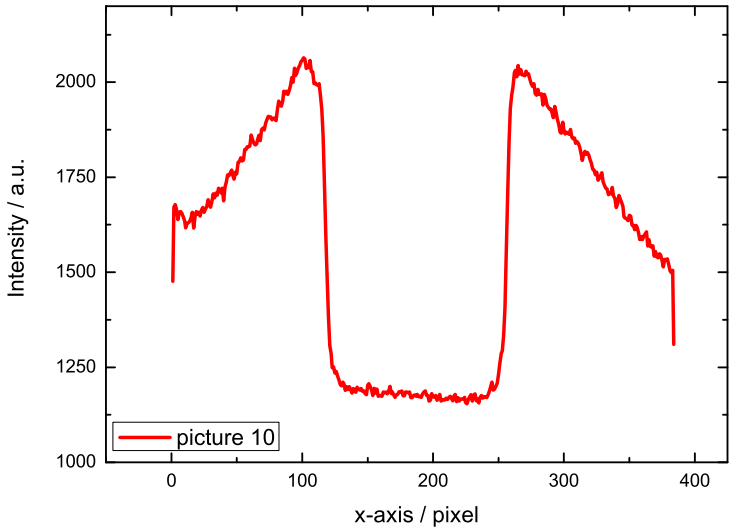

Figure 21: Profile from figure 20.

last picture. The influence of the self-radiation is in the same size as the depth of the undisturbed profile. No evaluation is possible. Number 1 indicates the undisturbed low-level of the profile. Number 2 indicates the 'shoulder' from the self-radiation of the wire. It is on the same level as the undisturbed high-level of the profile.

The penultimate picture is displayed in figure 23. The distance from shoulder to undisturbed low-level (2-1) is indeed approximately 0.65 times this distance in figure 22. The correct evaluation of the diameter would be in the middle of the dashed lines (half maximum of undisturbed high- and low-level), indicated by the solid line. Without the shielding, the evaluation would be done on the level of the red line. The obtained diameter would exceed the correct value!

In the antepenultimate picture the half maximum will be too high as well. But the influence is reduced by a factor of 0.62.

One picture after the last picture the profile no longer exists (see figure 24). Without shielding the intensity record from the wire would exceed the intensity from the flashlight, thus leading to a flipped profile. This can not be used for a diameter evaluation, because the edges are not sharp.

In summary, the conclusion is that the last data-points of expansion can have a deviation to higher values. By looking at figure 10 again, one can now see this deviation. As soon as the traces diverge from the linear behavior, the data-points have to be excluded because of a systematic error in the

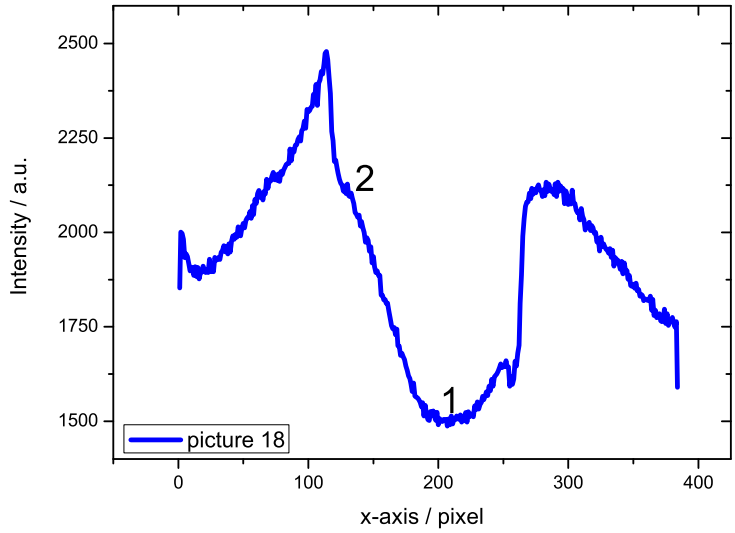

Figure 22: Disturbed profile from figure 20. No evaluation is possible. 1: low-level of undisturbed profile, 2: 'shoulder' from self radiation of wire on the same level as upper level of undisturbed profile.

evaluation.

Nevertheless, the assumptions made in this chapter hold for water and nitrogen experiments. The Stefan-Boltzmann law is only correct for the whole spectrum of wavelengths. Filtering (see transmission of water, figure 14) leads to different results. This could lead to a difference in the influence of self-radiation between water and nitrogen experiments. But because the multi-channel-plate is doing an increased filtering as well (see figure 18), the effect exists all the time, independent of 'water-filtering'.

4.5 Double wire experiments

The quantification of self-radiation was the first business which was raised at the end of chapter 4.3. The second one was the confirmation of whether the charge-coupled device delivers plausible results when a pre-set configuration is investigated. But the measurementconditions during pulse-heating are not static. Therefore, this goal is contradictory: One needs to pulse-heat without pulse-heating. Believe it or not, this is possible via double-wire-experiments.

Usually, the wire under investigation is clamped on both sides. The clamps act as feed cables. To get a sample in pulse-heating conditions with-

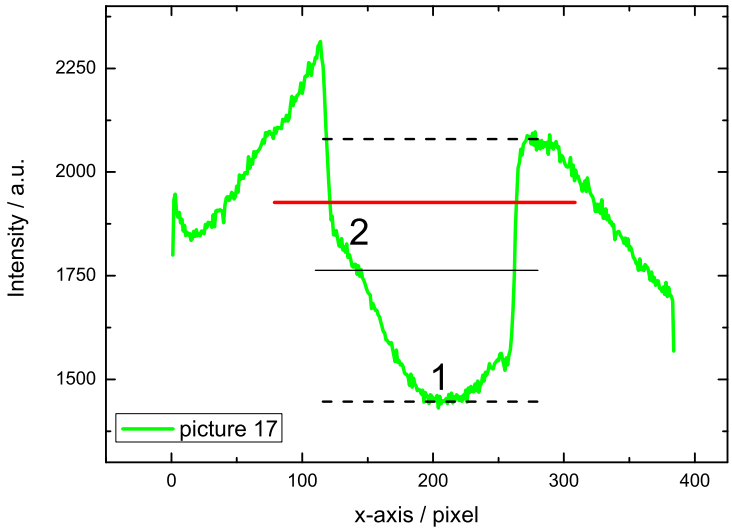

Figure 23: Disturbed profile from figure 20. Dashed lines: undisturbed high- and low-level, 1: low-level of undisturbed profile, 2: 'shoulder' from self radiation of the wire, black solid line: correct half maximum, red line: defective evaluation of diameter yielding too big values.

out pulse-heating it, the author placed a second wire parallel to the first one. This 'scale-wire' is not clamped. It is fixed by two pellets of plasticine - an insulating modeling clay. The distance to the first wire is 0.5 - 1.5 mm. Figure 25 shows the sequence of CCD-images during heating. The wire on the left hand side is the 'scale-wire' (it does not change during heating), the wire on the right is the heated wire (it expands during heating).

The evaluation is identical to the ordinary experiments. Figure 26 shows a profile of a double-wire-experiment performed in water atmosphere.

Any disturbing effect which happens during heating only (it is already known that all other disturbing effects would cancel each other out because of ratioing D^2/D_0^2) - summing up of dark current, lens effect, shock waves - would be visible on the 'scale-wire'. The diameter of the scale-wire should not change during pulse-heating. Figure 27 shows the results from nitrogen-experiments. The diameter of the heated wire expanded as expected. The diameter of the scale-wire remained constant until the very end.

Figure 28 shows the results for experiments in water atmosphere. Again, the scale-wire remained constant. Again, the heated wire expanded as measured earlier in water atmosphere.

These extraordinary experiments were a turning point in the investiga-

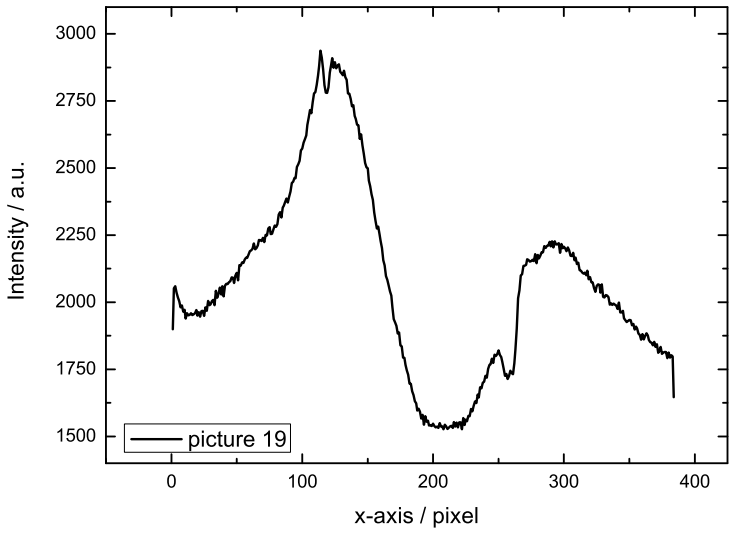

Figure 24: Profile from figure 20: Radiance from the wire exceeds the radiance from the backlighting.

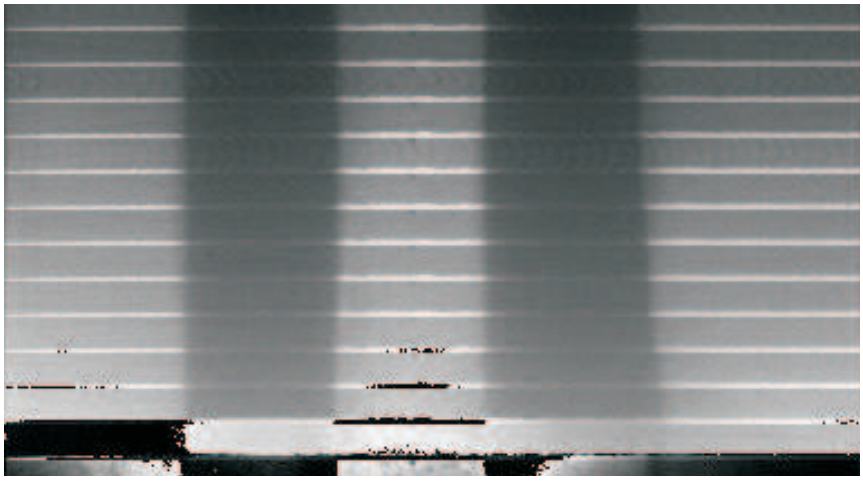

Figure 25: CCD-record of double-wire-experiment.

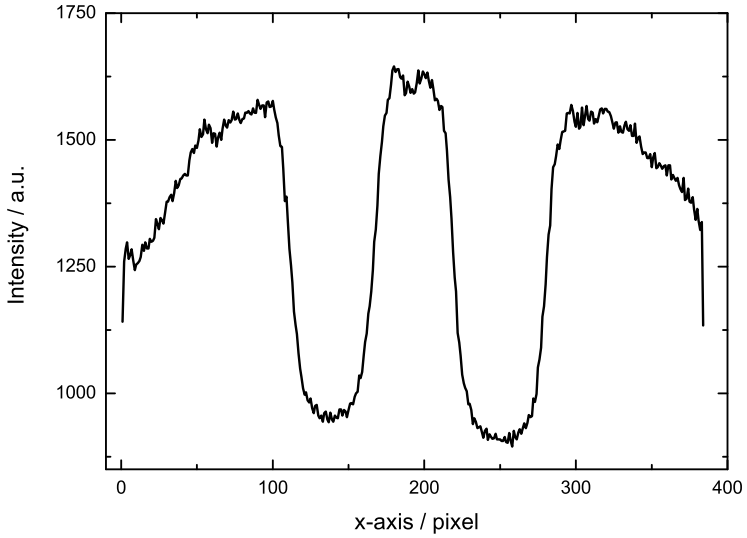

Figure 26: Profile of a double-wire-experiment.

tions. Up to this day all exploratory research aimed at finding an error in the imaging system. Nobody thought that the expansion would really be enlarged because of water or high pressure. The clear results of the double-wire experiments stimulated new questions. If the enlarged expansion was real, what could be the physical explanation?

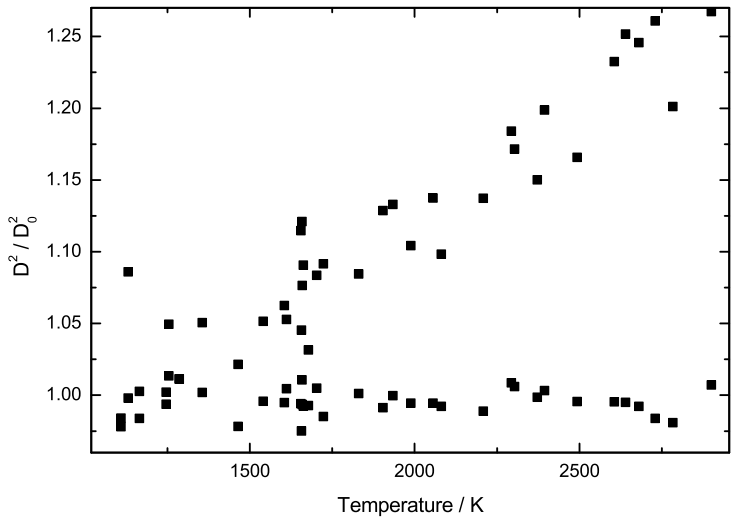

Figure 27: Evaluated double-wire-experiments in nitrogen atmosphere.

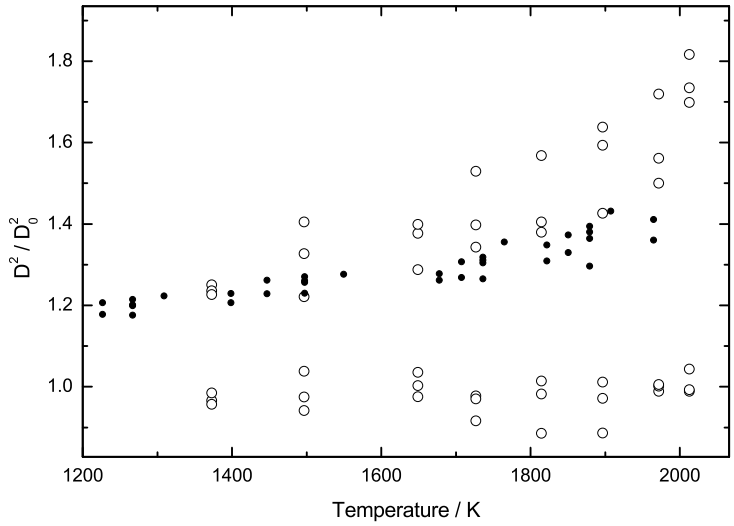

Figure 28: Evaluated double-wire-experiments in water atmosphere (open circles). Full circles: previous results.

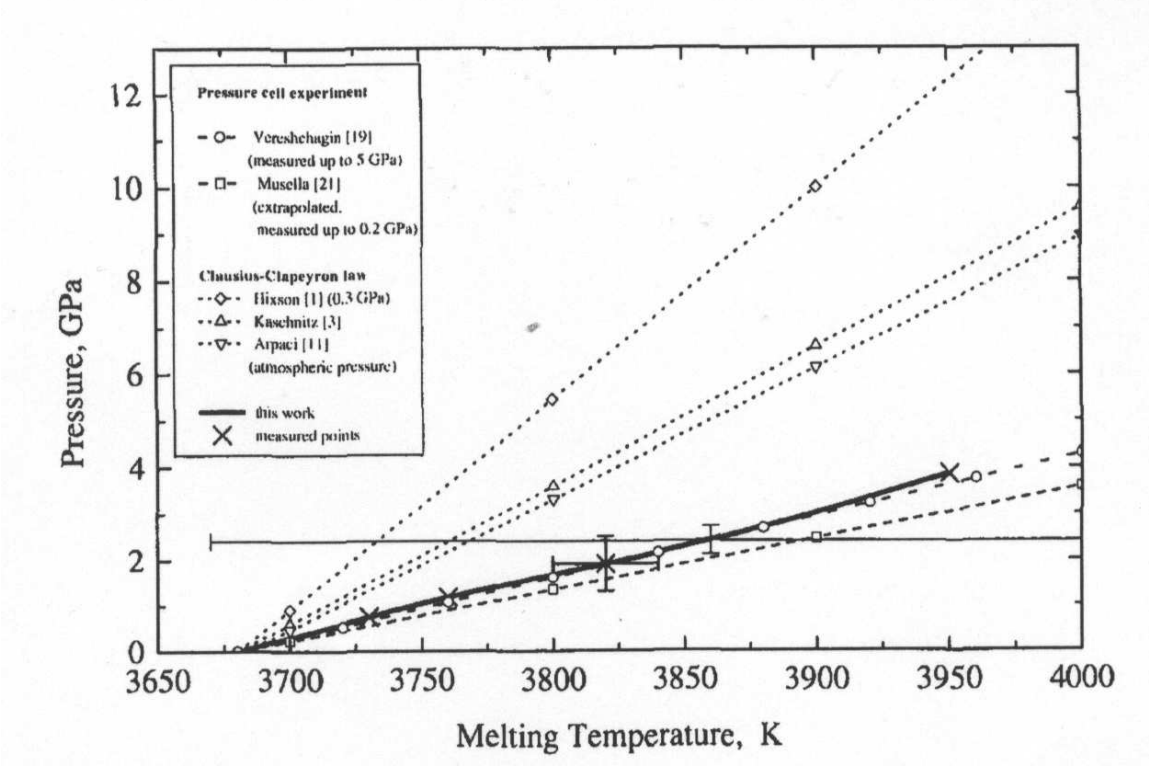

Figure 29: Melting curves of tungsten. [A. Kloss, H. Hess, H. Schneidenbach, R. Grossjohann, 'Scanning the Melting Curve of Tungsten by a Submicrosecond Wire-Explosion Experiment', Int. J. Thermophys., 20 (4), 1999].

4.6 Elevation of melting point

The temperature measurement in all experiments was conducted as follows: The known melting temperature (from the literature) is assigned to the melting plateau, which is visible on the pyrometer output record ('indirect calibration' of pyrometer). Then the other pyrometer output values are scaled according to Plancks law.

The same temperature was assigned to water and nitrogen experiments. But from the phase-diagrams of pressure vs. temperature it is known that the melting point is pressure dependent! The higher the pressure the higher the melting point (compare the famous anomaly of water). This is called the melting curve. If the melting point in the high pressure experiments was enlarged by 500 K, it would explain the results: The data-points with 'enlarged expansion' would have to be drawn at higher temperatures. The increase of relative expansion with increasing temperature is the expected behavior. So the author looked at the absolute value of the pyrometer output at melting to see if the height of the plateau would change by increasing the pressure. But no change could be observed between 500 and 2800 bar.

Literature values for melting curves exhibit that the effect is orders of magnitude too small to explain the findings. Figure 29 displays a graph from Kloss on tungsten. Approximately 60 000 bar would be necessary to reach an increase of the melting point of 500 K.

The elevation of the melting point is not the reason for the apparent increased expansion.

4.7 Change of resistance

If the increase of expansion was real, it should be visible in the resistance record of the sample, too. Increasing the diameter decreases the resistance.

This time one has to deal with the methodological trickiness in a different way because the high pressure setup is not calibrated for resistance measurements. The voltage drop has to be measured over the wire plus power cables and discharge vessel. Hence, the obtained values can not be compared to the low pressure setup which measures the voltage drop by two knife-edge contacts directly placed on the wire. Only changes using the same setup can be compared.

Firstly, the author did experiments with the low pressure setup as usual. Then the same parameters were used but with water filled into the vessel. As mentioned above, the expansion is no longer analyzable in this setup because of the possible formation of a steam-tube surrounding the wire. But the resistivity evaluation is still correct. The water had no influence on the resistance of the wire.

Secondly, the author did experiments with the high pressure setup. Starting at 1 bar (again invalid expansion evaluation) a pressure range up to 2800 bar was covered. No significant change of resistance could be found.

These experiments reanimate the suspicion that the enlarged expansion in the high pressure setup is only an artifact.

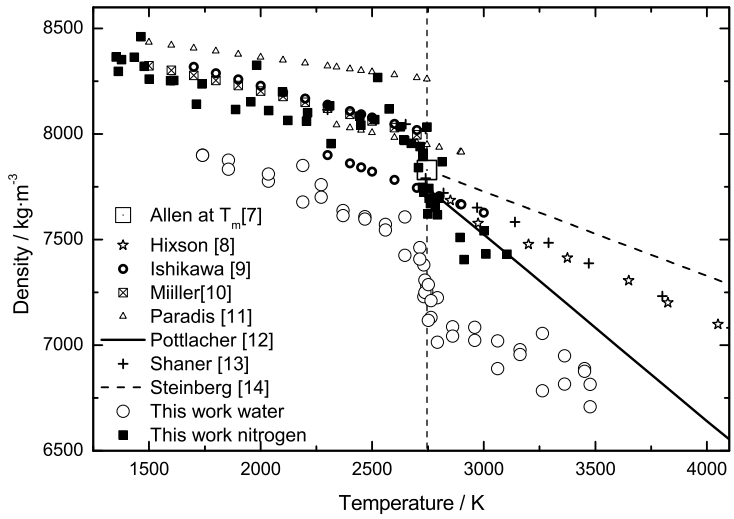

Figure 30: Density of niobium as a function of temperature including literature values (see [12]).

4.8 Literature comparison

Figure 30 displays the literature comparison which is described in [12]. Although the consistency is low, this comparison is a point for the low pressure results of thermal expansion. The high pressure results (open circles) deliver a density which is significantly lower than any other reference.

Additionally, in private communications with John Arblaster, who is conducting a lot of crosschecking of literature databases, the stated expansion values e. g. for palladium and hafnium, possess a high acceptation. All results for thermal expansion published by the workgroup refer to low pressure measurements.

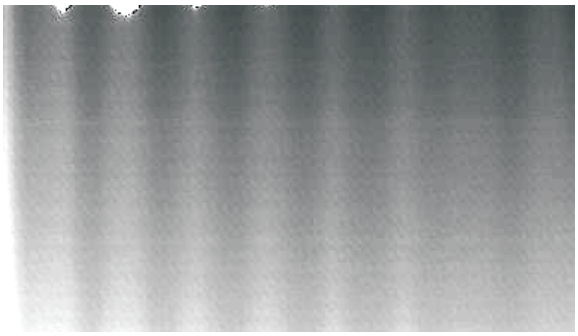

Figure 31: Diffraction pattern as alternative approach to the diameter evaluation.

5 Future steps

Dilatometer

The workgroup would profit from a cooperation with a laboratory with a dilatometer. This device can measure the thermal expansion with high precision up to about 1800 K. A systematic analysis of different materials could give additional information about the quality of the results obtained under pulse-heating conditions.

Diffraction patterns

Some of the earlier mentioned possible reasons for an erroneous expansion measurement were justified on the basis of optics. This raises the question of whether the imaging process could be done using effects which can only be explained by the wave-properties of light (compare dualism). Such an effect is the diffraction of light. With the use of lasers, coherent light with a very narrow spectrum can be obtained. The detection of a diffraction pattern would not be sensitive to any self-radiation of the specimen because the latter contribution is not coherent and therefore does not change the position of interference maxima or minima.

Figure 31 displays a diffraction pattern obtained in the pulse-heating setup. A laser with 532 nm wavelength was directed on the wire instead of the backlighting by the photoflash. This leads to a diffraction pattern which can be detected with the CCD-camera. Again, it is operated as streak-camera delivering 16-lines-pictures each 5 μs. In figure 31 the first order maximum is outside of the detector. The picture was taken prior to the heating process. By measuring the distance from minimum to minimum the diameter of the sample can be obtained. A relative change of this distance during heating would be inverse proportional to the relative change of the diameter. Figure 32 displays a possible way to evaluate the intensity profiles.

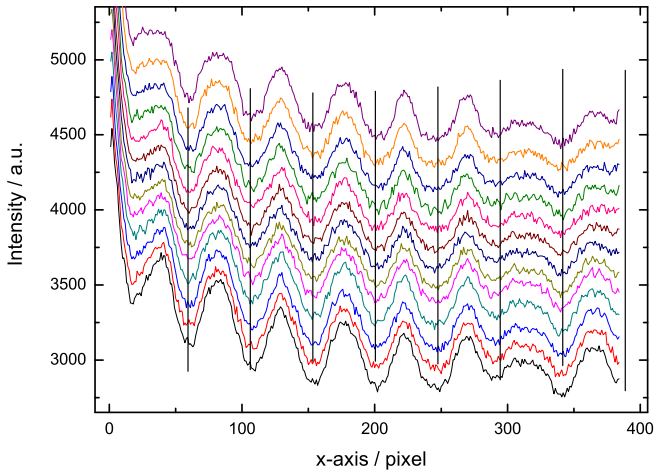

Figure 32: Intensity profiles of diffraction pictures. Vertical lines: positions of minima.

Unfortunately, the usage of diffraction patterns had to be abandoned very early on because of difficulties with the adjustment.

This method will probably be reinstalled in the future with the help of new tools.

Electromagnetic levitation

Another promising technique for analytical comparison with the pulse-heating results for thermal expansion is electromagnetic levitation. Thereby, metallic droplets are levitated by a high frequency electromagnetic field which is applied by a coil (see figure 33).

The induced current heats up the sample. Once the material is molten, it forms a sphere due to its surface tension. A precise measurement of the geometry of this droplet (e.g.: with a CCD-camera) delivers the thermal expansion as a function of temperature (for more information see [Georg Lohöfer, *SIAM J. Appl. Math.* **49**, 1989, p. 567.]).

An electromagnetic levitation apparatus from the DLR Cologne was transferred to the TU Graz. Once it is in operation, the results can easily be compared to the results obtained by fast pulse-heating.

Figure 33: Liquid droplet in an electromagnetic levitation experiment. Picture by courtesy of DLR Cologne, Germany.

6 Summary

Pulse-heating experiments deliver several thermophysical properties of electrically conducting samples simultaneously. Especially the liquid state can be investigated. Additionally, high pressures of about 5000 bar can be applied using a high pressure setup.

During the compilation of results a discrepancy between the high pressure and the low pressure setup appeared. Expansion in water at high pressure is larger than in nitrogen at low pressure. This demanded a closer look at the expansion measurement. The thermal expansion is measured via a sequence of pictures obtained with a fast CCD-camera.

Several possible explanations have been put to the test:

1. *Probe laser*: A laser which is directed through the vessel lateral to the wire is not deflected during the pulse-heating process.

2. *Lens effect*: The two parameters which could have an influence on the formation of a 'lens' due to shock waves are the heating-rate and the pressure. No dependency of expansion on the heating-rate or the pressure was detected.

3. *Detector properties*: Dark current has an influence on the obtained pictures. During ratioing the effect is canceled out. The spectral transmission of water is different from that of air, but because of the spectral response of the MCP, which causes even stronger filtering, it has no effect.

4. *Self-radiation*: The radiation from the heated wire can increase the

expansion obtained from the last two pictures in the sequence. As such a behavior can be easily identified these data-points should be left out.

5. *Double-wire experiments*: These experiments permit the measurement of a pre-set configuration in the dynamic process of pulse-heating. They prove that the evaluation delivers correct values for a non-heated wire which is parallel to the heated wire at a distance of about 1 mm.

6. *Elevation of melting point*: The increase of the melting point due to an increase of the pressure is much too small to be the reason for the discrepancy.

7. *Change of resistance*: An increased expansion would decrease the resistance of the sample. No such correlation could be detected.

8. *Literature comparison*: The low pressure results for thermal expansion agree much better with the literature values than the high pressure results.

A dilatometer would be a convenient complement to compare expansion results. The evaluation of expansion from diffraction patterns is possible. It is an alternative to the current evaluation method. Additionally, an apparatus for electromagnetic levitation experiments will be set up at the TU Graz. This method is able to provide data for thermal expansion as well.

7 Publications

1. G. Pottlacher, T. Hüpf, *A review of expansion measurements for subsecond ohmic pulse-heating experiments*, submitted to ITCC in Pittsburgh 2009.

2. T. Hüpf, C. Cagran, B. Wilthan, G. Pottlacher, *Thermophysical properties of rhodium obtained by fast pulse-heating*, Journal of Physics: Condensed Matter 21, 2009.

3. C. Cagran, T. Hüpf, B. Wilthan, G. Pottlacher, *Selected thermophysical properties of Hf-3%Zr from 2200 K to 3500 K obtained by a fast pulse-heating technique*, High Temperatures-High Pressures, 37, 2008.

4. T. Hüpf, C. Cagran, G. Lohöfer, G. Pottlacher, *Electrical resistivity of high melting metals up into the liquid phase (V, Nb, Ta, Mo, W)*, Journal of Physics: Conference Series 98, 2008.

5. T. Hüpf, C. Cagran, G. Lohöfer, G. Pottlacher, *Electrical resistivity of high temperature metallic melts - Hf-3%Zr, Re, Fe, Co, and Ni*, High Temperatures-High Pressures 37, 2008.

6. C. Cagran, T. Hüpf, G. Pottlacher, *Electrical resistivity of high melting metals (W, Mo, Re, Ta, Nb, Ir, and Hf) up into the liquid phase*, Proceedings of the Seventh International Conference on Tungsten, Refractory & Hardmaterials, 2008.

7. T. Hüpf, C. Cagran, G. Pottlacher, G. Lohöfer, *Specific*, Poster presented at the 14th Lähnwitzseminar on calorimetry, Warnemünde, Deutschland, 2008.

8. T. Hüpf, C. Cagran, E. Kaschnitz, G. Pottlacher, *Thermophysical properties of Ni80Cr20*, Thermochimica Acta 494, 2009.

9. T. Hüpf, C. Cagran, E. Kaschnitz, G. Pottlacher, *Thermophysical properties of five binary copper-nickel alloys*, Int. J. Thermophys., accepted in March 2010.

10. T. Hüpf, C. Cagran, G. Pottlacher, *Two ways of looking at the intermediate position of binary alloys*, Poster presented at the ÖPG in Innsbruck, 2009.

11. T. Hüpf, C. Cagran, G. Pottlacher, *Thermophysical properties of 22 pure metals in the solid and liquid state - The pulse-heating data collection*, submitted to LAM 14, Rome, July 2010.

12. T. Hüpf, C. Cagran, G. Pottlacher, *Thermal expansion in pulse-heating - a status report*, submitted to ITCC, Pittsburgh, USA September 2009.

7.1 A review of expansion measurements for subsecond ohmic pulse-heating experiments

G. Pottlacher, T. Hüpf, *A review of expansion measurements for subsecond ohmic pulse-heating experiments*, accepted at ITCC in Pittsburgh, USA, 2009.

The paper is a review of expansion measurements; around the globe and at the TU Graz as well.

Comments: The paper was written by myself in close collaboration with Prof. Pottlacher who provided all the information.

Cover sheet

Title: *A Review of Expansion Measurements for Subsecond Ohmic Pulse-Heating Experiments*

Authors: Gernot Pottlacher
Thomas Hüpf

Affiliation: Graz University of Technology
Institute of Experimental Physics
Petersgasse 16
8010 Graz
Austria

ABSTRACT

During fast pulse-heating experiments wire shaped specimens are rapidly ohmic heated by a short current ‘pulse’. Within such a measurement various quantities can be recorded in a subsecond time regime. Amongst electrical current, voltage drop, and temperature the geometry of the sample (or its density) and its change during one experiment is an important parameter.

The ultrashort experimental duration is a specific characteristic of pulse-heating and it is a major difficulty as well, because data recording has to be fast enough. Several laboratories around the globe have approached this requirement differently, and the developments of new electronic devices have arisen new possibilities of measurements. Expansion measurements can be categorized into two groups: Interferometric techniques and optical imaging techniques. The workgroups considered in this review are for the millisecond time regime – NIST (former NBS) Gaithersburgh Maryland USA, INRIM (former IMGC) Turin Italy, and ÖGI Leoben Austria – as well as for the submicrosecond time regime – Christian Albrecht University Kiel Germany (several parts of their equipment moved later to TU Graz), Group M6 Los Alamos National Laboratory USA, CEA Valduc France, INP University of Greifswald Germany, and the Russian Academy of Sciences Moskow Russia.

The development of expansion measurements during the last 25 years especially at the workgroup of subsecond thermophysics at TU Graz will be highlighted.

INTRODUCTION

Density is an important parameter in material science. In addition to thermal conductivity, heat capacity and the melting range this property is of high priority for the metal working industry [1]. For instance, it is used as input parameter for numerical simulations i.e. of casting processes.

Classical measurement methods like Archimedes principle or measurement of geometry and weighing are not applicable for hot samples and even less for liquids. During pulse-heating the demands on the measurement technique are even higher, because the experimental durations are very short.

Pulse-heating experiments with millisecond or even microsecond timescale inherently create a big advantage regarding density measurement, as the mass of the sample usually does not change during the heating process. Therefore, only geometric expansion has to be recorded. The mass can be measured prior to the experiment. Moreover, commonly only the thermal expansion is stated as a function of temperature and density can be calculated on the basis of known room temperature densities, which are obtained to much higher precision by other techniques [2].

The established expansion measurement method under static conditions is the push-rod dilatometer [3].

Different methods of thermal expansion measurements under pulse-heating conditions have been developed. They can be separated into two groups: interferometric techniques and optical imaging techniques.

TECHNIQUES

Interferometric expansion measurement

The basic idea of interferometric methods is to shape the specimen in such a way, that it can act as a mirror (called ‘optical flat’). If the mirror is not the specimen itself, the reflecting surface has to provide a representation of the whole sample’s change in geometry (expansion) due to a thought-out mounting. This assembly then is placed inside an interferometer. Consequently, the recording of expansion is done by fringe counts or phase detection. More sophisticated methods like double-interferometers can make the measurement inherently insensitive to translational motion. However, a multitude of arrangements can be imagined.

When the specimen is the mirror itself the method is limited to the solid phase only. This approach, especially suitable for millisecond pulse-heating experiments, was pursued by two laboratories: NIST (formerly National Bureau of Standards) and ÖGI (Österreichisches Gießerei-Institut Leoben).

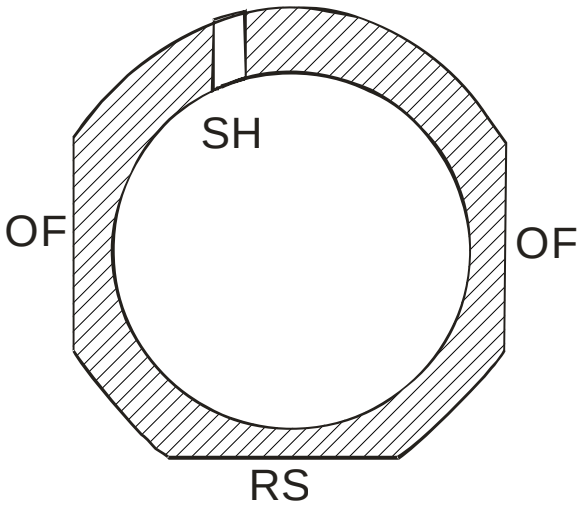

Figure 1: Cross section of the sample which is placed inside the interferometer, outside radius: 3.4 mm, OF: optical flats, RS: optical flat to monitor rotational stability, SH: sighting hole for optical temperature measurement.

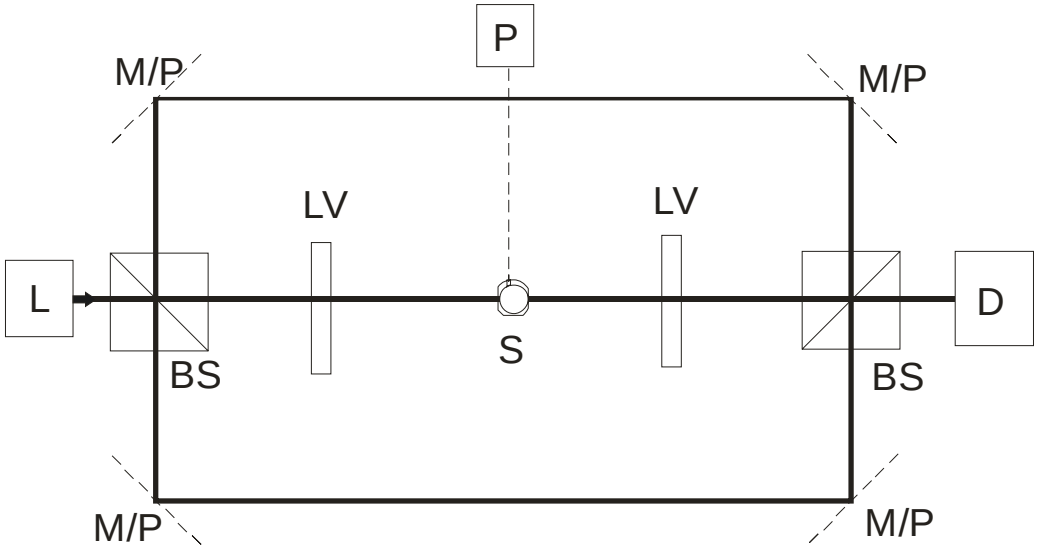

Figure 2: Sketch of interferometer: L: laser, D: detector, S: sample, BS: beam-splitter, M/P: mirror or prism (details omitted), LV: quarter wave plate.

NIST

The interferometric method was chronologically the second type of expansion measurement at the laboratory of A. Cezairliyan. The first type – a kind of 'shadowgraph method' – will be discussed in section 'Optical Imaging'.

As mentioned above, the specimen is designed as a tube with parallel optical flats on opposite sides [4]. Figure 1 displays two more features: a small rectangular sighting hole to provide an approximation of blackbody conditions for optical temperature measurement and a third optical flat to monitor the rotational stability of the sample.

The specimen is acting as a double-reflector inside a Michelson interferometer (figure 2). The coherent light source is a plane-polarized He-Ne laser (632.8 nm). A typical measurement of metals between room temperature and the melting point corresponds to a cumulative fringe shift of 400 – 500 fringes. The linearly polarized light is split into two beams by a polarizing beam splitter (in and perpendicular to the interferometer plane).

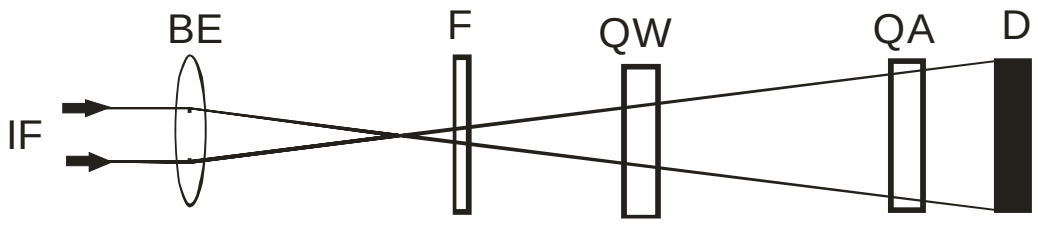

Figure 3: Detection-system at NIST and ÖGI: IF: light from interferometer, BE: beam expander, F: bandpass filter, QW: quarter wave plate, QA: four quadrant analyzer, D: detector.

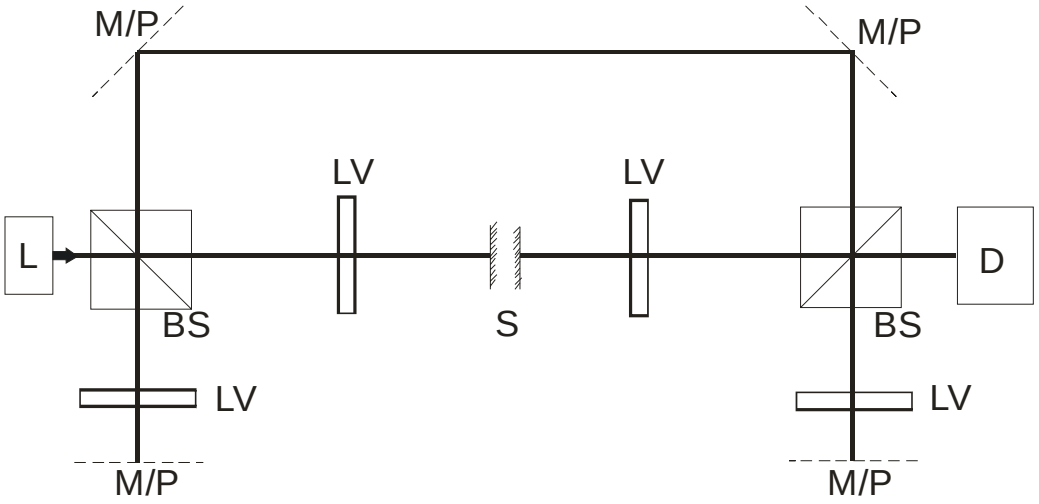

Figure 4: Different arrangement of interferometer at ÖGI, L: laser, D: detector, S: sample, BS: beam-splitter, LV: quarter wave plate, M/P: mirror or prism.

Passing a quarter wave plate, the now circularly polarized light is reflected on the optical flat thus changing its handedness. After passing the quarter wave plate again, the phase can be changed depending on the distance (which is destined by the sample).

The detection system is displayed in figure 3. The light from the interferometer passes through a beam expander and a filter with a narrow bandpass at the laser-wavelength. A quarter wave plate, oriented 45° to the interferometer plane, gives right and left handed circularly polarized light beams which combine to linearly polarized light when their intensity is adjusted to be equal. The angle of this linearly polarized light depends on the phase-shift of the two beams. It is recorded by a four quadrant analyzer with a silicon detector. For more details see [4]. Please mind, the system does not count fringes but ‘rounds’.

ÖGI

E. Kaschnitz spent a year at NIST where he got familiar with the interferometric expansion measurement. Consequently, an apparatus quite similar to the one at NIST was set up in Leoben as PhD thesis of Peter Reiter [5].

As mentioned, different arrangements were employed: One similar to NIST (see figure 2) and a second one slightly different (see figure 4). The latter is less sensitive to changes in the refractive index of the surrounding air (e.g. caused by temperature gradients) but two more quarter wave plates are necessary.

The detection system is the same as described above.

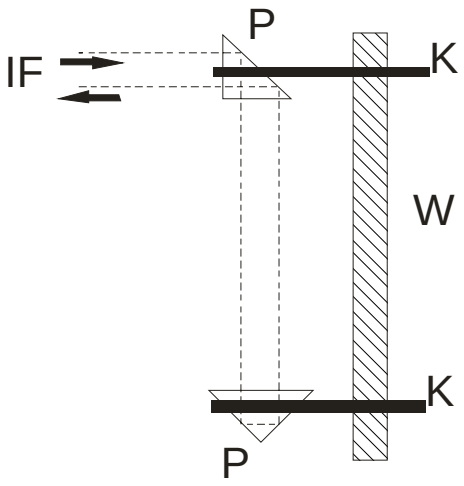

Figure 5: Interferometer directly mounted on the sample, IF: entrance of light, P: prism, K: clamps, W: wire (specimen).

INRIM

In Italy, F. Righini developed an interferometric expansion measurement technique (name of the institute at that time: IMGC). The interferometer is directly mounted on the sample (figure 5). Consequently the method is limited to the solid phase. Temperature is measured with a high speed scanning pyrometer. Longitudinal expansion is obtained as a function of temperature. The experiments are carried out in vacuum [6].

Optical Imaging

There are many possibilities to obtain an image. They have to involve background lighting (conventional photoflash, laser, etc.), optics (e.g. lenses for magnification) and detection (photographic films, diodes, CCD-arrays, etc.).

These techniques are not limited to the solid phase. Therefore they are the method of choice in fast pulse-heating experiments, which are especially interested in the liquid phase. Thin wires are used as samples and the experiments are operated on a submicrosecond time scale. Because of the short time scale the detection system has to be very fast. The major developments concern the handling of this demand for high speed detection.

Most of the following methods do not measure the diameter of the expanding wire on an absolute scale. Instead, the ratio of a ‘cold’ picture (prior to the heating process) and a ‘hot’ picture (during heating) is calculated.

NIST

As mentioned earlier, the first method of expansion measurement at this laboratory (NBS) was some kind of ‘shadowgraph method’ [7]: A constant radiance source delivers parallel light to the specimen which is enclosed in a rectangular aperture (figure 6). The light which can pass through specimen and aperture is detected by a pyrometer. An expansion of the specimen leads to a decrease of transmitted light.

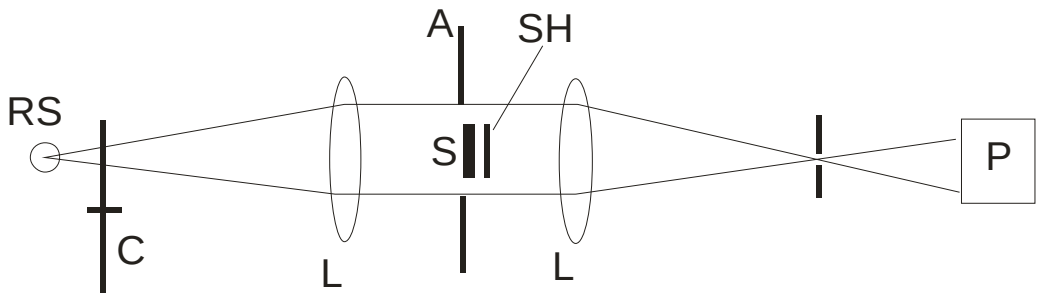

Figure 6: Sketch of shadowgraph-method, RS: radiation source, C: chopper, L: lens, A: aperture, S: sample, SH: shield.

Proper calibration is necessary to establish a relation between the decrease of pyrometer output and the increase of specimen volume. The self-radiation of the hot specimen is blocked by a shield. As the expanding specimen becomes bigger than the shield additional chopping of the light is performed to obtain offset correction.

M6

A crafty method to obtain high resolution in time without modern electronic devices is a streak camera. Thereby, a narrow image (through a slit) is moved over the detection area (e.g. with a rotating mirror) during measurement. Consequently, a certain distance on the detector corresponds to a certain distance in time.

At Los Alamos two types of imaging systems were used simultaneously: a streak camera with a laser as light source and a single image photography which delivers one picture of the entire sample at a defined moment in time (figure 7) [8].

The surrounding atmosphere was argon at elevated pressures [9].

CEA

At CEA in France the experimental setup is very similar to the one used already ealier in Los Alamos. Again a streak camera image was used to obtain radial expansion. A continuous NdYAG laser provides background lighting.

Additionally, such a setup can be used to measure the speed of sound. This was performed at Los Alamos and CEA. Thereby, the propagation of the impact of a laser pulse perpendicular to the backlighting laser through the liquid sample can be monitored on the streak record. From its traveling time and distance the speed of sound is calculated [10].

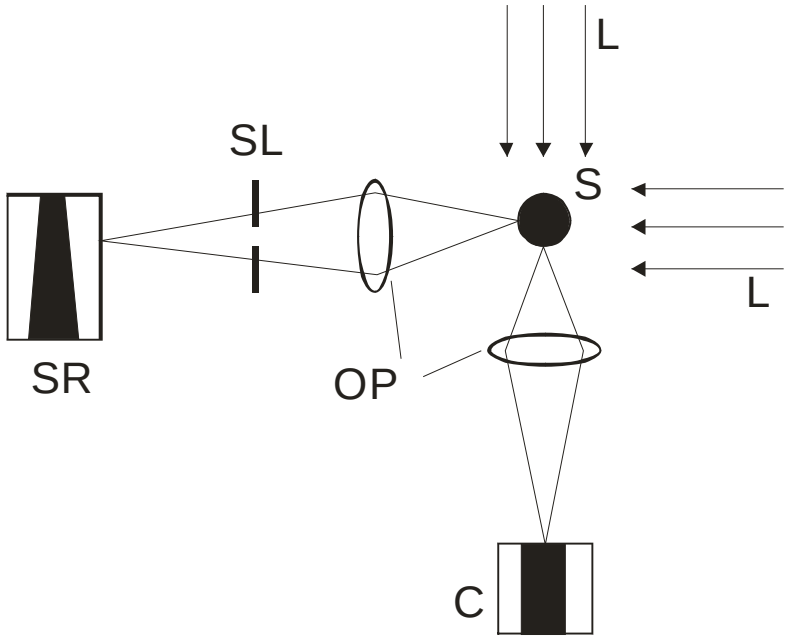

Figure 7: Optical imaging at Los Alamos and CEA, from right to left: optical axis of streak camera, from top to bottom: optical axis of single image recording system, SR: streak record, OP: optic devices, SL: slit,, C: conventional photography, S: sample, L: laser as backlighting.

KIEL

A very special feature was employed in the apparatus at Kiel, Germany: The backlighting is provided by a second wire explosion in air, which starts prior to the heating of the sample under investigation. The vessel is filled with water (figure 8). Picture detection is done with a single frame image converter camera (Marco Scientific. M7) with shutter speeds down to 3 ns, yielding one image per experiment. While shifting the point in time of exposure a sequence of pictures can be obtained which deliver radial expansion as a function of time [11]. In the beginning 80ies the experiment in Kiel was dismantled and several parts were transferred to TU Graz. This was the initiation of the subsecond thermophysics group at the Institute of Experimental Physics.

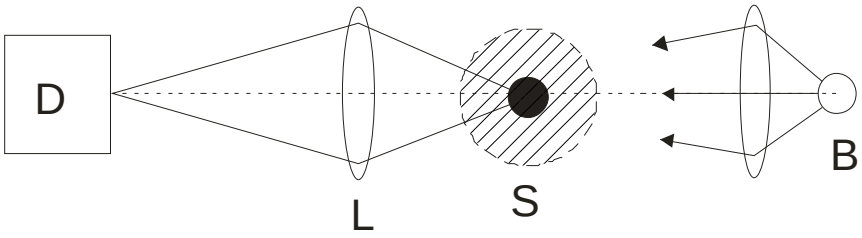

Figure 8: Experimental setup at Kiel, D: detector, L: lens, S: sample inside vessel which is filled with water, B: backlighting provided by wire explosion in air.

INP

In Greifswald, Germany, a streak camera (Hadland, Imacon 500) records the radial development of one cross section of the wire. The overall geometry and the occurrence of surface discharges are observed with a framing camera (Hadland, Imacon 468), which takes four images, each with an exposure time of 10 ns.
At the beginning of the heating process backlighting was necessary, for the later time the self-radiation of the wire was used to obtain radial expansion [12].

Mechanical expansion measurement

Different from all other methods are the experiments performed at the Russian Academie of Sciences [13]. There, the pulse-heated wire is contained in a capillary which has a slightly larger diameter than the wire. When the wire expands to a certain degree it fills the capillary completely. This can be identified in the records of current and voltage (due to a sudden increase of pressure). By varying the gap between capillary and wire thermal expansion can be obtained up into the liquid phase by this mechanical method. Beside that also optical methods are used [14].

STAGES OF DEVELOPMENT AT TU GRAZ

At the Subsecond Thermophysics Workgroup Graz many of the above mentioned optical imaging techniques have been performed for a certain period of time. They will be discussed in their historical order. Therefore it is adequate to call this chapter ‘stages of development’. Additionally, the surrounding atmosphere used varies from nitrogen or argon at ambient pressure to distilled water with pressures from 1 bar up to 5000 bar.

Shadowgraph method

The very first measurements were performed with a shadowgraph method. The expanding wire led to a shielding of the detector (Si-photodiode). Proper calibration allowed estimations of the wire diameter from the detector output traces on a memory oscilloscope (figure 9).

In a first step an experiment without backlighting is performed to obtain the self radiation of the sample (figure 9, bottom). The second step is to calibrate the detection system by applying defined shadowing (figure 9, top). Then a measurement can be recorded (figure 9, middle). The signal is corrected for offset and the self radiation subtracted. The remaining output is compared with the calibration traces to obtain thermal expansion of the expanding wire.

Kerrcell

When performing conventional photography (photoflash as backlighting, photographic film as detector) one needs a fast shutter to obtain a picture which is just a snapshot during the heating process. This is the purpose of the Kerrcell. It is an electro-optic device which delivers an exposure time of 30 ns (Optronics FOA 2-10) [15].

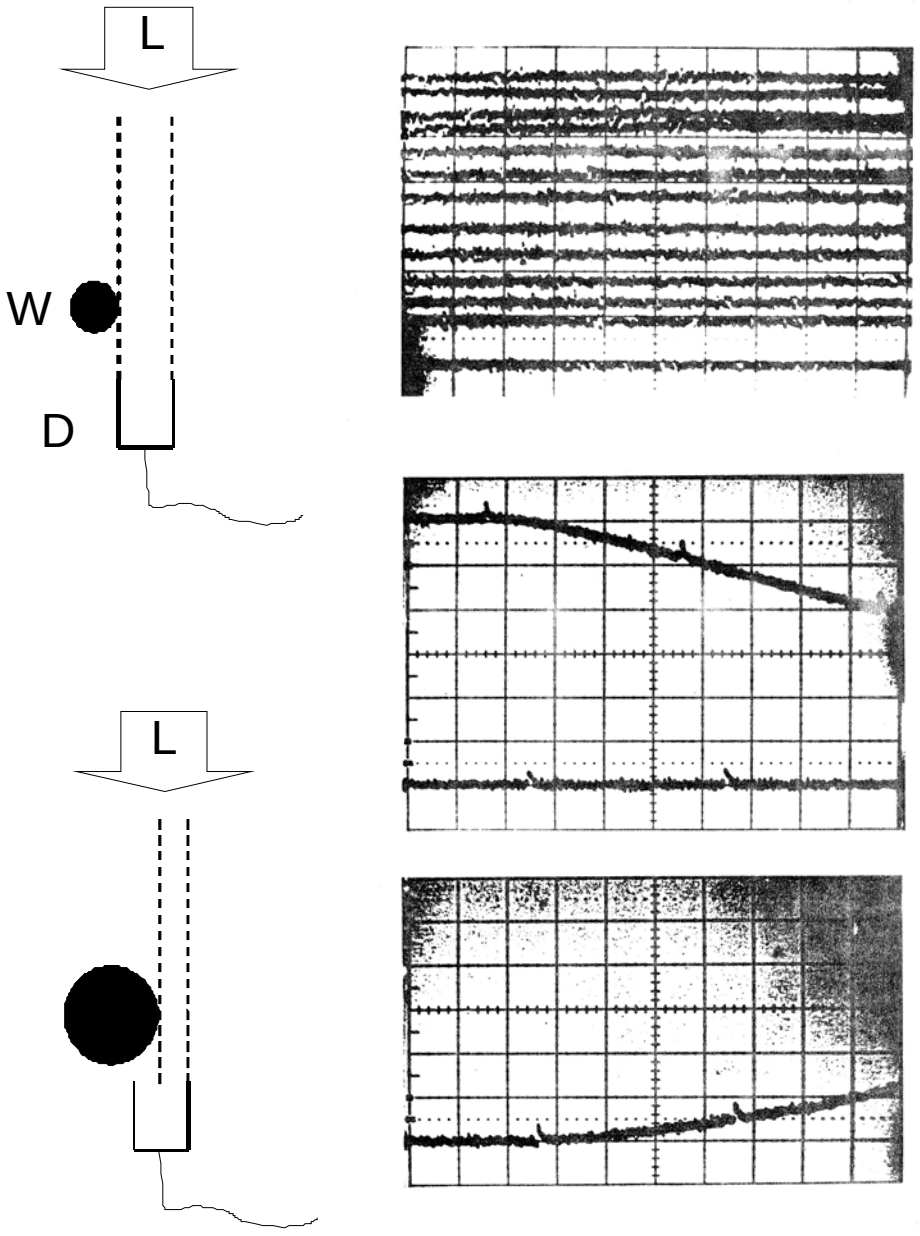

Figure 9: left: sketch of shadowgraph method (details omitted), W: cross section of wire, D: detector, L: light source, right: output-traces on oscilloscope, top: calibration, middle: decreasing signal and zero-line, bottom: self-radiation of hot sample.

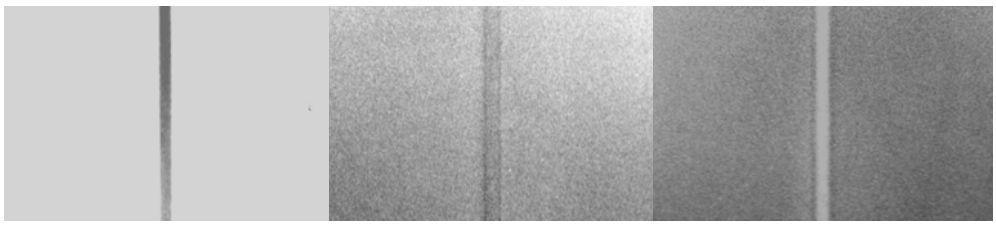

Figure 10: Kerr-cell pictures on conventional photographic film, left: early picture during the heating process, middle: wire expanded, right: visible self-radiation of the wire.

The photographic film (Ilford HP5) has to be prepared thoroughly: After adjusting the optical devices, the image of the sample is diffused by a Fresnel-lens. Now the film is ‘preexposed’ three times (3 x 30 ns) to achieve best sensitivity. After removing the Fresnel-lens the apparatus is ready for measurement.

The obtained pictures (one per experiment) are ordered according to time (figure 10). Thermal expansion is obtained by comparison of photographs of wire-diameters at different times. All the photographs have to have the same optical magnification.

Schlierenphotography

The German word ‘Schlieren’ could be translated with streak. Again the sample is focused onto a rectangular diaphragm. A timeresolved picture is detected on photographic film by means of a fast rotating mirror. Therefore the sample is seen as a vertical line in figure 11 in the middle of the picture, beginning on the top. This setup mainly was used to analyze the plasma discharge but not to monitor thermal expansion (figure 11). It was combined with a spectral analysis of the emitted light [16]. In figure 11 one can see two shock-waves: the first one from the top of the picture (see index 1) is associated with the melting transition of the wire, the second one (see index 2) is associated with the start of plasma discharge. It is noticeable that this ignition starts in the middle of the sample, which in exploding wire terminology is called ‘axial discharge’, as opposed to a ‘peripheral discharge’ [16].

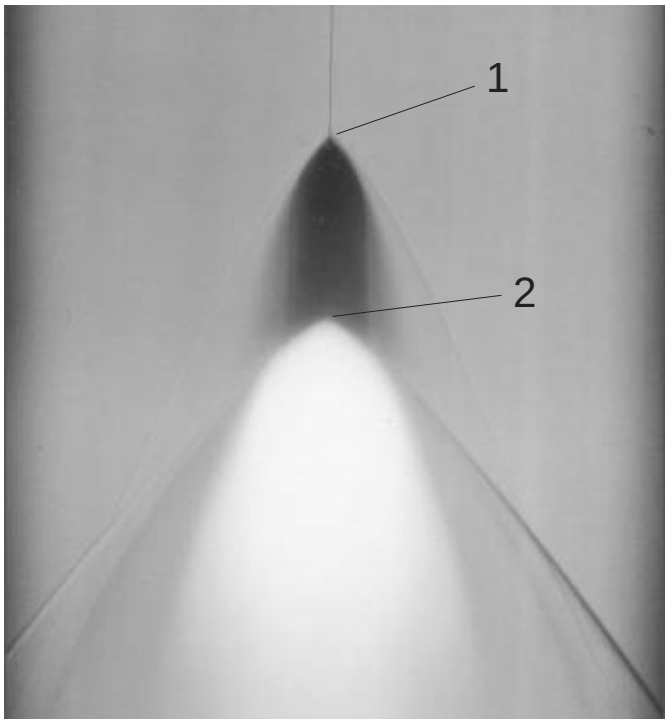

Figure 11: ‘Schlieren’-photography of exploding wire, time axis from left to right, shockwaves from the melting transition (1) and from the start of plasma-discharge (2) are visible (by courtesy of Prof. Neger, TU Graz).

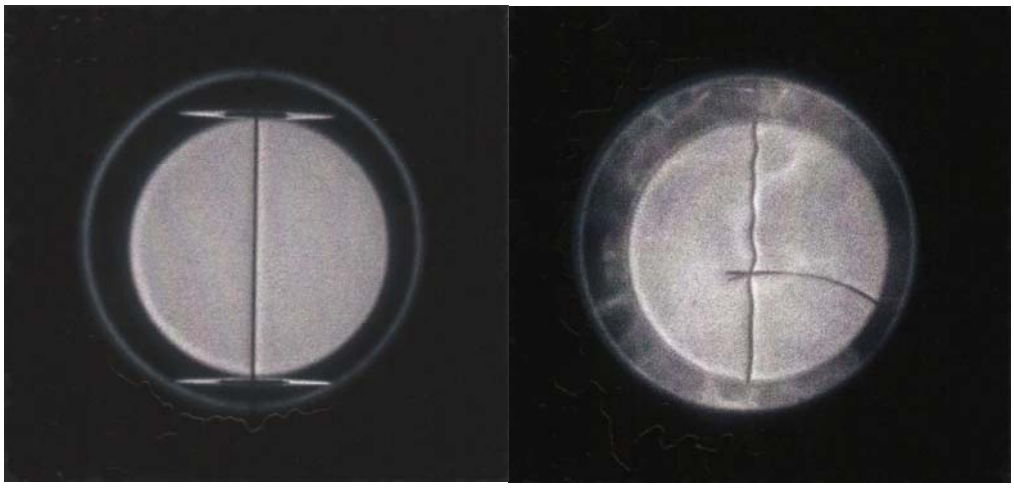

Figure 12: Dicam pictures, left: straight wire, right: extraordinary picture of wire bending because of too small heating rate (picture by Claus Cagran), wire is contacted by two knife-edges (one is visible) to measure voltage-drop.

Dicam pro

This camera is able to take two pictures in fast succession (figure 12). We use it to monitor if the overall geometry of the wire remains constant during the heating process (when the heating rate is too small, the wire will automatically bend). When talking about bending, one usually thinks of a sample bending like a bow. Figure 12 shows an extraordinary picture with an alternative outcome: a sinuous line. It is the result of two interacting forces: a sideward one because of longitudinal expansion and the inertia which is 'reacting' on every acceleration. Its dominant presence gives a unique feeling of the circumstances in these short-time-scale experiments.

CCD-camera

The setup we use nowadays for expansion measurements is a specially designed CCD-camera. It consists of a multi-channel-plate (MCP) which acts as amplifier and fast shutter and a one to one image onto a CCD-array. To get a fast succession of pictures the common way to get images (reading out the entire chip) was abandoned. Instead, only a small portion of the chip is open for exposure. The rest (which is the storage area) is masked.

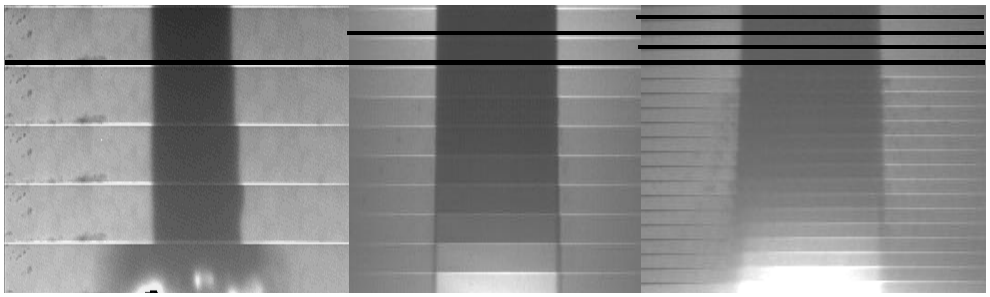

Figure 13: CCD-camera pictures, time axis from top to bottom, left: 32 lines shifted, middle: 16 lines shifted, right: 8 lines shifted.

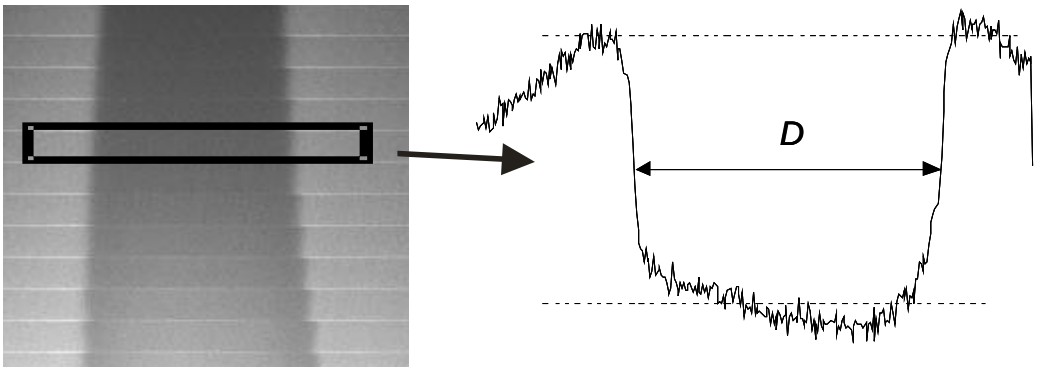

Figure 14: Diameter evaluation from intensity profile, left: 32-line-configuration picture, rectangle corresponds to one picture (exposure time 0.6 µs), right: intensity profile, D: diameter at FWHM.

Pictures are obtained by a fast succession of exposures (usually 0.6 µs) and of shifting this content into the storage area. The obtained images look like a streak with discrete steps (figure 13). The first camera system started with shifting 32 lines, then decreased to 16 and now is shifting 8 lines. This leads to a frame rate of 2.5 µs approximately [17].

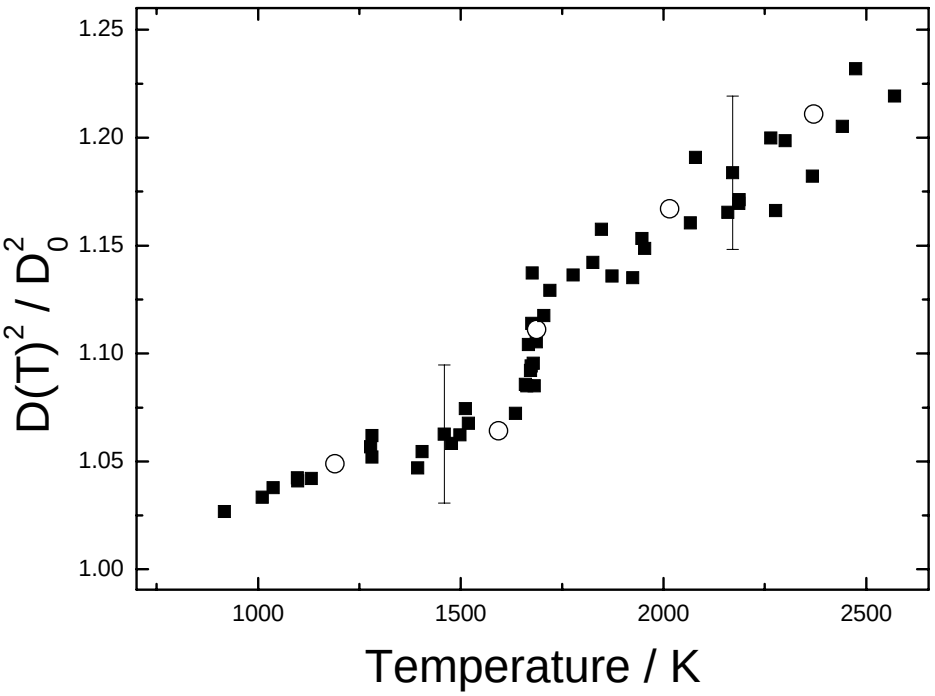

Figure 15: Typical result: thermal expansion (D^2/D_0^2) of Ni80Cr20 as a function of temperature (sum of several independent measurements), circles: data-points from one streak, uncertainty bars: 3% relative uncertainty with coverage factor k = 2.

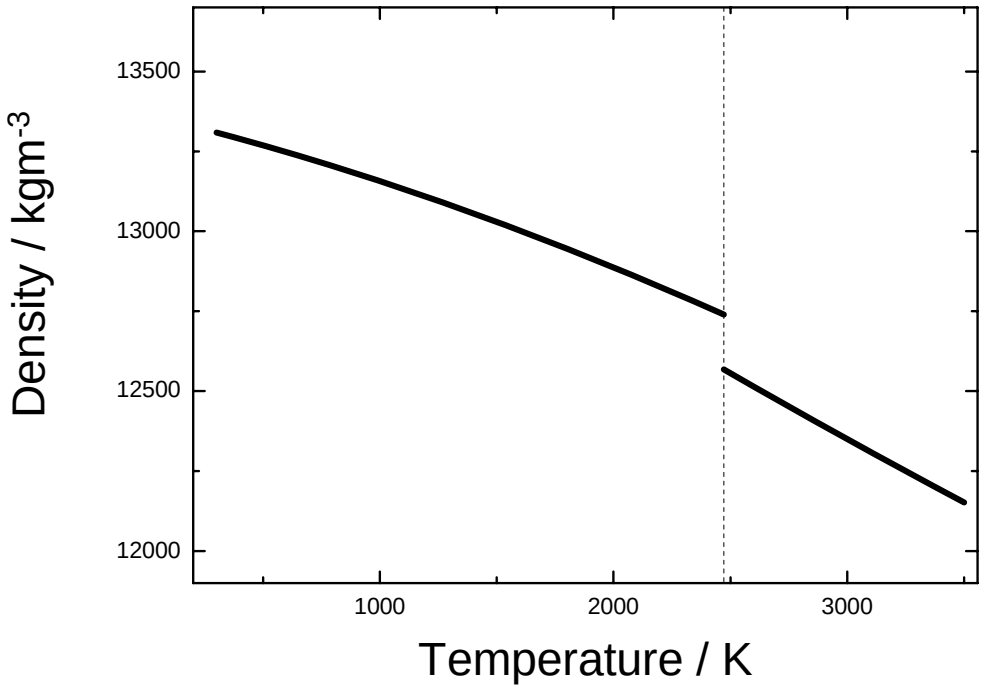

Figure 16: Typical result: density of hafnium as a function of temperature calculated from room temperature density and thermal volume expansion; dashed line: melting point.

The evaluation of the wire diameter is done by calculating full-width-half-maximum (FWHM) from the intensity profiles (figure 14). As a result we display the diameter at room temperature D_0 squared over diameter at temperature T squared (figure 15). The circles in figure 15 correspond to the pictures which are obtained in one experiment. To have a more 'continuous' trace the start of the camera-sequence is shifted in steps of 1 µs. Ten independent measurements were performed to obtain the graph in figure 15.

With the known room temperature density of the material under investigation and the volume expansion we obtain density as a function of temperature (figure 16).

UNCERTAINTY

The earlier measurements were performed, the less uniformity was present concerning uncertainty analysis. What was called estimation is now standardized in GUM [18].

Interferometers can be very precise. [4] states an uncertainty for linear thermal expansion of tantalum of 1% at 2000 K and <2% at 3000 K. [19] states an imprecision (standard deviation of individual point) of 0.5% and an uncertainty ('estimated total error') of 3% for thermal expansion α.

At TU Graz we performed an uncertainty analysis according to GUMs result category B (uncertainty propagation of each input quantity, mind figure Profil) and a statistic standard deviation approach as well, yielding approx 3% (for more details see [20]).

SUMMARY

Density as a function of temperature under pulse-heating conditions is obtained by measuring the expansion of the sample during the heating process. The different approaches of workgroups mentioned can be ‘explained’ by the need for high-speed detection. The commercial progression of electronic devices has been implemented through individual developments, including lasers for interferometry, electro-optic devices such as Kerr-cells, photodiodes, streak cameras, image converters and CCD-arrays. Exceptional methods are a wire explosion in air as light source and a ‘mechanical’ method of expansion estimation.

It is observable that the exchange of know-how is a driving force to install new applications. Unfortunately, it has to be mentioned that most of the pulse-heating apparatuses are currently not functional. As the one at TU Graz is still operating and as it includes many of the noted features it is legitimate to illustrate its ‘stages of development’ as paradigm and review.

Acknowledgement

This work was supported by the Austrian Space Applications Programme (ASAP) by the FFG, Vienna, Austria.

REFERENCES

[1] Industry survey by University of Ulm, http://www.uni-ulm.de/aktuelles/aktuelles_thema/aktuell0411/index.html, September 2009.

[2] Arblaster, J.W. 1989. “Densities of Osmium and Iridium”, *Platinum Metals Rev.*, 33(1): 14-16.

[3] Technical note by Anter corporation, November 2009 at http://www.anter.com/TN69.htm

[4] Miiller, A.P., A. Cezairliyan. 1982. “Transient Interferometric Technique for Measuring Thermal Expansion at High Temperatures: Thermal Expansion of Tantalum in the Range 1500 – 3200 K,” *Int. J. Thermophys.*, 3: 259-288.

[5] Reiter, Peter. 2001. “Entwicklung eines Millisekunden Pulsheizsystems zur Messung thermophysikalischer Daten von Metallen”, *PhD-Thesis*, Graz University of Technology.

[6] Righini, F., R.B. Roberts, A. Rosso, P.C. Cresto. 1986. “Thermal Expansion by a Pulse-Heating Method: Theory and Experimental Apparatus,” *High Temp. – High Pres.*, 18: 561-571.

[7] Cezairliyan, A. 1970. “A High Speed Method of Measuring Thermal Expansion of Electrical Conductors,” *The Rev. of Scient. Instr.*, 42(4): 540-541.

[8] Shaner, J.W., G.R. Gathers, C. Minichino. 1976. “A new apparatus for thermophysical measurements above 2500 K”, *High Temp. – High Pres.*, 8: 425-429.

[9] Hixson, R.S., M.A. Winkler, M.L. Hodgdon. 1990. “Sound speed and thermophysical properties of liquid iron and nickel”, *The American Physical Society, Review B*, 42(10): 6485-6491.
[10] Boivineau, M. 2001. “What’s new on plutonium up to 4000 K?,” *J. Nuclear Materials*, 297: 97-106.
[11] Seydel, U., W. Kitzel. 1979. “Thermal Volume Expansion of Liquid T, V, Mo, Pd, and W,” *J. Phys. F: Metal Phys.*, 9(9): 153-160.
[12] Kloss, A., T. Motzke, R. Grossjohann, H. Hess. 1996. “Electrical Conductivity of Tungsten Near Its Critical Point,” *The Am. Phys. Soc.: Phys. Rev. E*, 54(5): 5851-5854.
[13] Savvatimski, A.I. 1996. “Experiments on Expanded Liquid Metals at High Temperatures,” *Int. J. Thermophys.*, 17(2): 495-505.
[14] Korobenko, V.N., M.B. Agranat, S.I. Ashitkov, A.I. Savvatimskiy. 2002. “Zirconium and Iron Desities in a Wide Range of Liquid States”, *Int. J. Thermophys.*, 23(1): 307-318.
[15] Jäger, H., W. Neff, G. Pottlacher. 1992. “Improved Thermophysical Measurements on Solid and Liquid Tantalum”, *Int. J. Thermophys.*, 13(1): 83-93.
[16] Neger, T., 1981. “Relative Übergangswahrscheinlichkeiten und Starkeffektbreiten von Cu I - und Cu II - Linien”, *PhD-Thesis*, Graz University of Technology.
[17] Otter, C., 1994. “Bestimmung thermophysikalischer Daten von Zink im Überhitzungsbereich der flüssigen Phase bis zum kritischen Punkt”, *PhD-Thesis*, Graz University of Technology.
[18] GUM: *Guide to the Expression of Uncertainty in Measurement* 1993 (Geneva: ISO)
[19] Cezairliyan, A. 1997. “Advances in measurements of thermophysical properties by dynamic techniques”, *High Temp. – High Pres.*, 11: 9-27.
[20] Hüpf, T., C. Cagran, E. Kaschnitz, G. Pottlacher. 2009. “Thermophysical Properties of Ni80Cr20”, *Thermochimica Acta*, 494: 40-44.

7.2 Thermophysical properties of rhodium obtained by fast pulse-heating

T. Hüpf, C. Cagran, B. Wilthan, G. Pottlacher, *Thermophysical properties of rhodium obtained by fast pulse-heating*, Journal of Physics: Condensed Matter 21, 2009.

This paper is suitable as an introduction because it describes the standard procedure of investigations on pure metals.

Comments: The text was written by myself and I gave an oral presentation on this topic at the ECTP in Pau, France, in 2008. Dr. Claus Cagran was my coworker in the project this paper is assigned to, but due to his competence and experience he was more of a supervisor to me providing help whenever he was asked to do so. Dr. Boris Wilthan, at that time working at NIST, Washington, USA, had performed measurements on this element too. He gave me the data along with a lot of advice. Both were taken into consideration in the paper. Prof. Gernot Pottlacher was the supervisor of this project. He was involved in all decisions especially regarding final text revisions.

J. Phys.: Condens. Matter **21** (2009) 125701 (6pp) doi:10.1088/0953-8984/21/12/125701

Thermophysical properties of rhodium obtained by fast pulse-heating

T Hüpf, C Cagran, B Wilthan and G Pottlacher

Institut für Experimentalphysik, Technische Universität Graz, Petersgasse 16, A-8010 Graz, Austria

E-mail: pottlacher@tugraz.at

Received 11 November 2008, in final form 29 January 2009
Published 26 February 2009
Online at stacks.iop.org/JPhysCM/21/125701

Abstract

The so-called *platinum metals* are Ru, Rh, Pd, Os, Ir and Pt. Our workgroup has already published data on Pd, Ir and Pt. The present work will focus on measurements of the thermophysical properties of rhodium, which have been carried out recently. The scarce literature data available emphasize the need for new measurements.

Using a rapid pulse-heating technique, wire-shaped specimens are ohmic-heated by the passage of a large current pulse. This fast heating drives the sample from room temperature up into the liquid phase in typically 50 μs and thus prevents chemical reactions and gravitational distortions. Enthalpy, electrical resistivity and volume expansion can be obtained as a function of temperature. From these results, heat of fusion, heat capacity and change of density can be calculated as a function of temperature. A set of data of the mentioned quantities will be presented and the comparison to literature values will be discussed within this study. Additionally we will contrast the results for rhodium with the respective results for Pd, Ir and Pt.

The conformity of data published decades ago with our new measurements is fairly high. Rhodium does not show unexpected behaviour regarding the comparison to Pd, Ir and Pt.

1. Introduction

The workgroup of Subsecond Thermophysics at TU Graz has a long tradition in performing measurements on metals up to very high temperatures by means of a fast pulse-heating method. Heating rates of typically 10^8 K s^{-1} allow investigations of the liquid phase.

In the course of our collaboration project with the DLR in Cologne, Germany, we have started to recapitulate our measurements and work on those elements which still have not been investigated at our laboratory. One of them is rhodium (Greek, *rhodon*: rose). The colour is associated with many rhodium alloys [1] and its salts give a rosy solution [2]. Wollaston discovered rhodium in the years 1803–1804 in crude platinum ore [3].

The metal is silvery white and at red heat slowly changes in air to the sesquioxide. At higher temperatures it converts back to the element. Rhodium has a higher melting point and lower density than platinum. (T_m: 2236 K [4] density at RT: 12 423 kg m^{-3} [5]). Its major use is as an alloying agent to harden platinum and palladium. Such alloys are used for furnace windings, thermocouple elements, bushings for glass fibre production, electrodes for aircraft spark plugs and laboratory crucibles. It is useful as an electrical contact material as it has a low electrical resistance, a low and stable contact resistance and is highly resistant to corrosion. Plated rhodium, produced by electroplating of evaporation, is exceptionally hard and is used for optical instruments. It has a high reflectance and is hard and durable. Rhodium is also used for jewelry, for decoration and as a catalyst.

2. Experiment and data reduction

The measurements were performed during fast resistive pulse-heating experiments. Herein the electrical energy is stored in a capacitor bank of 500 μF which is then discharged over the sample. Its ohmic resistivity leads to a rapid self-heating. This process is so fast (10^8 K s^{-1}) that the sample maintains its initial position during the transition from room temperature up to the end of the liquid phase where the wire explosion takes place. The experimental duration of such an experiment is typically 50 μs. This has two advantages: on the one hand, the manipulation of the samples can be done without a container—and without any crucible reactions—and, on the

Table 1. Results of the present study given as least squares fits (where applicable) including the temperature range of applicability. (Fits are given in the form $a + bT + cT^2$, where a, b and c are the fitted parameters and T is the temperature.) H: enthalpy, ρ_{IG}: electrical resistivity with initial geometry, ρ: electrical resistivity considering thermal volume expansion, $V(T)\ V_0^{-1}$: volume expansion, λ: thermal conductivity, a: thermal diffusivity. Temperature range for λ and a see section 3.

	Solid state			Liquid state		
	a	b	T range (K)	a	b	T range (K)
H (kJ kg^{-1})	−486.154	0.523	$1950 < T < 2236$	−98.980	0.448	$2236 < T < 3150$
ρ_{IG} ($\mu\Omega$ m)	−0.126	3.085×10^{-4}	$1950 < T < 2236$	0.635	6.975×10^{-5}	$2236 < T < 3150$
ρ ($\mu\Omega$ m)	−0.202	3.617×10^{-4}	$1950 < T < 2236$	0.516	1.680×10^{-4}	$2236 < T < 3150$
$V(T)\ V_0^{-1}$ (1)	0.943	5.994×10^{-5}	$1400 < T < 2236$	0.893	1.055×10^{-4}	$2236 < T < 3500$
	a	b	c	a	b	c
λ (W m^{-1} K^{-1})	157.611	−0.046	7.255×10^{-6}	10.661	0.029	-2.932×10^{-6}
$a \times 10^{-5}$ (m^2 s^{-1})	2.349	-6.157×10^{-4}	1.046×10^{-7}	0.071	6.052×10^{-4}	-3.558×10^{-8}

other hand, chemical reactions like oxidation can be avoided. The surrounding atmosphere in our case was nitrogen with a pressure of 2.3 bar.

Our rhodium samples were purchased from Goodfellow Cambridge Limited. The wire was cut into pieces of about 50 mm length. The diameter was 0.509 mm and the purity 99.9% (lot no. RH005120/9).

In all the measurements *temperature* was determined with pyrometers working at either 1570 nm or 650 nm, selected by interference filters with a bandwidth of 84 nm and 37 nm, respectively. The melting plateau in the temperature records was used to assign the voltage output of the pyrometer to the freezing point of rhodium of 2236 K [4]. Then the temperature was calculated by Planck's radiation law using the assumption of a constant emissivity in the liquid phase. The contribution of a possible change of emissivity throughout the liquid phase is not considered in the uncertainty analysis. This enables the researcher to recalculate temperature and its uncertainty with any supplementary data on emissivity. In our experience the influence thereof on thermophysical data is small [6, 7].

Due to the electronics of the pyrometer used the temperature range is limited from 1000 to 3500 K.

Furthermore *current* was measured with an induction coil and the *voltage drop* along the wire was measured with two molybdenum foil knife-edges directly placed on the wire.

All these quantities were recorded as a function of experimental duration. The simultaneous temperature measurement allows a description of all quantities as a function of temperature, which will be presented subsequently.

During the investigations, two values for a series resistor were used (0.25 and 0.50 Ω), leading to two different heating rates and two different experimental durations (40 and 80 μs).

The two different heating rates have no influence on the *electrical* data obtained (specific enthalpy, specific electrical resistivity and quantities derived from them), but the experimental duration is one of the parameters which has to be optimized in matters of the *optical* measurements.

The *volume expansion* of the wire is measured optically with a CCD camera. Thereby the wire is backlit with a photoflash and a magnified picture is mapped on a multi-channel plate which acts as a fast shutter. This picture is then imaged one by one on the CCD. As the picture rate of this device is limited, a longer experimental duration means more pictures per experiment and consequently an increased accuracy. Therefore two different heating rates have been used.

A detailed description of the apparatus can be found in [8].

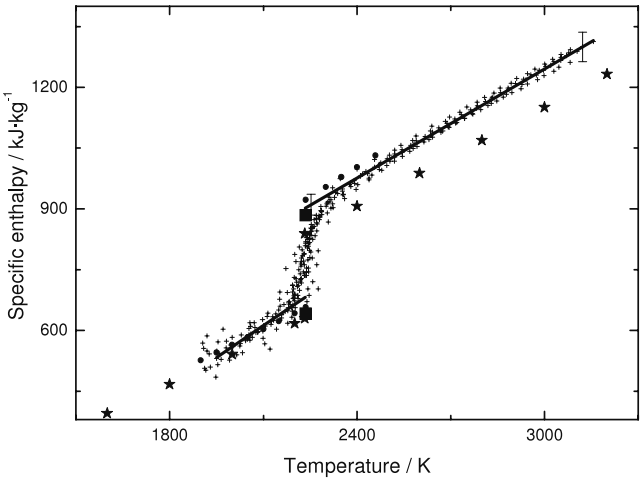

Figure 1. Specific enthalpy of rhodium versus temperature. Crosses: measurement data from the present study, solid lines: linear fits to the data points, filled squares: values of Martynyuk [9], stars: values of Jaeger [10], filled dots: values of Chekhovskoi [11].

3. Results

All the calculations were done with a melting temperature T_m of 2236 K [4] and a density at RT of 12 423 kg m^{-3} [5].

Specific enthalpy, H, given in kJ kg^{-1} is plotted in figure 1 as a function of temperature. It was calculated using the equation

$$H(t) = \frac{1}{m} \int I(t) U(t)\, \mathrm{d}t \qquad (1)$$

where m is the mass of the sample, I: current and U: voltage drop. The polynomials for the linear fits are given in table 1. Numerical results are given in table 2. Values at the melting transition: H_s (T_m) 683.3 kJ kg^{-1} and H_l (T_m) 902.7 kJ kg^{-1}, which deliver a heat of fusion ΔH of 219.4 kJ kg^{-1}.

In figure 1 the enthalpy values at the beginning and at the end of the melting transition measured by Martynyuk are also depicted (ΔH: 242.9 kJ kg^{-1}) [9], as well as literature values

Table 2. Numerical results of the present study. H: enthalpy, ρ_{IG}: electrical resistivity with initial geometry, ρ: electrical resistivity considering thermal volume expansion, $V(T)\ V_0^{-1}$: volume expansion, λ: thermal conductivity, a: thermal diffusivity.

T (K)	H (kJ kg^{-1})	ρ_{IG} ($\mu\Omega$ m)	ρ ($\mu\Omega$ m)	$V(T)V_0^{-1}$ (1)	λ (W m^{-1} K^{-1})	$a \times 10^{-5}$ (m^2 s^{-1})
1950	533.7	0.476	0.503	1.060	95.5	1.55
2000	559.8	0.491	0.521	1.063	94.6	1.54
2050	586.0	0.506	0.539	1.066	93.8	1.53
2100	612.1	0.522	0.558	1.069	93.0	1.51
2150	638.3	0.537	0.576	1.072	92.2	1.51
2200	664.4	0.553	0.594	1.075	91.5	1.50
2236s	683.3	0.564	0.607	1.077	91.0	1.50
2236l	902.7	0.791	0.892	1.129	60.8	1.25
2250	909.0	0.792	0.894	1.130	61.1	1.25
2300	931.4	0.795	0.902	1.136	61.9	1.27
2400	976.2	0.802	0.919	1.146	63.4	1.32
2500	1021.0	0.809	0.936	1.157	64.8	1.36
2600	1065.8	0.816	0.953	1.167	66.2	1.40
2700	1110.6	0.823	0.970	1.178	67.6	1.45
2800	1155.4	0.830	0.986	1.188	68.9	1.49
2900	1200.2	0.837	1.003	1.199	70.1	1.53
3000	1245.0	0.844	1.020	1.210	71.3	1.57
3100	1289.8	0.851	1.037	1.220	72.4	1.61
3150	1312.2	0.855	1.045	1.225	72.9	1.62

of Jaeger [10] and Chekhovskoi [11], which yield a ΔH of 208.9 kJ kg^{-1} and 265.2 kJ kg^{-1}, respectively. Paradis [12] reports a heat of fusion of 223.5 kJ kg^{-1}.

The enthalpy records, as shown in figure 1, show very good agreement in the solid state and at the melting transition. In the liquid phase our values are in between the results of Chekhovskoi [11] and Jaeger [10] (regardless of the fact that Jaeger's values for rhodium are only guiding values in this temperature range). Our heat of fusion outcome matches the result of Paradis best.

This work obtains for *isobaric heat capacity* c_p in the solid state right before melting $c_{p,s}$ 523 J kg^{-1} K^{-1} and in the liquid phase $c_{p,l}$ 448 J kg^{-1} K^{-1} (calculated from the slope of the $H(T)$ curves). Paradis [12] reports 312.9 J kg^{-1} K^{-1} at T_m (liquid phase). The values of Jaeger [10] are 384.0 J kg^{-1} K^{-1} (solid) and 406.7 J kg^{-1} K^{-1} (liquid).

The isobaric heat capacity shows large variations: our value for the solid state is higher than the recommended value of Touloukian [13]. In the liquid state the correlation to Touloukian is better. Values from Paradis [12] for the supercooled liquid are lower.

Figure 2 plots the results for *specific electrical resistivity*, ρ, as a function of temperature. It was calculated using the equation

$$\rho_{IG}(t) = \frac{U(t)\pi r_0^2}{I(t)l} \tag{2}$$

where r_0 is the sample radius at room temperature and l the length. The average of different measurements was fitted with linear least squares fits. This gives the results for electrical resistivity with initial geometry (index IG). But the volume expansion has to be taken into account to obtain ρ.

According to equation (3), this is achieved via a multiplication of two independent measurements: electrical resistivity (with initial geometry) and thermal expansion (square of the relative change of diameter). As the temperature in this kind of dynamic experiments is a measured quantity—not an 'applied' one—the experimental points from independent measurements happen to be located at slightly different temperatures. Consequently a multiplication of quantities can only be performed on the basis of fits or interpolations.

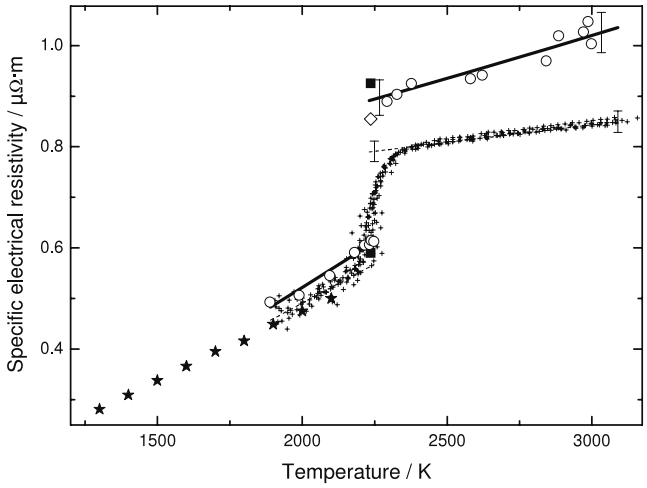

Figure 2. Specific electrical resistivity of rhodium versus temperature. Crosses: measurement data from the present study, dashed lines: linear fits to the specific electrical resistivity with initial geometry (IG), open circles: values including volume expansion, solid lines: linear fits to specific electrical resistivity including volume expansion, filled squares: values of Martynyuk [9], open diamonds: values of Savvatimskii [14], filled stars: values of Filippow [15].

To preserve the characteristic distribution of points, which can be used to estimate the quality of the measurement, we combined the fit for electrical resistivity at initial geometry with the data points of thermal expansion. In this way it is also possible to follow the uncertainty contribution of thermal expansion as the basic value for derived quantities. It can be seen in figures 2 and 4 that its influence, though it seems to be

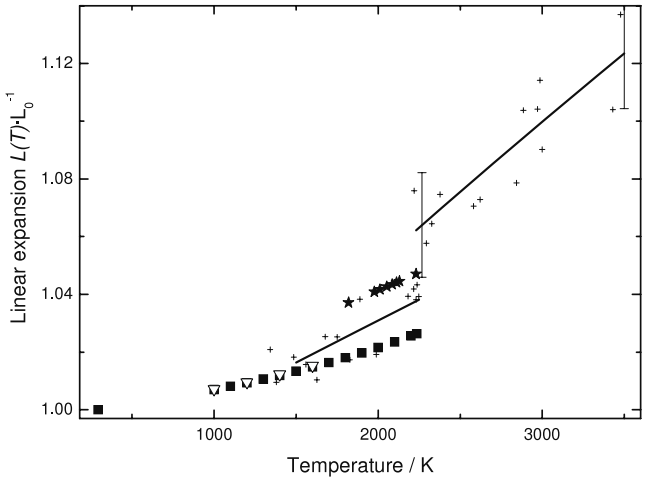

Figure 3. Linear thermal expansion of rhodium versus temperature. Crosses: measurement data from the present study, solid lines: linear fits to the data points, full stars: values of Paradis [12] for supercooled liquid Rh, full squares: values of Arblaster [5], open down triangle: recommended values of Touloukian [13].

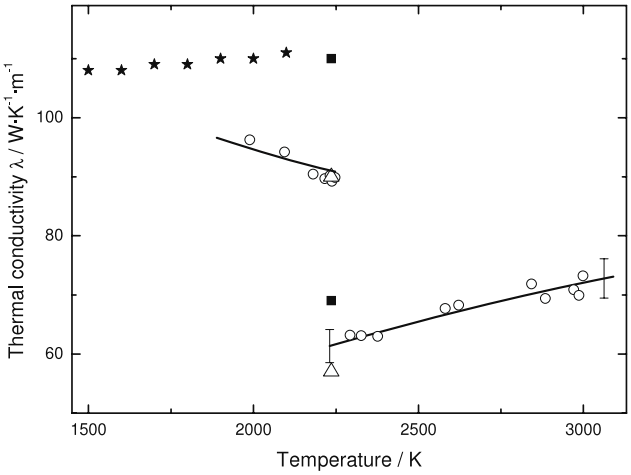

Figure 4. Thermal conductivity of rhodium versus temperature. Open circles: data from the present study, solid lines: fits to the data points, solid squares: value from the NPL report [16], open triangle: values of Vlasov [17], full stars: values of Filippow [15].

a highly scattered measurement with high uncertainty, on the derived quantities is small (GUM vocabulary: its index in the uncertainty budget is small).

The relevant polynomials for ρ are given in table 1. Numerical results are given in table 2. The values at the melting transition are for resistivity with initial geometry: $\rho_{IG,s}$ 0.564 $\mu\Omega$ m and $\rho_{IG,l}$ 0.791 $\mu\Omega$ m and with the volume expansion included: ρ_s 0.607 $\mu\Omega$ m and ρ_l 0.892 $\mu\Omega$ m (an increase of $\Delta\rho_{IG}$ 0.227 $\mu\Omega$ m and $\Delta\rho$ 0.285 $\mu\Omega$ m is observed).

The plot also shows the results of Martynyuk [9] and Savvatimskii [14], who have measured ρ_s: 0.590 $\mu\Omega$ m, ρ_l: 0.925 $\mu\Omega$ m ($\Delta\rho$: 0.335 $\mu\Omega$ m) and ρ_s: 0.610 $\mu\Omega$ m, ρ_l: 0.855 $\mu\Omega$ m ($\Delta\rho$: 0.245 $\mu\Omega$ m), respectively. Filippow [15] did measurements in the solid phase.

The results (see figure 2) do almost coincide when approaching the melting temperature. Our value for ρ_l lies in between the results of Martynyuk [9] and Savvatimskii [14].

To be able to account for the *volume expansion* of the wire it is necessary to know the cross section at a given temperature. This is done via a measurement of the diameter during the heating process as described in section 2. For the comparison to literature values we chose the quantity $L(T)L_0^{-1}$ (length of the sample at temperature T divided by the length at room temperature L_0) and converted each result accordingly (the length in our case is the diameter, shown in figure 3).

Notice that for the calculation of ρ out of ρ_{IG} (see equation (3)) the square of this quantity has to be used. The (squared) data points were fitted linearly, separated into the solid and liquid phase.

These polynomials are given in table 1. Numerical results are given in table 2:

$$\rho(t) = \rho_{IG}(t)\frac{L(t)^2}{L_0^2} \tag{3}$$

where L_0^2 is the diameter at room temperature squared. A conversion from density to $L(T)/L_0$ (which was necessary for the levitation measurements of Paradis [12]) was done using 12 423 kg m^{-3} as the value for density at 293.15 K [5]. Figure 3 compares our measurements to values for the supercooled liquid [12] and to recommended values of Touloukian [13] and values of Arblaster [5] for the solid phase.

In the low temperature regime scattering is high and values of Arblaster [5] and recommended values of Touloukian [13] are lower than the values of the present work. At the onset of melting the situation is the same for the comparison to the measurements of Paradis [12]. The values are still within the error bars: however, he has measured supercooled liquid rhodium.

Thermal conductivity, λ, may be estimated by using the Wiedemann–Franz law:

$$\lambda(T) = \frac{LT}{\rho(T)}. \tag{4}$$

With a Lorentz number $L = 2.45 \times 10^{-8}$ V^2 K^{-2} a value of 91.0 W K^{-1} m^{-1} is obtained at the onset of melting and 60.8 W K^{-1} m^{-1} at the end of melting.

Figure 4 only depicts thermal conductivity, because the behaviour of *thermal diffusivity*, a, is very similar:

$$a(T) = \frac{\lambda(T)}{c_P(T)d(T)} \tag{5}$$

where c_p is the isobaric heat capacity and $d(T)$ the density. The relevant polynomials are given in table 1. Numerical results are given in table 2. At the onset of melting the value for a_s is 1.50×10^{-5} m^2 s^{-1} with a decrease to a_l: 1.25×10^{-5} m^2 s^{-1} at the end of melting. It has to be considered that, due to the fact that we obtain just one constant value for the isobaric heat capacity c_p in the solid phase, the relevance of a is limited to the region near the melting point. The thermal diffusivity of the liquid state does not suffer from this situation.

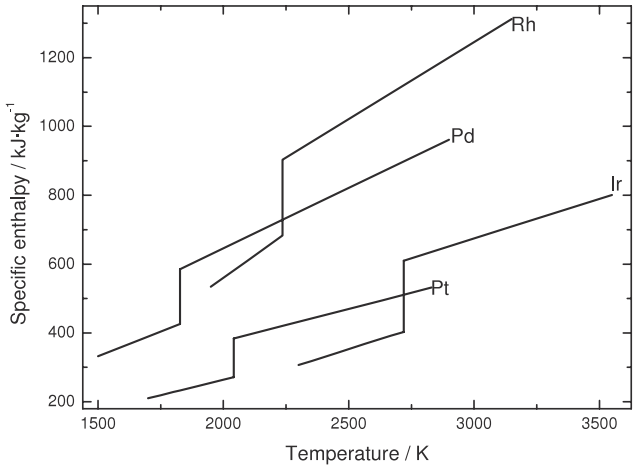

Figure 5. Specific enthalpy of Rh, Pd, Pt and Ir as a function of temperature. Rh: values from the present work. Pd, Pt and Ir: values from [18–20].

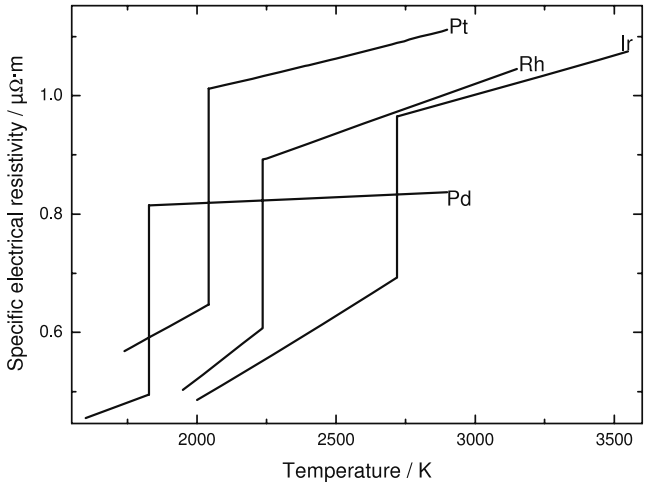

Figure 6. Specific electrical resistivity of Rh, Pd, Pt and Ir as a function of temperature. Rh: values from the present work. Pd, Pt and Ir: values from [18–20].

The plot shows the values at melting from the NPL report [16] (λ_s 110 W K^{-1} m^{-1} and λ_l 69 W K^{-1} m^{-1}) and values from Vlasov [17] (λ_s 90 W K^{-1} m^{-1} and λ_l 57 W K^{-1} m^{-1}). Filippow [15] reports values for the solid state. Surprisingly the solid state values of Filippow [15] do precisely aim at NPL's value for λ_s whereas our measurements hit the value of Vlasov. At the beginning of the liquid state our results lie in between the NPL and Vlasov.

4. Discussion

The available data of thermodynamic properties of rhodium, especially in the liquid state, are very scarce. However, the existing data give quite a good match to the values reported in this work (see section 3).

To set rhodium in context with the other platinum metals, we have compared the results to our already published data on Pd, Ir and Pt [18–20].

Figure 5 shows *specific enthalpies* as a function of temperature. The conformity of the results is high. It can be observed (as described for the first time in [21]) that Rh is linked with Pd and Pt with Ir. This can be explained by their position in the periodic table of the elements (fifth period and sixth period elements).

Figure 6 shows *specific electrical resistivities* as a function of temperature. The graph shows that Pd differs from Pt, Rh and Ir, which are very similar regarding their electrical resistivities. The trace for Pd is almost constant throughout the liquid phase, whereas the traces for Pt, Rh and Ir are increasing with similar slopes and the absolute resistivity value of Pd is significantly lower. A possible reason for the diverse behaviour of Pd is the electron configuration: it is the only element (out of Rh, Pd, Ir and Pt) with an empty outermost s orbital (Rh: [Kr]4d^{8}5s^1, Pd: [Kr]4d^{10}5s^0, Ir: [Xe]4f^{14}5d^{7}6s^2, Pt: [Xe]4f^{14}5d^{9}6s^1).

In summary, the infrequent appearance of rhodium in the literature is more likely to be a result of its seldom occurrence on Earth than of its peculiar thermodynamic properties, because the latter are not peculiar but 'good-natured' for they are very similar to those of the other platinum metals.

5. Uncertainties

In accordance with the guide to the expression of uncertainty in measurement (GUM 1999 [22]), uncertainties reported here are expanded relative uncertainties with a coverage factor of $k = 2$. For the calculated thermophysical properties the following uncertainties have been obtained (liquid phase): enthalpy, H_l: 2.8%, volume expansion, $V(T)V_0^{-1}$: 3%, electrical resistivity with initial geometry, ρ_{IG}: 2.5%, electrical resistivity including volume expansion, ρ: 3.9%, thermal conductivity, λ: 4.6% and thermal diffusivity, a: 8.8%.

6. Conclusion

The present study describes measurements on rhodium. It delivers a complete dataset of thermophysical properties, as literature values for liquid rhodium are sparse.

However, the accordance with these literature values—some published decades ago—is high (see figures 1–4).

In figures 5 and 6 rhodium is set in context with the other platinum metals Pd, Ir and Pt, measured under the same experimental conditions. Again, consistency is high. Rhodium shows no unexpected behaviour.

Acknowledgments

The project *Electrical Resistivity Measurement of High Temperature Metallic Melts* is sponsored by the Austrian Space Applications Programme (ASAP) of the FFG.

References

[1] 2008 http://periodic.lanl.gov/elements/45.html
[2] 2008 http://environmentalchemistry.com/yogi/periodic/Rh.html#Overview

[3] Lide D R 2004 *CRC Handbook of Chemistry and Physics* 85th edn (Boca Raton, FL: CRC Press)
[4] Bedford R E, Bonnier G, Maas H and Pavese F 1996 *Metrologia* **33** 133–54
[5] Arblaster J W 1997 *Platinum Met. Rev.* **41** 184–9
[6] Pottlacher G and Seifter A 2002 *Int. J. Thermophys.* **23** 1281–91
[7] Cagran C, Brunner C, Seifter A and Pottlacher G 2002 *High Temp.–High Pressures* **34** 669–79
[8] Kaschnitz E, Pottlacher G and Jäger H 1992 *Int. J. Thermophys.* **13** 699–710
[9] Martynyuk M M and Tsapkov V I 1974 *Fiz. Met. Metalloved.* **37** 49–54
[10] Jaeger F M and Rosenbohm E 1932 *Rec. Trav. Chim.* **51** 1–46 in Hultgren R, Desai P D, Hawkins D T, Gleiser M, Kelley K K and Wagman D D 1973 *Selected Values of the Thermodynamic Properties of the Elements* (Metals Park, OH: American Society for Metals)
[11] Chekhovskoi V Y and Kats S A 1981 *High Temp.—High Pressures* **13** 611–6
[12] Paradis P-F, Ishikawa T and Yoda S 2003 *Int. J. Thermophys.* **24** 1121–36
[13] Touloukian Y S 1970 *Thermophysical Properties of Matter* vol 12 *Thermal Expansion* (New York: IFI/Plenum)
[14] Savvatimskii A I 1973 *Teplofiz. Vys. Temp.* **11** 1182–7 Savvatimskii A I 1974 *High Temp.* **11** 1057–62 (Engl. Transl.)
[15] Filippow L P 1973 *Int. J. Heat Mass Transfer* **16** 865–85
[16] Mills K C, Monaghan B J and Keene B J 1997 *Thermal Conductivities of Molten Metals* (Teddington: National Physical Laboratory)
[17] Vlasov B V, Taluts S G, Zinovyev V E and Korenovskii N A 1992 *Phys. Met. Metallogr.* **74** 371–7
[18] Cagran C and Pottlacher G 2006 *Platinum Met. Rev.* **50** 140–5
[19] Cagran C and Pottlacher G 2007 *Int. J. Thermophys.* **28** 697–710
[20] Wilthan B, Cagran C, Brunner C and Pottlacher G 2004 *Thermochim. Acta* **415** 47–54
[21] Hüpf T, Cagran C, Lohöfer G and Pottlacher G 2008 *High Temp.—High Pressures* **37** 239–46
[22] *Guide to the Expression of Uncertainty in Measurement* 1993 (Geneva: ISO)

7.3 Selected thermophysical properties of Hf-3%Zr from 2200 K to 3500 K obtained by a fast pulse-heating technique

C. Cagran, T. Hüpf, B. Wilthan, G. Pottlacher, *Selected thermophysical properties of Hf-3%Zr from 2200 K to 3500 K obtained by a fast pulse-heating technique*, High Temperatures-High Pressures, 37, 2008.

The section 'estimation of uncertainties' gives additional insight into the details of the uncertainty analysis according to GUM.

Comments: The paper was written by Dr. Cagran. Measurements were performed by myself. Dr. Wilthan did the uncertainty analyses. Prof. Pottlacher was the supervisor of this work.

High Temperatures-High Pressures, Vol. 37, pp. 205–219
Reprints available directly from the publisher
Photocopying permitted by license only

Selected thermophysical properties of Hf-3%Zr from 2200 K to 3500 K obtained by a fast pulse-heating technique†

CLAUS CAGRAN, THOMAS HÜPF, BORIS WILTHAN AND GERNOT POTTLACHER*

Institute of Experimental Physics, Graz University of Technology, Petersgasse 16, 8010 Graz, Austria

Received: November 21, 2007. Revised: May 20, 2008. In Final Form: July 4, 2008.

Wire shaped samples of commercially available Hf-3%Zr are resistively volume heated as part of a fast capacitor discharge circuit. Time resolved electrical measurements with sub-μs resolution include the current through and the voltage drop across the specimen. Surface radiance from the sample (to measure the temperature) is detected by pyrometers and the thermal expansion of the sample is monitored by means of a custom-made fast CCD-camera. Based on these measured quantities, temperature-dependent thermophysical properties such as enthalpy, isobaric heat capacity, electrical resistivity and thermal expansion are deduced. Further properties such as thermal conductivity/diffusivity are calculated using the Wiedemann-Franz law. This work presents a set of thermophysical data for Hf-3%Zr in the solid and the liquid states, an uncertainty statement, as well as a comparison of the obtained results to existing literature values.

Keywords: Enthalpy, Hf-3%Zr, liquid metal, pulse-heating, resistivity, thermal conductivity, thermal diffusivity, thermophysical properties.

1 INTRODUCTION

Hafnium is a silvery gray, ductile, tetravalent transition metal that is corrosion resistant and chemically very similar to zirconium. Although Mendeleev had

*Corresponding author: E-mail: pottlacher@tugraz.at

†Paper presented at the 8th International Workshop on Subsecond Thermophysics, September 26–28, 2007, Moscow, Russia.

already implicitly predicted a heavier analog of titanium and zirconium in 1869, it took until 1923 before hafnium was finally discovered. The physical properties of hafnium are markedly affected by remaining zirconium contents acting as impurities, as these two metals are among the most difficult ones to separate. There are only two notable physical differences between hafnium and zirconium: their densities (hafnium is more than twice as dense as zirconium, 13310 $kg \cdot m^{-3}$ versus 6520 $kg \cdot m^{-3}$ [1]) and their neutron capture cross-sections (the one of Hf being 600 times that of zirconium). Chemically, both elements are extremely similar.

The main use for hafnium is in control rods for nuclear reactors due to its good ability to absorb thermal neutrons, its excellent mechanical properties and exceptional corrosion-resistance. Although its importance in nuclear technology, not many published data on thermophysical properties of hafnium can be found. Either because the data are still being considered confidential or because pure hafnium is very hard to separate and mostly contaminated by zirconium and/or oxygen; both can drastically influence the measured properties.

A recent study by Milošević and Maglić [2] presents data of hafnium in the solid α and β phases up to temperatures of 2400 K, the authors also compile the available literature data for comparison reasons. However, no results at melting or in the liquid state are given. This is the scope of this manuscript which presents recently obtained results for thermophysical properties of Hf-3%Zr (the purest commercially available form of hafnium) from about 2200 K (solid β phase) up to 3500 K in the liquid state.

2 EXPERIMENTAL SETUP

Pulse-heating consists of passing a large current pulse (with the energy being pre-stored in a suitable device) through the material under investigation which is part (mounted in series) of a discharge circuit. Due to its (ohmic) resistivity the sample can be self-heated from room temperature (RT) up to the boiling point within several microseconds.

The pulse-heating apparatus at TU Graz consists of a capacitor bank (500 μF) acting as an energy storage, a variable shunt resistor (0.25 or 0.5 Ω) to shape the current pulse, two ignitrons to accurately switch the experiment, and an experimental (so-called discharge) chamber with several windows for optical diagnostics. To maintain a controlled ambient atmosphere (or to create a pressure of about 1.5 bar) the chamber may be purged either with argon or nitrogen; the latter was used for the hafnium measurements.

Typical charging voltages of 5.5 kV have been used for hafnium experiments resulting in an average experimental duration of about 35 μs to span the entire temperature range from RT to the boiling point (corresponding to a heating rate of about 1.4×10^8 K/s). During this short period the sample is not affected by gravitational distortions and maintains its cylindrical geometry

throughout the entire experiment (even in the liquid state) until the temperature reaches the boiling point where the material will be disintegrated by the sudden volume increase. The setup at TU Graz has been extensively described in earlier publications [3,4].

2.1 Directly measured properties

Several quantities are directly accessible during such a pulse-heating experiment which is mainly limited by the short duration. These obtained quantities can be grouped in electrical and optical properties: the first group contains current through and voltages at a portion of the sample, the second group consists of properties such as thermal radiance (to measure the temperature) and thermal expansion. All other properties have to be deduced from these electrical and optical signals and are not directly accessible. It has to be stated that all electrical and optical properties are recorded as a function of experimental duration (time) first and are scaled to temperatures later once the radiance signal is evaluated.

2.1.1 Electrical quantities – current and voltage drop

The current through the system (and thus the sample) is measured at the feed line by a current monitor (induction coil with included integration element) purchased from Pearson Electronics. To obtain the voltage drop along a metered section of the sample, two knife-edge contacts are placed on the sample's surface. Both voltages are measured with respect to a known potential (ground); after deduction of the inductive contribution to the signals, both voltages are subtracted yielding the ohmic contribution of the voltage drop. All electrical signals are fed through voltage dividers to optimize the signals for the data acquisition system placed inside a shielded room to protect the electronics from the occurring electro-magnetic gradients.

2.1.2 Temperature

According to the international temperature scale of 1990 (ITS-90 [5]) temperatures above the freezing point of silver (1234.93 K) are to be measured by means of radiation thermometry deploying Planck's law. Such radiometric devices (radiometers or pyrometers) detect the spectral radiance emitted from a sample surface which later, in a second step, can be converted to temperature units given the system is calibrated with well-known fixed-points. In the case of hafnium, a pyrometer with f/2.4 (with the f-number of an optical system being the focal length divided by the aperture diameter, yielding a quantitative measure of lens speed) optics operating at a center-wavelength of 649.7 nm (and a FWHM of 37 nm) was utilized; the fixed-point used to calibrate the system (during each experiment separately) was the well-known melting temperature of hafnium at 2471 K [6]. Melting can be seen as a plateau (constant voltage signal of the radiometer) in the recorded radiance-versus-time traces.

The drawback of this in situ approach is the neglect of any possible changes in emissivity in the liquid state (as reported in [7]) as all temperatures are

calculated by ratioing the voltage output of the radiometer to the voltage at the melting transition, thus assuming a constant emissivity (the not explicitly known value at melting). Although this approach may not result in metrologic temperature accuracy, it is proven to be sufficiently exact for the determination of thermophysical properties and their practical applications.

2.1.3 Expansion

The sample's thermal expansion during pulse-heating measurements is optically monitored by a fast CCD-Camera system. Basically, a magnified shadowgraph image (small section of the entire sample, magnification of about 5) of the specimen is focused onto a channel-plate/CCD-chip combination. The former sets the pre-defined exposure time, the latter records and stores the images. For being able to record several images of the expanding sample during one single experiment the CCD-chip (Thomson TH 7863A, 384 pixels in horizontal direction and 576 lines) is masked and thus separated into an exposure- and a storage-zone. 16 out of total 576 lines can be exposed, the rest (35×16 lines) is used as storage. As shifting of exposed lines is several times faster than reading the entire chip's content, these first exposed 16 lines are shifted to the storage area and then automatically cleared. This procedure can be repeated (36 times) until the storage is full; it is slowly read-out after the experiment. The camera system has been improved recently and images the radial expansion of the sample about every 5 μs (slightly depending on the actual exposure time).

This technique can solely measure radial expansion, as only a small fraction of the respective specimen is monitored. However, experiments with another camera capable of imaging the entire (but only once during one experiment) specimen have proven that the samples only expand radially and do not show any longitudinal expansion above a sufficiently high heating rate (to be determined in pre-experiments) in the used set-up at TU Graz. At our understanding, this finding does not negate the existence of longitudinal expansion, but merely states that it can't be observed at the short time–scale due to effects like inertia of mass at extremely high heating rates. Therefore the actual sample volume only increases in radial direction (in 2 dimensions) which is measured by the camera system and used for combining electrical resistivity with thermal expansion.

A closer description of the original design is given in [8], a more detailed explanation of the modification will be published in the next future.

2.2 The specimen material – Hf-3%Zr

The specimen material under test for this study was a commercially available Hafnium-3%Zirconium wire (0.5 mm in diameter) purchased from Alfa Aesar, Germany (LOT# A06N08); the manufacturer states the purity to be 99.95% hafnium in the metal basis excluding the Zr content of nominally 3%.

The oxygen is estimated to be 300–400 ppm. Hafnium (at standard pressure) has a hcp structure and undergoes an $\alpha - \beta$ phase transition (into

the bcc structure) at about 2030 K [9]. It shows for zirconium [10] that the phase transition temperature depends on the oxygen content (transition temperature increases with higher oxygen concentration), which is expected for hafnium too.

For pulse-heating experiments, pieces of about 65–70 mm in total length are cut and the actual diameter was measured to be 0.509–0.510 mm (variations are due to non-uniform diameter) by means of a laser-micrometer (Keyence LS-7010, measurement accuracy $\pm 0.5\,\mu$m, repeatability $\pm 0.06\,\mu$m). A maximum of 3 measurement values have been taken for each test specimen and the respective diameter was used for data evaluation.

3 DATA EVALUATION AND RESULTS

3.1 Temperature

As mentioned earlier, a melting temperature value of $T_m = 2471\,\mathrm{K}$ [6] was used as a reference fixed-point to scale the pyrometer output in situ in temperature units omitting possible changes in emissivity.

3.2 Thermal expansion

The ratio of the cross section of the wire at temperature T to the cross section at room temperature equals the ratio of the diameters, D, squared. The fit to the measurements for the solid phase is:

$$D^2(T)/D_0^2 = 0.996 + 1.288 \times 10^{-5} T + 2.766 \times 10^{-9} T^2, \quad 1500\,\mathrm{K} < T < 2471\,\mathrm{K} \qquad (1)$$

and for the liquid phase:

$$D^2(T)/D_0^2 = 0.972 + 3.623 \times 10^{-5} T. \quad 2471\,\mathrm{K} < T < 3500\,\mathrm{K} \qquad (2)$$

3.3 Electrical resistivity

The specific electrical resistivity with initial geometry ρ_{IG} (not considering any thermal expansion) can be calculated via the equation:

$$\rho_{\mathrm{IG}}(T) = \frac{U(T) \cdot \pi \cdot r^2}{I(T) \cdot l}. \qquad (3)$$

With U being the voltage drop across the sample, I is the current trough the setup, r is the initial radius of the wire at RT, and l is the length between the two knive edge contacts. It should be noted here that ρ_{IG} is not only an intermediary result during calculation of electrical resistivity ρ (which incorporates thermal expansion) but is used to calculate thermal diffusivity (which itself is also independent on thermal expansion).

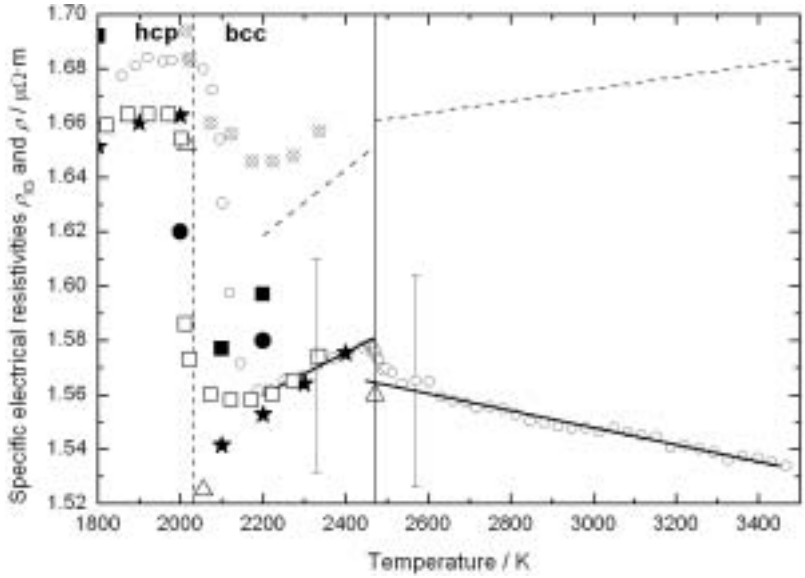

FIGURE 1
Specific electrical resistivity of Hf-3%Zr as a function of temperature. Open circles with respective solid lines: results for ρ_{IG} of this work with linear least-squares fits; dashed line: results for ρ (including thermal expansion) of this work; vertical solid line: melting temperature (2471 K), vertical dashed line: temperature of phase transition (2030 K). Literature data: open squares: values of [2] (sample 2); slashed diamonds: [2] (sample 1), full squares: values of [11], open triangles [12], full stars [13], full circles [9].

Specific electrical resistivity ρ as a function of temperature is obtained by multiplying ρ_{IG} with the thermal diameter expansion. Results for Hf-3%Zr are shown in Figure 1 and according values are listed in Table 1. At melting $\rho_{IG}(T_m)$ decreases from 1.581 μΩ·m to 1.564 μΩ·m, resulting in a total change of $\Delta\rho_{IG}(T_m)$ of 0.017 μΩ·m. The linear fit to the solid β-phase data is:

$$\rho_{IG}(T) = 1.389 + 7.753 \times 10^{-5} T, \quad 2200\,\mathrm{K} < T < 2471\,\mathrm{K} \qquad (4)$$

and for the liquid phase:

$$\rho_{IG}(T) = 1.642 - 3.142 \times 10^{-5} T. \quad 2471\,\mathrm{K} < T < 3500\,\mathrm{K} \qquad (5)$$

Including the radial expansion the equations change to:

$$\rho(T) = 1.352 + 1.212 \times 10^{-4} T, \quad 2200\,\mathrm{K} < T < 2471\,\mathrm{K} \qquad (6)$$

and:

$$\rho(T) = 1.606 + 2.219 \times 10^{-5} T. \quad 2471\,\mathrm{K} < T < 3500\,\mathrm{K} \qquad (7)$$

At melting $\rho(T_m)$ increases from 1.651 μΩ·m to 1.661 μΩ·m, resulting in a $\Delta\rho(T_m)$ of 0.01 μΩ·m.

T/K	$\rho_{IG}/\mu\Omega\cdot$m	$\rho/\mu\Omega\cdot$m	H/kJ·kg^{-1}	$D^2(T)/D_0^2$
1858*	1.677*	1.727*	260.5*	1.029
1907*	1.682*	1.734*	278.7*	1.030
1958*	1.683*	1.736*	290.5*	1.032
1999*	1.685*	1.740*	303.6*	1.033
2056*	1.680*	1.737*	316.9*	1.034
2096*	1.654*	1.712*	332.3*	1.035
2146*	1.572*	1.629*	358.5*	1.036
2200	1.560	1.619	372.8	1.038
2250	1.563	1.625	384.5	1.039
2300	1.567	1.631	396.2	1.040
2350	1.571	1.637	407.9	1.042
2400	1.575	1.643	419.6	1.043
2450	1.579	1.649	431.3	1.044
2471 (s)	1.581	1.651	436.2	1.045
2471 (l)	1.564	1.661	518.5	1.062
2500	1.563	1.661	526.0	1.063
2550	1.562	1.663	539.0	1.064
2600	1.560	1.664	551.9	1.066
2700	1.557	1.666	577.8	1.070
2800	1.554	1.668	603.7	1.073
2900	1.551	1.670	629.6	1.077
3000	1.548	1.673	655.5	1.081
3100	1.545	1.675	681.4	1.084
3200	1.541	1.677	707.3	1.088
3300	1.538	1.679	733.2	1.092
3400	1.535	1.681	759.1	1.095
3500	1.532	1.684	785.0	1.099

TABLE 1
Summary of measurement results. T: temperature, ρ_{IG}: specific resistivity related to initial geometry, ρ: specific resistivity (including thermal expansion), H: specific enthalpy, $D^2(T)/D_0^2$: thermal radial expansion. Note: Values marked with an asterisk are directly measured values and cannot be calculated from the respective least-squares fits.

3.4 Enthalpy and isobaric heat capacity

Specific enthalpy H is calculated from the electrical signals (current and voltage drop) by equation:

$$H(t) - H(293\,\mathrm{K}) = \frac{1}{m}\int I(t)\cdot U(t)\mathrm{d}t. \tag{8}$$

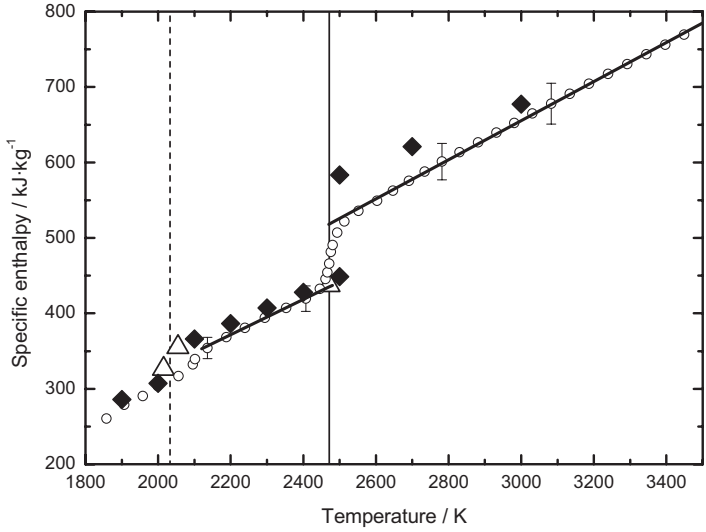

FIGURE 2
Specific enthalpy of Hf-3%Zr as a function of temperature. Open circles and respective solid lines: results from this work with linear least-squares fits; solid vertical line: melting temperature (2471 K); vertical dashed line: phase transition (2030 K); open triangles: literature values of [12]; full diamonds: [14].

Herein m represents the mass of the sample obtained from geometry and density at RT (13310 kg·m^{-3} [1]). Results for H are shown in Figure 2 and listed in Table 1. Linear fits representing the measurement results are

$$H_s(T) = -142.0 + 0.234T, \quad 2200\,\mathrm{K} < T < 2471\,\mathrm{K} \tag{9}$$

for the solid phase and

$$H_l(T) = -121.5 + 0.259T, \quad 2471\,\mathrm{K} < T < 3500\,\mathrm{K} \tag{10}$$

for the liquid state. At melting, $H_s(T_m) = 436.2\,\mathrm{kJ{\cdot}kg^{-1}}$ and $H_l(T_m) = 518.5\,\mathrm{kJ{\cdot}kg^{-1}}$; thus a heat of fusion of $\Delta H = 82.3\,\mathrm{kJ{\cdot}kg^{-1}}$ is obtained.

Isobaric heat capacity c_p can be obtained from the slope of the enthalpy versus temperature function. $c_{p,s} = 234\,\mathrm{J{\cdot}kg^{-1}{\cdot}K^{-1}}$ and $c_{p,l} = 259\,\mathrm{J{\cdot}kg^{-1}{\cdot}K^{-1}}$ are obtained for the solid and liquid states, respectively. Heat capacity in the solid state should be regarded as a rough estimate and is limited to a narrow temperature range before the onset of melting.

3.5 Thermal conductivity and thermal diffusivity

The thermal conductivity λ is calculated using the Wiedemann-Franz law, which states a proportionality of the thermal conductivity/electrical conductivity ratio to the temperature of a metal based on the free electron model

(Drude model). Thus, λ may be obtained by:

$$\lambda(T) = \frac{L \cdot T}{\rho(T)}, \tag{11}$$

with L being the Lorenz-number ($L = 2.45 \times 10^{-8}\,\mathrm{V^2{\cdot}K^{-2}}$ [15]). Linear fit results for λ (in $\mathrm{W{\cdot}K^{-1}{\cdot}m^{-1}}$) to our measurements are given by

$$\lambda(T) = 6.042 + 1.239 \times 10^{-2} T, \quad 2200\,\mathrm{K} < T < 2471\,\mathrm{K} \tag{12}$$

for the solid, and by

$$\lambda(T) = 1.691 + 1.408 \times 10^{-2} T, \quad 2471\,\mathrm{K} < T < 3500\,\mathrm{K} \tag{13}$$

for the liquid state. Thermal diffusivity a is calculated via a modified Wiedemann-Franz equation, as this time only ρ_{IG} and the density at RT are needed as input data:

$$a(T) = \frac{L \cdot T}{\rho_{\mathrm{IG}} \cdot c_p \cdot d}. \tag{14}$$

The linear fits for the solid and liquid states of a (in $10^{-5}\,\mathrm{m^2{\cdot}s^{-1}}$) are:

$$a_s(T) = 0.135 + 4.433 \times 10^{-4} T \quad 2200\,\mathrm{K} < T < 2471\,\mathrm{K} \tag{15}$$

$$a_l(T) = -0.081 + 4.866 \times 10^{-4} T \quad 2471\,\mathrm{K} < T < 3500\,\mathrm{K} \tag{16}$$

Results for thermal conductivity and thermal diffusivity are graphically presented in Figures 3 and 4, respectively.

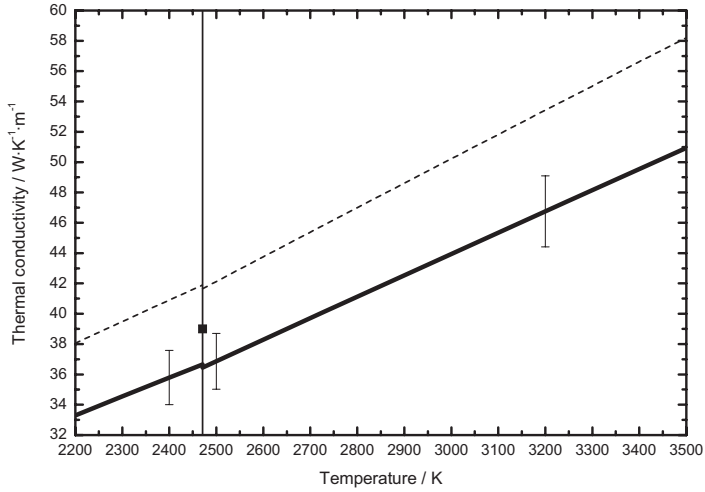

FIGURE 3
Thermal conductivity of Hf-3%Zr as a function of temperature. Solid line: results of this work using $L = 2.45 \times 10^{-8}\,\mathrm{V^2/K^2}$; dashed line: values calculated with $L = 2.8 \times 10^{-8}\,\mathrm{V^2/K^2}$ from [2]; full square: value as reported by [16]; solid vertical line: melting temperature (2471 K).

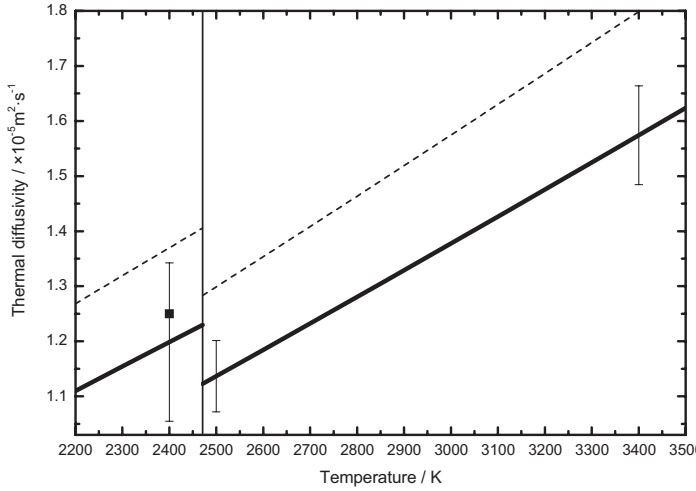

FIGURE 4
Thermal diffusivity of Hf-3%Zr as a function of temperature. Solid line: results from this work using $L = 2.45 \times 10^{-8}\,\mathrm{V^2/K^2}$; dashed line: values calculated with $L = 2.8 \times 10^{-8}\,\mathrm{V^2/K^2}$ from [2]; full square: value of [9]; solid vertical line: melting temperature (2471 K).

4 DISCUSSION

One of the main measurement challenges with Hf-3%Zr was the difference in pyrometric radiance signals at melting for independent trials, which showed an unusual wide scatter. Heavy abrasion of the samples' surface helped a little but signal differences still remained and prevented the usage of pre-calibrated pyrometers. Therefore, the in situ calibration approach (as described in the 'Temperature' section) was chosen to still obtain accurate and reproducible temperatures. Possible explanations for this seldom behaviour of a pure metal might be found in the contamination with 3%Zr (which effectively makes Hf-3%Zr more an alloy than a pure metal) or the unknown exact content of oxygen and a possible subsequent oxidation.

For the interpretation of all measurement results in the solid state it has to be kept in mind, that hafnium (at standard pressure) has a hcp structure and undergoes an $\alpha - \beta$ phase transition (into the bcc structure) at about 2030 K [9] which shows up in the measured voltage signals and the subsequently deduced properties.

4.1 Thermal expansion and density

As described earlier within this manuscript, no (or at least very little) longitudinal expansion of the samples under fast pulse-heating conditions was observed. Possible explanations for such a behaviour might be (some of

them circulate in the literature): (i) The samples compensate the missing longitudinal component by more radial expansion, or (ii) the samples do not expand in longitudinal direction but are compressed by the expansion instead.

When comparing the solid state thermal expansion data from this work with the values collected in [17] the former hypothesis is proven wrong, as a very good agreement between the radial expansion from the measurements and two-dimensional expansion listed in [17] (calculated from the linear expansion coefficient assuming equal expansion in all 3 dimensions) is found. However, this still does not prove the latter hypotheses right, which moreover is not the aim of the recent work.

Assuming the monitored expansion only represents the two-dimensional expansion in radial direction and mathematically accounting for the missing longitudinal expansion component (half of the expansion in 2 dimensions) enables the calculation of density at melting, by dividing the samples' density at RT by its actual volume. Following this approach for Hf-3%Zr we obtain for the density at melting (in the liquid state) $d(T_m) = 12170\,\mathrm{kg{\cdot}m^{-3}}$. As a comparison, Peterson *et al.* [18] report a value of $d(T_m) = 11100\,\mathrm{kg{\cdot}m^{-3}}$ and Allen [19] reports $d(T_m) = 12000\,\mathrm{kg{\cdot}m^{-3}}$, which is in good agreement considering possible compositional variations of the sample material and the stated uncertainty of our measurements.

4.2 Electrical resistivity

The electrical resistivity ρ_{IG} was measured in the temperature range from 1850 K to 3500 K and shows a characteristic drop in the solid at the $\alpha-\beta$ phase transition but is smooth elsewhere. Metals usually show a resistivity increase during melting, which was found to be very small for the investigated Hf-3%Zr and ρ_{IG} even decreases in the subsequent liquid state; the latter effect only appears for measurements not considering the actual geometry of the sample due to thermal expansion. Inclusion of thermal expansion data restores the anticipated resistivity increase with temperature.

In comparison to literature (see Figure 1) the values show some scatter in the range from 1850 K to 2400 K, especially at the phase transition, which might once again be due to the contamination with Zr and/or oxygen. The values from this present study lie in-between the data reported in earlier investigations by Peletskii [11], Martynyuk [12], or Filippow [20]. After the phase transition, which occurred at some 70 K higher temperatures than reported by [9] (usually due to superheating at these high pulse-heating rates), the reported resistivities of this study are in good agreement with literature [13]. The change in resistivity at the phase transition was very reproducible and yields $\Delta\rho_{\alpha-\beta} = 0.124\,\mu\Omega{\cdot}\mathrm{m}$.

Results for resistivity including thermal expansion of the sample ρ are also plotted in Figure 1 but unfortunately no comparison values have been found in the literature.

4.3 Enthalpy and isobaric heat capacity

In accordance with resistivity, values for specific enthalpy are also available in the range from 1850 K to 3450 K. The $\alpha - \beta$ phase transition appears as well (but less dominant) in the enthalpy trace (see Figure 2) and is also shifted some 70 K, which is in fact little surprising, as electrical resistivity and enthalpy are deduced from the same electrical signals, namely U and I. Keeping this shift in mind, the values in the solid state do agree very well with Martynyuk [12] and Hultgren [14], but are in the liquid state lower than the values reported in [14].

As already stated earlier, the isobaric heat capacity in the solid state changes with temperature and is therefore only compared at temperatures close to melting: Milošević and Maglić [2] report $c_p = 197.0\,\mathrm{J{\cdot}kg^{-1}{\cdot}K^{-1}}$ at 2336 K, the value of Hultgren [14] at 2400 K is $206.3\,\mathrm{J{\cdot}kg^{-1}{\cdot}K^{-1}}$, Cezairliyan and McClure [13] report $c_p = 209\,\mathrm{J{\cdot}kg^{-1}{\cdot}K^{-1}}$ at 2400 K; all these values are lower than the $234\,\mathrm{J{\cdot}kg^{-1}{\cdot}K^{-1}}$ obtained in the present work. For the liquid state we obtain a constant $c_p = 259\,\mathrm{J{\cdot}kg^{-1}{\cdot}K^{-1}}$.

4.4 Thermal conductivity and thermal diffusivity

Literature data for thermal conductivity and diffusivity are sparse. For liquid hafnium no literature data could be found. Mills *et al.* [16] suggest a value of $39.0\,\mathrm{W{\cdot}K^{-1}{\cdot}m^{-1}}$ for thermal conductivity at T_m. This work yields a value of $36.7\,\mathrm{W{\cdot}K^{-1}{\cdot}m^{-1}}$ by using the Lorenz number $L = 2.45 \times 10^{-8}\,\mathrm{V^2/K^2}$. Although L is not always a constant and may vary for different materials [21] as well as with temperature (e.g. [22]), a good agreement for calculated properties containing L (thermal conductivity/diffusivity) with other techniques has been observed for metals [23] and even alloys [24]. However, if a more accurate value for L would become evident, the results could easily be adjusted.

The thermal diffusivity at 2400 K reported by Zinovyev [9] is $1.25 \times 10^{-5}\,\mathrm{m^2{\cdot}s^{-1}}$, which is slightly higher than our value of $1.20 \times 10^{-5}\,\mathrm{m^2{\cdot}s^{-1}}$. Thermal conductivities and diffusivities reported by [2] only reach 1600 K. Filippow [20] also reported thermal conductivity/diffusivity data which are again limited to the solid state below the $\alpha - \beta$ phase transition ($T \leq 2100$ K) and thus omitted from this comparison.

As stated earlier, different values for the Lorenz number lead subsequently to different results when deducing thermal conductivity/diffusivity. Extrapolating the values reported in [2] for the range from 800 K to 1400 K would lead to $L = 2.8 \times 10^{-8}\,\mathrm{V^2/K^2}$ and thus to higher conductivities/diffusivities. In order to show the influence of altering the Lorenz number a second set of calculated data (using the before-mentioned extrapolated value of [2]) is also shown in the graphs for thermal conductivity/diffusivity.

Since even this number is not proven, the authors decided to hold on to the theoretical value leaving possible recalculations (upon discovery of a more accurate Lorenz number) to the reader. As with alloys [21], it might even become necessary for a better characterization of Hf-3%Zr to consider and add a lattice component to the Lorenz number (see [19], for example).

5 ESTIMATION OF UNCERTAINTIES

An elaborate uncertainty analysis of all possible measurements using the entire pulse-heating setup at TU Graz according to GUM [25] has been performed as part of [26]. A detailed description well exceeds the scope of this report and has therefore to be omitted; however, the final deduced maximum uncertainties (with a coverage factor of $k = 2$) for each property will be stated instead.

As a demonstration, the results of the temperature-dependent uncertainty analysis for enthalpy are shown in Figures 5a and 5b. The former figure shows the evolution of the expanded ($k = 2$) and relative expanded uncertainties with temperature and, as can be seen from Figure 5b, temperature itself is the predominant contribution to overall uncertainty. The weaker signal-to-noise ratio of the pyrometer at lower temperatures leads to a larger uncertainty but becomes less important at higher temperatures. The uncertainty in the vicinity of the melting transition tends to infinity which is mathematically caused by the temperature-derivative. This results in an extreme sensitivity to the actual uncertainty in temperature although the uncertainty in the temperature signal is constant at melting. Figure 5b gives an overview which part of the setup contributes the most to the overall uncertainty in enthalpy. As can be seen, the uncertainty in temperature and the accuracy of the diameter are the biggest contributors.

Accordingly, the uncertainty analysis specifically for Hf-3%Zr yields the following uncertainties: temperature T : 4%; enthalpy H_s : 4% and H_l : 3.2%;

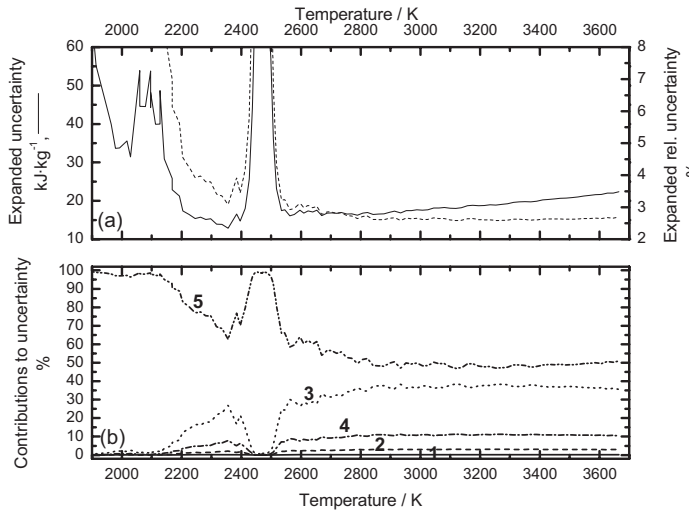

FIGURE 5
(a) Expanded ($k = 2$) uncertainty estimation for enthalpy of Hf-3%Zr according to GUM. (b) Individual contributions to the total uncertainty. 1: A/D interface board in the PC (U, I measurements); 2: length of wire; 3: diameter of wire; 4: density at RT; 5: temperature.

heat of fusion ΔH: 8%; specific heat capacity $c_{p,s}$: 11.2%, $c_{p,l}$: 3.4%; thermal expansion D^2/D_0^2: 3%; density at melting $d(T_m)$: 5%; specific electrical resistivity (with initial geometry) ρ_{IG}: 2.5%; electrical resistivity (including expansion) ρ: 3.9%; thermal conductivity λ: 5%; thermal diffusivity a_s: 12% and a_l: 5.7%.

Uncertainties are also given for thermal conductivity/diffusivity, the two properties that include the Lorenz number. As stated in the respective sections, the value of L might differ (even if the actual value is currently unknown) from the one used within this work and therefore the Lorenz number was treated as an exact number (like a constant) throughout the uncertainty estimation. Following this approach, stated uncertainties for thermal conductivity/diffusivity only include all experimental inherent and do not account for any variations of L.

6 CONCLUSION

Pulse-heating measurements have been performed at TU Graz to obtain thermophysical properties for Hf-3%Zr, as this is the purest form of hafnium commercially available. Among the presented data, results for enthalpy, electrical resistivity and thermal expansion are given in the temperature range from about 1850 K in the solid state to about 3500 K in the liquid state. Whenever possible, the recent results have been compared to sparse literature data for hafnium.

Additionally, the isobaric heat capacity is calculated from the temperature-dependent enthalpy traces and the Wiedemann-Franz law is deployed to estimate thermal conductivity/diffusivity using two constant Lorenz numbers. The results are presented in graphs and in tabular form as well as expressed in terms of least-squares fits. An uncertainty analysis according to GUM has been performed and respective expanded uncertainties are stated for each property including a more detailed demonstration of the uncertainty results for enthalpy.

ACKNOWLEDGEMENTS

This work has been supported by the Austrian *FWF*, "*Fonds zur Foerderung der wissenschaftlichen Forschung*", Grant P-15055 and by the *Austrian Space Applications Programme (ASAP)* under project "High temperature metallic melts".

REFERENCES

[1] Lide D. R (Ed.), *CRC Handbook of Chemistry and Physics*, 85th edition, CRC Press, Boca Raton, 2004.

[2] Milošević N. D. and Maglić K. D. *Int. J. Thermophys.* **27**(2) (2006), 530–553.

[3] Kaschnitz E., Pottlacher G. and Jäger H. *Int. J. Thermophys.* **13**(4) (1992), 699–710.

[4] Cagran C., Wilthan B., Pottlacher G., Roebuck B., Wickins M. and Harding R. A., *Intermetallics* **11** (2003), 1327–1334.

[5] Preston-Thomas H. *Metrologia* **27** (1990), 3–10 and 107.

[6] Cezairliyan A. and McClure J. *J. Res. Nat. Bur. Stand.* **80A**(4) (1976), 659–662.

[7] Cagran C., Brunner C., Seifter A. and Pottlacher G. *High Temp.-High Press.* **34** (2002), 669–679.

[8] Nussbaumer G. *Master thesis (Diplomarbeit)*, Technische Universität Graz, Austria, Graz, 1993.

[9] Zinovyev V. *Metals at High Temperatures—Standard Handbook of Properties.* Hemisphere Publishing Corporation, New York, 1990.

[10] Webster R. T. *Specific Metals and Alloys: Zirconium and Hafnium, ASM Handbook, Volume 2, Properties and Selection: Nonferrous Alloys and Special-Purpose Materials*, ASM International, 1990, in ASM Handbook on CD-ROM: ASM International and The Dialog Corporation, 1999.

[11] Peletskii V. and Druzhinin V. Translated from *Teplofizika Vysokikh Temperatur* **9**(3) (1971), 539–545.

[12] Martynyuk M. and Tsapkov V. *Russian Metallurgy* **2** (1974), 108–112.

[13] Cezairliyan A. and McClure J. *J. Res. Nat. Bur. Stand.* **79A**(2) (1975), 431–436.

[14] Hultgren R., Desai P. D., Hawkins D. T., Gleiser M., Kelley K. K. and Wagman D. D. *Selected Values of the Thermodynamic Properties of the Elements*, 1990. American Society for Metals, Metals Park, 1973.

[15] Weißmantel Ch. and Hamann C. *Grundlagen der Festkörperphysik.* Springer, Berlin, 1980, pp. 324.

[16] Mills K., Monaghan B. and Keene B. *Thermal Conductivities of Molten Metals*—NPL Report CMMT(A) 53. NPL, Teddington, 1997.

[17] Touloukian Y. S., Kirby R. K., Taylor R. E. and Desai P. D. *Thermophysical Properties of Matter—Volume 12: Thermal Expansion—Metallic Elements and Alloys*, IFI/Plenum, New York, 1975.

[18] Peterson A. W., Kedesdy H., Keck P. H. and Schwarz E. *J. Appl. Phys.* **29** (1958), 213.

[19] Allen B. C. *Trans. AIME* **227** (1963), 1175 & *Trans. AIME* **230** (1964), 1357.

[20] Filippow L. P. *Int. J. Heat Mass Transfer* **16** (1973), 865–885.

[21] Klemens P. G. and Williams R. K. *Int. Met. Rev.* **31**(5) (1986), 197–215.

[22] Tye R. P. and Hayden R. W. *High Temp.-High Press.* **11** (1979), 597–605.

[23] Pottlacher G. *J. Non-Crystall. Solids* **250–252** (1999), 177–181.

[24] Wilthan B., Reschab H., Tanzer R., Schützenhöfer W. and Pottlacher G. *Int. J. Thermophys.* **29**(1) (2008), 434–444.

[25] *Leitfaden zur Angabe der Unsicherheit beim Messen*, 1995. DIN Deutsches Institut für Normung, 1. Beuth Verlag GmbH. Original: *Guide to the Expression of Uncertainty in Measurement*, ISO Geneva, 1993.

[26] Wilthan B. *PhD Thesis (Dissertation)*, Technische Universität Graz, Austria, Graz, 2005.

7.4 Electrical resistivity of high melting metals up into the liquid phase (V, Nb, Ta, Mo, W)

T. Hüpf, C. Cagran, G. Lohöfer, G. Pottlacher, *Electrical resistivity of high melting metals up into the liquid phase (V, Nb, Ta, Mo, W)*, Journal of Physics: Conference Series 98, 2008.

On the one hand this paper puts pulse-heating in context to other measurement techniques (electromagnetic levitation) and on the other hand it introduces the approach of making investigations on systematic behavior on the basis of comparison (V, Nb, Ta, Mo, W).

Comments: The text was written by myself with the help of Dr. Claus Cagran. The referred measurements are a combination of new data and 'old' results obtained by my predecessors in the workgroup of subsecond thermophysics. Dr. Georg Lohöfer was our partner working on electromagnetic levitation at the DLR in Cologne. Prof. Pottlacher was the supervisor of this collaboration project.

Journal of Physics: Conference Series **98** (2008) 062002 doi:10.1088/1742-6596/98/6/062002

Electrical resistivity of high melting metals up into the liquid phase (V, Nb, Ta, Mo, W)

T Hüpf[1], C Cagran[1], G Lohöfer[2] and G Pottlacher[1]

[1]Institute of Experimental Physics, Graz University of Technology, Petersgasse 16 8010 Graz, Austria
[2]Institute of Materials Physics in Space, DLR, Porz-Wahnheide, Linder Höhe, 51147 Cologne, Germany

thomas.huepf@tugraz.at

Abstract. Objective of the collaboration of TU Graz and DLR Cologne is the measurement of specific electrical resistivity comparing pulse-heating and levitation results. The TU Graz measurements on V, Nb, Ta, Mo and W will be presented and discussed with regard to volume expansion and resistivity.

1. The ASAP Project

The Subsecond Thermophysics Group in Graz has a long tradition in performing pulse-heating experiments (see TU Graz Experimental Setup). These deliver thermophysical properties of metals up into the liquid phase as a function of temperature [1]. We started to team up with the Institute of Materials Physics in Space at DLR (German Aerospace Center) in Cologne, which also performs experiments on liquid metals by means of electromagnetic levitation [2]. On one hand both setups, at TU Graz and DLR Cologne, have the same field of research, but on the other hand our investigations are very different: Pulse-heating experiments have a time-scale of microseconds (typically 50 µs for the transit from room temperature to 4000 K) whereas levitation can be seen as a quasistatic method.

This cooperation covers the valuable possibility to create a compilation of electrical resistivity data with the excellence of being verified in two completely different approaches, pulse-heating and levitation. The latter is further planned to be carried out under micro gravity (µg) conditions at the ISS. The prearrangements to this more precise experiment in space e. g. material selection, also have to be done in terms of comparability. The ensure TU Graz's ability to take part in these spaceflight networks the Austrian Space Applications Program (ASAP) delivers financial support (see last paragraph).

2. TU Graz Experimental Setup

A wire shaped specimen is assembled into a discharge circuit. A capacitor bank of 500 µF is charged with a high voltage power supply and then discharged through the wire. Its ohmic resistivity leads to a rapid increase in temperature. Heating rates of 10^8 K/s eliminate chemical reactions between the wire and the surrounding atmosphere and the cylindrical sample maintains its shape until the end of the liquid phase. This leads to an experimental duration of about 50 µs.

The current is measured with an induction coil. The voltage drop is measured with two knife edges placed on the wire. Temperature has to be detected pyrometrically using Planck's law of black-body radiation. These records deliver the electrical resistivity with initial geometry ρ_{IG} as a function of temperature. As thermal expansion leads to smaller densities, which affects the calculation of the

specific electrical resistivity ρ, the volume expansion has to be taken into account. At TU Graz the change of the diameter D can be measured with a fast CCD camera as a shadowgraph when the wire is backlit with a photoflash.

3. Results

For each material, the results are given as a function of temperature T in polynomial fits, split into solid and liquid phase (see table 1). Melting temperatures and references: V: 2201 K, [3], Nb: 2745 K, [4, 5], Ta: 3270 K, [6, 7], Mo: 2895 K, [8, 9], W: 3687 K, [4, 10]. Plots see figure 1 and figure 2.

Table 1: Polynomial least-squares fits (Value = a + bT + cT^2 + dT^3). D: diameter, D_0: diameter at room temperature, ρ_{IG}: specific electrical resistivity with initial geometry, ρ: specific electrical resistivity, ρ_{IG} and ρ given in $\mu\Omega \cdot \mathrm{m}$, decimal places according to references.

Vanadium:	range / K	a	b	c	d
D^2/D_0^2	1800 - 2201	0.990	3.137×10^{-5}	1.261×10^{-9}	
D^2/D_0^2	2201 - 2900	0.910	7.727×10^{-5}		
ρ_{IG}	1800 - 2201	-0.22754	1.120×10^{-3}	-2.15791×10^{-7}	
ρ_{IG}	2201 - 2900	1.486	-3.305×10^{-4}	5.188×10^{-8}	
ρ	1800 - 2201	-0.280	1.180×10^{-3}	-2.174×10^{-7}	
ρ	2201 - 2900	1.418	-1.730×10^{-4}	6.012×10^{-8}	
Niobium:					
D^2/D_0^2	2745 - 3700	0.963	-2.5×10^{-5}	3.14×10^{-8}	-1.17×10^{-12}
ρ_{IG}	473 - 1573	0.023	4.839×10^{-4}	-8.899×10^{-8}	
ρ_{IG}	1790 - 2745	0.199	2.441×10^{-4}		
ρ_{IG}	2745 - 3700	0.972	5.527×10^{-6}		
ρ	2745 - 3700	0.6833	1.477×10^{-4}		
Tantalum:					
D^2/D_0^2	2750 - 3250	-1.3393	2.4883×10^{-3}	-0.86945×10^{-6}	0.1026×10^{-9}
D^2/D_0^2	3300 - 5000	0.95634	5.6199×10^{-5}	-2.6656×10^{-9}	3.7798×10^{-13}
ρ_{IG}	2750 - 3250	0.2307	2.7007×10^{-4}		
ρ_{IG}	3300 - 5000	1.3401	-6.243×10^{-5}	5.503×10^{-9}	
ρ	2750 - 3250	0.2037	2.9027×10^{-4}		
ρ	3300 - 5000	1.19622	4.40644×10^{-5}		
Molybdenum:					
D^2/D_0^2	2895 - 3600	0.969	5.768×10^{-5}		
ρ_{IG}	400 - 2895	-0.0384	2.8436×10^{-4}	-1.0970×10^{-8}	3.6622×10^{-12}
ρ_{IG}	2895 - 3600	0.9535	-1.1498×10^{-5}		
ρ	2895 - 3600	0.93106	3.95726×10^{-5}		
Tungsten:					
D^2/D_0^2	3680 - 5000	0.95062	6.344×10^{-5}		
D^2/D_0^2	5000 - 6000	1.34989	-1.0333×10^{-4}	1.73957×10^{-8}	
ρ_{IG}	423 - 1723	-0.021	2.456×10^{-4}	1.201×10^{-8}	
ρ_{IG}	2390 - 3687	-0.059	3.166×10^{-4}		
ρ_{IG}	3687 - 5400	1.833	-2.573×10^{-4}	2.169×10^{-8}	
ρ	3687 - 5400	2.313	-4.585×10^{-4}	5.65×10^{-8}	

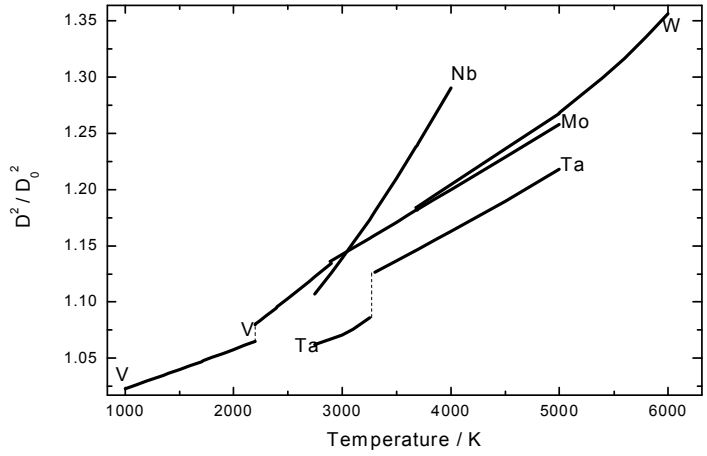

Figure 1: Diameter expansions, D^2/D_0^2, as a function of temperature.

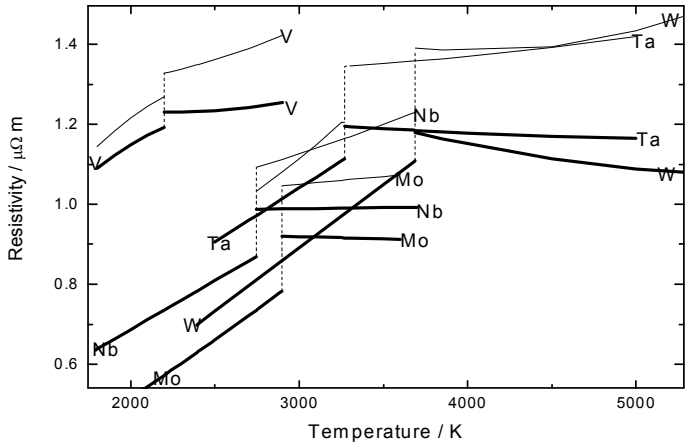

Figure 2: Electrical resistivities, ρ, as a function of temperature. Thin lines: values including volume expansion, dashed lines: melting transitions.

4. Discussion

The pulse-heating setup contains some peculiarities concerning the volume-correction of the electrical resistivity, which shall be considered first. In the formula for the specific electrical resistivity $\rho = U \cdot I^{-1} \cdot r^2 \pi \cdot l^{-1}$, with U: voltage drop, I: current, r: radius, l: length, one can see, that the consideration of thermal expansion requires knowledge of the change in radius (or diameter) and length. In our case, the wire can not change its length, because of the mechanical clamping. Due to improper experimental adjustments (e. g. unsatisfactory slow heating-rate) the wire will bend when its length increases leading to inoperative results. Hence the described monitoring of the cross-section is the best considered method: It delivers the thermal expansion of the diameter (later expressed as

D^2/D_0^2) and it will indicate, if the wire maintained its position during the heating process. The CCD camera delivers a picture of the diameter every 5 µs. The relation with the simultaneous temperature measurement yields the diameter D as a function of temperature.

As can be seen in figure 1, the five elements are not very different in their thermal expansions, except for niobium. The slope of Nb is steeper compared to the other metals. From this follows that the expansion of Nb in the solid phase has to be much lower than in the liquid phase as the ratio D^2/D_0^2 equals unity at room temperature. This common trend is approved by the two elements vanadium and tantalum, where solid state values are plotted too. They also show the typical increase at the melting-point.

The comparison of electrical resistivities exhibits a different behavior: Here vanadium is the element being outside of the bulk. It has the highest resistivity. W, Ta and Mo show a decreasing resistivity in the liquid state. This characteristics disappears when volume-expansion is taken into account.

It is easily noticeable from figure 2, that the temperature range is different for each material. Although pulse-heating would provide the possibility to measure resistivity values up to the end of the liquid phase, this additional experimental effort is barely appreciated within this project's framework: No change in liquid phase behavior is expected at higher temperatures and the comparison with the results of our partners, obtained though levitation experiments, will be done some hundred degrees around the melting-point region.

Uncertainty consideration: The expanded relative uncertainty with a coverage factor of $k = 2$ of the electrical resistivity with initial geometry is 4%. The calculation for the thermal expansion in terms of GUM [11] is still missing, but even broad estimations of 0.04 (3.5%) for D^2/D_0^2 will only increase the uncertainty for specific resistivity to 6%.

5. Conclusion

We have presented our measurements of specific electrical resistivity on V, Nb, Ta, Mo, and W. The results shall be compared with the results obtained at our partner's laboratory by means of levitation. This is one topic to be done in the course of our collaboration project.
TU Graz will proceed with the compilation of resistivity measurements. The improvement of density measurements with the pulse-heating method is the active research at TU Graz, because density values at high temperatures are sparse.

Acknowledgement

The project *Electrical Resistivity Measurement of High Temperature Metallic Melts* is sponsored by the Austrian Space Applications Program (ASAP) of the FFG, Sensengasse 1, 1090 Wien, Austria.

References

[1] Gallob R, Jäger H and Pottlacher G 1986 *Int. J. Thermophys.* **7** (1) 139
[2] Richardsen T and Lohöfer G 1999 *Int. J. Thermophys.* **20** 1029
[3] Pottlacher G, Hüpf T, Wilthan B and Cagran C 2006 *Thermo. Acta* DOI: 10.1016/ j.physletb.2003.10.071
[4] Wilthan B, Cagran C and Pottlacher G 2005 *Int. J. Thermophys.* **26** 1017–29
[5] Gallob R, Jäger H and Pottlacher G 1985 *High Temp. – High Press.* **17** 207–13
[6] Pottlacher G and Seifter A 2002 *Int. J. Thermophys.* **23** 1267–80
[7] Jäger H, Neff W and Pottlacher G 1978 *Int. J. Thermophys.* **83** 127
[8] Cagran C, Wilthan B and Pottlacher G 2004 *Int. J. Thermophys.* **25** 1551–66
[9] Pottlacher G, Kaschnitz E and Jäger H 1991 *J. Phys. Condens. Matter* **3** 5783–92
[10] Kaschnitz E, Pottlacher G and Windholz L 1990 *High Pressure Research* **4** 558–60
[11] GUM 1993 *Guide to the Expression of Uncertainty in Measurement* (Geneva: ISO)

7.5 Electrical resistivity of high temperature metallic melts - Hf-3%Zr, Re, Fe, Co, and Ni

T. Hüpf, C. Cagran, G. Lohöfer, G. Pottlacher, *Electrical resistivity of high temperature metallic melts - Hf-3%Zr, Re, Fe, Co, and Ni*, High Temperatures-High Pressures 37, 2008.

This paper is again dedicated to systematic materials comparisons with regard to their position in the periodic system of the elements (PSE). Additionally, a discussion about sample purity and supplier is contained in the text.

Comments: The paper was written by myself with the help of Dr. Claus Cagran. Again, the mentioned results are 'old' and new ones. Dr. Lohöfer was a partner in the project from which this paper received financial support. Prof. Pottlacher was the supervisor of this work.

High Temperatures-High Pressures, Vol. 37, pp. 239–246
Reprints available directly from the publisher
Photocopying permitted by license only

Electrical resistivity of high temperature metallic melts – Hf-3%Zr, Re, Fe, Co, and Ni†

THOMAS HÜPF[1,*], CLAUS CAGRAN[1], GEORG LOHÖFER[2] AND GERNOT POTTLACHER[1]

[1]*Institute of Experimental Physics, Graz University of Technology, Petersgasse 16, 8010 Graz, Austria*
[2]*Institut für Materialphysik im Weltraum, DLR, Porz-Wahnheide, Linder Höhe, 51147 Köln, Germany*

Received: November 21, 2007. Revised: April 30, 2008. In Final Form: May 6, 2008.

Electrical Resistivity Measurement of High Temperature Metallic Melts is an Austrian Space Applications Programme (ASAP) project, sponsored by the FFG. The project's main intent is the refinement of electrical resistivity data via a comparison between two very different experiments: fast pulse-heating and electromagnetic levitation. The latter is planed to be carried out under μg-conditions at the ISS beginning in 2010. This arrangement comprehends subsecond ohmic versus quasistatic inductive heating and ground-based versus space-flight facility.

This paper gives a general survey of the project's approaches and present results of the pulse-heating experiment for Hf-3%Zr, Re, Fe, Co, and Ni with respect to *enthalpy, resistivity* and *volume-expansion* up into the liquid phase.

Keywords: Cobalt, enthalpy, hafnium-3%zirconium, iron, liquid metals, metallic melts, nickel, pulse-heating, resistivity, rhenium, volume-expansion.

1 INTRODUCTION

The workgroup of Subsecond Thermophysics at Graz University of Technology has a long tradition in performing pulse-heating experiments. These allow

*Corresponding author: E-mail: thomas.huepf@tugraz.at

†Paper presented at the 8th International Workshop on Subsecond Thermophysics, September 26–28, 2007, Moscow, Russia.

investigations of electroconductive materials – basically metals. Thermophysical data, such as enthalpy, isobaric heat capacity and electrical resistivity, are obtained as a function of temperature [1].

The pulse-heating method is very prominent concerning measurements of liquid metals. Due to very high heating rates (in our case 10^8 K/s) thermophysical data can be obtained far in the liquid phase. Research on liquid metals is also frequently done using levitation devices. A collaboration project of TU Graz and DLR at Cologne, where research is done on electromagnetic levitation devices, is dedicated to measurements of electrical resistivities of liquid metals. The levitation measurements are also planned to be carried out under micro-gravity conditions (at the ISS or in flight experiments) and a prototype of this levitation device is ready for approbation (for the details on both experiments see [2,3]).

As resistivity measurements via electromagnetic levitation are very new, their results have to be compared with data obtained in another type of experiments. The Subsecond Thermophysics Workgroup will provide these data for pre defined liquid metals. For this purpose, new results and already published ones are revised and compiled. Additionally, it is scientifically highly stimulating to see, what the results of very fast experiments (as it is the case with fast pulse-heating) are, compared to even quasistatic methods (like levitation). The latter also covers the possibility – and the partners at Cologne make use of it widely – to investigate undercooled liquids. For example a crystalline short range order could possibly be seen in the resistivity curve. This is not possible at the TU Graz laboratory.

This work will focus on the pulse-heating results of hafnium, rhenium, iron, cobalt and nickel with regard to volume-expansion, enthalpy and resistivity. New results (Hf-3%Zr, Co, Re) are described as well as already published ones (Ni, Fe, Re).

2 MEASUREMENTS

The following quantities were measured: Current, I, with an induction coil. Voltage drop, U, with two knife-edges directly placed on the wire. The thermal radiance was measured with pyrometers working at a wavelength of either 1570 nm or 650 nm. The known melting temperature of each material (see Section 4.1) was assigned to the melting plateau in the pyrometer signal records and temperature, T, was calculated using Plancks radiation law.

The diameter, D, of the wire was measured with a fast CCD-camera. For this purpose, the wire was backlit with a photoflash.

The specimens have the shape of a wire, about 70 mm long and a diameter at room temperature of about 0.5 mm. The results are average values of several measurements. For more details see [4].

3 RESULTS

Data are recorded as a function of experimental duration, t. Due to the simultaneous temperature measurement, all time-dependent quantities can later be described as a function of temperature T [5]. Thermal expansion of the wire is taken into account by the ratio $D^2(T)/D_0^2$, with D_0 being the diameter at room temperature. The temperature dependences of $D^2(T)/D_0^2$ for Hf-3%Zr, Re, Fe, Co and Ni are shown in Figure 1.

Specific enthalpy $H(t)$ is calculated as

$$H(t) = \frac{1}{m} \cdot \int U(t) \cdot I(t)\,\mathrm{d}t, \tag{1}$$

m: mass, t: time. The dependence of enthalpy versus temperature for Hf-3%Zr, Re, Fe, Co and Ni is depicted in Figure 2.

Further specific resistivity with initial geometry $\rho_{\mathrm{IG}}(t)$ is calculated as

$$\rho_{\mathrm{IG}}(t) = \frac{U(t) \cdot r^2 \cdot \pi}{I(t) \cdot l}, \tag{2}$$

with l: length and r: radius of the wire. Specific resistivity including thermal expansion $\rho(T)$ is calculated as

$$\rho(T) = \rho_{\mathrm{IG}}(T) \cdot \frac{D^2(T)}{D_0^2}. \tag{3}$$

Both resistivities (with and without thermal expansion) for Hf-3%Zr, Re, Fe, Co and Ni are plotted in Figure 3.

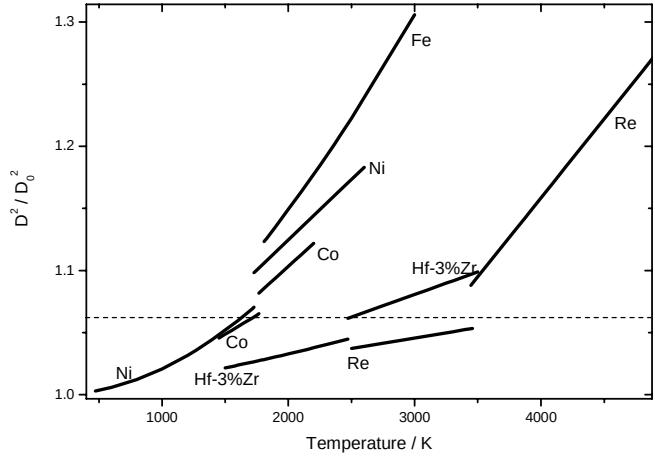

FIGURE 1
Thermal expansion versus temperature for Hf-3%Zr, Re, Fe, Co and Ni. Dashed line: lowest thermal expansion at the beginning of the liquid phase (hafnium-3%zirkonium).

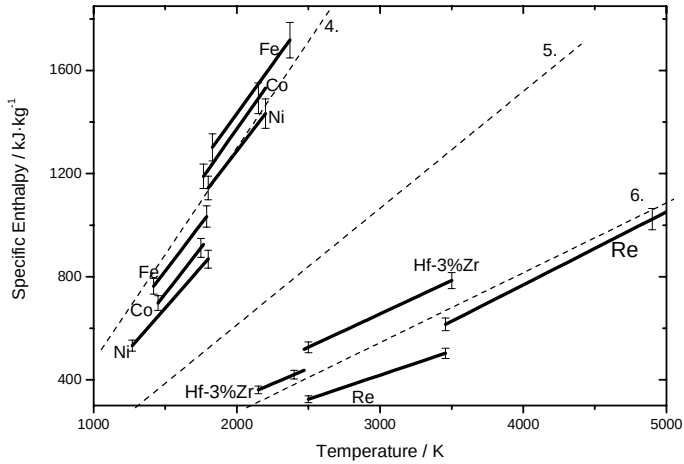

FIGURE 2
Specific enthalpy versus temperature for Hf-3%Zr, Re, Fe, Co and Ni. Dashed lines: approximate enthalpy values for 4th, 5th and 6th period elements.

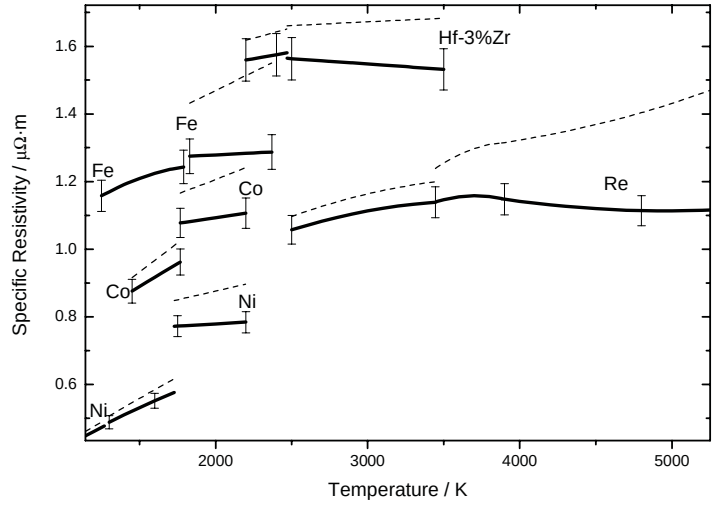

FIGURE 3
Specific resistivity with initial geometry versus temperature for Hf-3%Zr, Re, Fe, Co and Ni. Dashed lines: values including thermal expansion.

The corresponding polynomials for $D^2(T)/D_0^2$, $H(T)$, $\rho(T)$ and $\rho_{\mathrm{IG}}(T)$, which are presented as least-squares fits, are collected in Table 1.

Whenever possible the data were fitted with low order polynomials, although multiplication of polynomials would mathematically lead to a higher order.

Element or quantity	Range / K	a	b	c
Hafnium-3%Zr				
D^2/D_0^2	1500–2471	0.996	1.288×10^{-5}	2.766×10^{-9}
D^2/D_0^2	2471–3500	0.972	3.623×10^{-5}	—
H	2150–2471	−142.0	0.234	—
H	2471–3500	−121.5	0.259	—
ρ_{IG}	2200–2471	1.389	7.753×10^{-5}	—
ρ_{IG}	2471–3500	1.642	-3.142×10^{-5}	—
ρ	2200–2471	1.352	1.212×10^{-4}	—
ρ	2471–3500	1.606	2.219×10^{-5}	—
Rhenium*				
D^2/D_0^2	1500–3458	0.995	1.688×10^{-5}	—
D^2/D_0^2	3458–4500	0.650	1.271×10^{-4}	—
H	2500–3458	−140.2	0.186	—
H	3458–5000	−363.6	0.283	—
ρ_{IG}	2000–3458	0.354	4.229×10^{-4}	-5.665×10^{-8}
ρ_{IG}	3458–3880	−2.843	2.160×10^{-3}	-2.915×10^{-7}
ρ_{IG}	3880–4500	1.859	-3.001×10^{-4}	3.019×10^{-8}
ρ	2000–3458	0.338	4.446×10^{-4}	-5.650×10^{-8}
ρ	3458–3880	−3.682	2.540×10^{-3}	-3.235×10^{-7}
ρ	3880–4500	1.520	-1.753×10^{-4}	3.150×10^{-8}
Iron				
D^2/D_0^2	1808–3000	0.8465	1.5119×10^{-4}	—
H	1420–1790	−276.65	0.732	—
H	1830–2370	−107.306	0.770	—
ρ_{IG}	1250–1790	0.591	6.594×10^{-4}	-1.648×10^{-7}
ρ_{IG}	1830–2370	1.232	2.342×10^{-5}	—
ρ	1830–2370	1.0274	2.2094×10^{-4}	—
Cobalt				
D^2/D_0^2	1450–1768	0.967	4.835×10^{-5}	4.105×10^{-9}
D^2/D_0^2	1768–2200	0.918	9.269×10^{-5}	—
H	1450–1768	−337.1	0.714	—
H	1768–2200	−212.5	0.793	—
ρ_{IG}	1450–1768	0.484	2.703×10^{-4}	—
ρ_{IG}	1768–2200	0.961	6.593×10^{-5}	—
ρ	1450–1768	0.420	3.420×10^{-4}	—
ρ	1768—2200	0.858	1.738×10^{-4}	—
Nickel				
D^2/D_0^2	300–1728	1.000	-6.604×10^{-6}	2.738×10^{-8}
D^2/D_0^2	1728–2600	0.930	9.730×10^{-5}	—
H	1200–1715	−272.961	0.634	—
H	1740–2240	−151.913	0.720	—
ρ_{IG}	1300–1715	0.094	3.764×10^{-4}	-5.644×10^{-8}
ρ_{IG}	1750–2200	0.728	2.546×10^{-5}	—
ρ	1300–1715	0.106	3.456×10^{-4}	-2.920×10^{-8}
ρ	1750–2200	0.667	1.043×10^{-4}	—

TABLE 1
Summary of results. Values X given in $X = a + b \cdot T + c \cdot T^2$. D^2/D_0^2: thermal expansion, H: specific enthalpy, ρ_{IG}: specific resistivity with initial geometry, ρ: specific resistivity. H given in kJ/kg, ρ and ρ_{IG} in $\mu\Omega$ m. References: Re [2], Fe [6,7], Ni [6]. Star: results for rhenium purchased from Advent Research.

4 DISCUSSION OF RESULTS

4.1 Thermal expansion

Iron, cobalt and nickel have similar melting temperatures (Fe: 1808 K [8], Co: 1768 K [8], Ni: 1728 K [8]). Due to this fact, the differences in their respective thermal expansions can be seen easily in the graphic plot (see Figure 1). For iron, only the liquid phase was measured. For nickel, the data was expanded to lower temperatures, which could be done with every element, as the ratio D^2/D_0^2 has to equal unity at room temperature per definition. Hafnium and rhenium have higher melting temperatures (Hf: 2471 K [9], Re: 3458 K [10]). Hafnium shows the lowest expansion at the beginning of the liquid phase as indicated by the horizontal dashed line in Figure 1.

The differences in the temperature range derive from the particular combination of pyrometer and neutral gray filters depending on the requirements. This effect will be seen in every plot in this work.

4.2 Specific enthalpy

As can be seen in Figure 2, the enthalpy curves split into two groups: Fe, Co, Ni and Hf, Re. This is consistent with their respective position in the periodic table of the elements: The first ones belong to the 4th period, whereas Hf and Re belong to the 6th period. This congruence can be found with other metals too. It is indicated by the dashed lines, where 'bundles' of elements would be found: Ti, V, etc. along line 4, Nb, Zr, etc. around line 5 and Ta, Au, etc. line 6.

It can be deduced from this 'matching' situation, that the main physical reasons for the specific enthalpy results are quantities which are more or less classified in the periodic table of the elements. The precise classification is according to the number of protons and electronic shell models. Consequently a lot of quantities (if not all) do not appear randomly distributed but ordered in some way (atomic weight, density and even melting temperatures).

Nevertheless this observation is noteworthy, because this simple relation is *not* applicable for specific resistivities of metals, although this very quantity seems to be more than any other related to electronic structure.

4.3 Specific resistivity

As the resistivity with initial geometry is the 'directly measured' quantity in pulse-heating experiments, it is plotted as bold lines in Figure 3. The consideration of the volume expansion is displayed in dashed lines.

The results of the five elements cover a wide range. Nickel has the lowest, hafnium the highest resistivity. Only rhenium has a remarkable liquid phase behavior. It deviates from the linear increase. Additionally the results for rhenium depended on where the wires were purchased. The curve shown in Figure 3 belongs to the wire purchased at Advent Research Materials Ltd. with the highest purity (99.99%). Figure 4 also shows the results for the wire delivered by Alfa Aesar (purity 99.97%) and the measurements on a Goodfellow

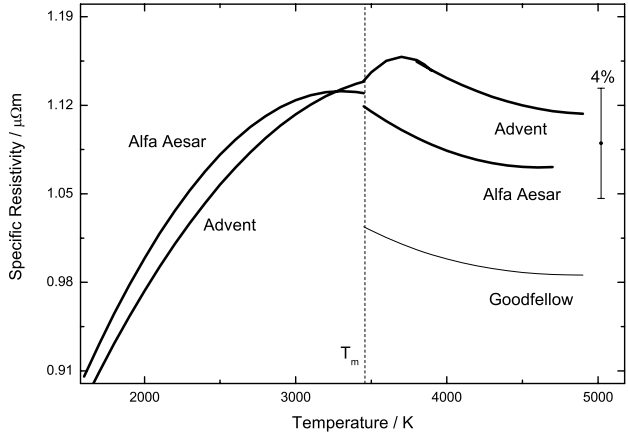

FIGURE 4
Comparison of different rhenium wires. Specific resistivity versus temperature for rhenium. Wire purchased 2007 from Advent Research (99.99% purity), Alfa Aesar 2003 (99.97%) and Goodfellow 1986 (99.9%), T_m: melting temperature.

wire published in 1986 [2] (purity 99.9%). In these former measurements, wires of 0.25 mm diameter were used and the heating rates were even higher, typically 10^9 K/s. These earlier results could not be verified recently.

Although the deviation between the Advent wires and the Alfa Aesar wires is significant and could be reproduced in several measurements, however, the total difference is small, considering the scale of Figure 3, and lies within the error bars of 4%. One reason for the different rhenium measurements might be the difference in purity. Additionally *new* measurements differ from those performed years ago, as the purity of purchased samples has strongly increased over the years.

Uncertainty

The expanded relative uncertainty with a coverage factor of $k = 2$, following the GUM [11] guidelines are: specific enthalpy, H: 4%, specific resistivity with initial geometry, ρ_{IG}: 4%. The calculation for the thermal expansion is still missing, but even broad estimations of 3.5% for D^2/D_0^2 will only increase the uncertainty for specific resistivity, ρ, to 6%.

5 CONCLUSION

This work presents the TU Graz pulse-heating results for hafnium-3% zirconium, rhenium, iron, cobalt and nickel, being one part of a collaboration project

together with DLR at Cologne, where investigations are done on levitation devices.

Polynomials are presented in Table 1. The thermal expansion of these five elements is shown in Figure 1. The specific enthalpy results depicted in Figure 2 reveal some kind of regularity that can be recovered in the periodic table of the elements. The specific resistivity results are shown in Figure 3. Figure 4 exhibits that the resistivity of rhenium strongly depends on quality parameters of the sample such as purity, manufacturer and decade of purchase.

ACKNOWLEDGEMENTS

The project "*Electrical Resistivity Measurement of High Temperature Metallic Melts*" is sponsored by the FFG by the Austrian Space Applications Programm (ASAP), Sensengasse 1, 1090 Wien, Austria.

REFERENCES

[1] Kaschnitz E., Pottlacher G. and Jäger H. *Int. J. Thermophys.* **13**(4) (1992), 699–710.

[2] Gallob R., Jäger H. and Pottlacher G. *Int. J. Thermophys.* **7**(1) (1986), 139–147.

[3] Richardsen T. and Lohöfer G. *Int. J. Thermophys.* **20** (1999), 1029–1039.

[4] Hess H., Kaschnitz E. and Pottlacher G. *High Pressure Research* **12** (1994), 29–42.

[5] Kaschnitz E., Nussbaumer G., Pottlacher G. and Jäger H. *Int. J. Thermophys.* **14**(2) (1993), 251–257.

[6] Wilthan B., Cagran C. and Pottlacher G. *Int. J. Thermophys.* **25** (2004), 1519–1534.

[7] Beutl M., Pottlacher G. and Jäger H. *Int. J. Thermophys.* **15**(6) (1994), 1323–1331.

[8] Bedford R., Bonnier G., Maas H. and Pavese F. *Metrologia* **33** (1996), 133–154.

[9] Cezairliyan A. and McClure J. *J. of Research of the National Bureau of Standards* **80A**(4) (1976), 659–662.

[10] Sims C., Craighead C. and Jaffee R. *J. Metals* **7** (1955), 168–178.

[11] GUM *Guide to the Expression of Uncertainty in Measurement*, Geneva (1993), ISO.

7.6 Electrical resistivity of high melting metals (W, Mo, Re, Ta, Nb, Ir, and Hf) up into the liquid phase

C. Cagran, T. Hüpf, G. Pottlacher, *Electrical resistivity of high melting metals (W, Mo, Re, Ta, Nb, Ir, and Hf) up into the liquid phase*, Proceedings of the Seventh International Conference on Tungsten, Refractory & Hardmaterials, 2008.

This paper is a summary of selected metals (refractory) which are especially accessible with the fast pulse-heating technique.

Comments: The text was written by Dr. Cagran and Prof. Pottlacher. Table and figures by Thomas Hüpf.

Tungsten, Refractory & Hardmaterials VII

Proceedings of the Seventh International Conference on Tungsten, Refractory & Hardmaterials sponsored by the Metal Powder Industries Federation in cooperation with the Refractory Metals Association and APMI International, June 8–12, 2008
Gaylord National Resort and Convention Center
On the Potomac at National Harbor, Maryland

Co-Chairmen:

Animesh Bose
Advanced Metalworking Practices, LLC

Robert J. Dowding
U.S. Army Research Laboratory

John A. Shields, Jr.
Mill Creek Materials Consulting, LLC

Metal Powder Industries Federation
105 College Road East
Princeton, New Jersey 08540-6692

Tel: (609) 452-7700 Fax: (609) 987-8523
www.mpif.org

ELECTRICAL RESISTIVITY OF HIGH MELTING METALS (W, Mo, Re, Ta, Nb, Ir, and Hf) UP INTO THE LIQUID PHASE

C. Cagran, T. Hüpf, G. Pottlacher

Institute of Experimental Physics
Graz University of Technology,
Petersgasse 16, 8010 Graz, Austria,

ABSTRACT

Pulse-heating techniques are capable of measuring thermophysical properties of electrically conducting samples from room temperature up into the liquid state. These properties are of technological interest for modern numeric simulations, e.g., casting simulations. Such devices have been developed and greatly improved since their first technological appearance in the late 1950s and have come a long way from their initial use as sources for dense plasmas or to generate high intensity light flashes.

For about 25 years the *Subsecond Thermophysics Group* in Graz is operating an ultrafast ohmic pulse-heating system which allows the investigation of thermophysical properties such as temperature-dependent electrical resistivity and density of liquid metals. Wire-shaped specimens are part of an electrical discharge circuit and heated up into the liquid phase within typically 50 µs by passage of a large current pulse. During this period the samples maintain their geometry without gravitational disturbances. Original measurements from our workgroup of electric resistivity as a function of temperature for solid and liquid W, Re, Ta, Mo, Nb, Ir, and Hf will be reviewed herein.

INTRODUCTION

The first resistive self-heating experiment reported in literature was performed by E. Nairne in 1773, when he demonstrated in front of the Royal Society in London an experiment in which he literally exploded an iron wire by passing the current from 64 charged Leyden jars (the predecessor of today's capacitors) over the test sample [1] which was used as a current estimating device.

It took until the mid 1950s until the pulse-heating technique became technologically of interest. At this time W. Chace and H. Moore published a series of books with the title 'Exploding Wires' discussing and presenting different applications of this technique [2].

Due to the increasing demand in the 1960s of thermophysical properties data of materials under extreme conditions and at high temperatures on one hand, and the rapid advances in fast electronics such as electrical pulse generation, data acquisition equipment, etc. on the other hand, dynamic pulse calorimetry became more popular and more commonly used.

Conventional steady-state and quasi steady-state techniques for measuring thermophysical properties of solid and liquid materials are generally limited to temperatures below 2500 K. These limitations are mainly due to severe difficulties in handling samples at these temperatures such as chemical reactions and contamination, heat transfer, evaporation, loss of mechanical strength and electric insulation, etc. due to the long exposure duration of the specimen to high temperature ranging from a few seconds to hours. This is where dynamic pulse calorimetry comes into play, as it allows to minimize such effects and to reach temperature ranges up to 10.000 K by passing a large electrical current over the sample during a short period of time.

EXPERIMENTAL

Rapid volume heating methods are limited to electrically conducting materials and involve resistive self-heating of the specimen by passing an electrical current pulse through it. Starting at room temperature, the measurements can be performed into the liquid phase of the investigated material. The energy is stored in a series of capacitors. The metal samples, usually wires, are contained in a controlled environment chamber and measurements are performed using inert gas (Ar or N_2) as an ambient medium under nearly isobaric conditions.

The main components of such a discharge circuit are typically the energy storage, the main switch (in our specific case a high voltage mercury vapor ignitron tube) and a specimen chamber with windows for optical diagnostics. Additional requirements are a crowbar switch to stop the experiment at any desired moment and a charging unit.

The time-dependent measured quantities are the current through the wire-sample, the voltage drop along a metered portion, the temperature of the material (which is determined by means of optical pyrometry), and other optical measurements, such as thermal expansion detected with a fast CCD-camera system taking a picture of the expanding sample every 5 μs [3]. The entire experiment is performed within about 50 μs, in which the sample is heated from room temperature up to the melting transition and then further into the liquid phase. In trade for the ability to obtain liquid state data inaccessible to other techniques, pulse-heating is a destructive method meaning the sample undergoes vaporization at the boiling point (at the latest) disintegrating the once solid material to a mist of nano-particles

The current, $I(t)$, is measured by means of a Pearson–probe (which is basically a kind of an induction-coil). The voltage drop along the sample is measured with two knive-edge probes and the signals are fitted to the A/D-cards' input requirements by means of ohmic voltage dividers. Inductive contributions to the voltage signals have actively to be subtracted from the measured voltage to finally obtain the voltage, $U(t)$, [4] which is used for all further calculations. The electrical resistivity, $\rho_{IG}(t)$, which represents the initial geometry at room-temperature without consideration of any thermal expansion can be calculated by means of Ohm's Law combined

with the sample geometry, which is still valid even at typical pulse-heating rates of about 10^8 K/s.

$$\rho_{IG}(t) = \frac{U(t) \cdot \pi \cdot r_o^{\,2}}{I(t) \cdot \ell}, \qquad (1)$$

where r is the actual sample radius obtained by the expansion measurement, and ℓ the length of the specimen.

The electrical resistivity $\rho(t)$ that accounts for the actual sample radius (due to thermal expansion) is calculated by

$$\rho(t) = \frac{U(t) \cdot \pi \cdot r(t)^2}{I(t) \cdot \ell}. \qquad (2)$$

Measurements of temperature, sample volume, and of electrical resistivity are on the same timescale thus electrical resistivity can also be given as a function of temperature.

RESULTS

As already mentioned, this paper reviews the temperature-dependent resistivity of refractory metals W, Re, Ta, Mo, Nb, Ir, and Hf at the end of the solid phase, at melting and in the liquid phase. Only Osmium is missing in this list, as it seems that Os cannot be drawn into wires of appropriate geometry to fit our experimental requirements (0.5 mm in diameter and 70 mm in length).

Within this manuscript own measurements that have been performed earlier are critically reviewed by ourselves to produce the best set of data to our knowledge, which might differ somewhat from earlier published values, as most of the refractory-metals have been remeasured for the sake of this review to confirm the validity of the presented temperature-dependent resistivity values. The comparison to literature has already been published in earlier papers, which are always indicated for each material, and thus will not be explicitly listed again. This comparison to literature data is not the aim of this review article but the collected resistivities for all available refractory metals. Readers with interest in a comparison to other literature data or in other thermophysical properties such as enthalpy, isobaric heat capacity, thermal conductivity, thermal diffusivity, and density (all as a function of temperature) for the high temperature solid and the molten states, as well as for normal spectral emittance (at a wavelength of 684.5 nm) are encouraged to locate those in the suggested references.

The results for each material are given in polynomial least-squares fits as a function of temperature, T, split into solid and liquid phase (see Table 1). For all refractory metals covered within this review, resistivity with initial geometry, ρ_{IG}, as a function of temperature is given in Fig. 1, whereas volume compensated resistivity, ρ, as a function of temperature is given in Fig. 2.

Tungsten (W):

Melting temperature used for data evaluation: 3687 K [5]. Density at RT (room temperature) 19300 kg·m^{-3} taken from [6]. Supplier of our samples: Goodfellow Cambridge Ltd., purity 99.95%.
At the onset of melting we obtain for resistivity with initial geometry, ρ_{IG}, (no correction for thermal expansion, index $_{IG}$) a value of 1.10 μΩ·m and at the end of melting a value of

1.18 μΩ·m, thus an increase of $\Delta\rho_{IG}$ = 0.08 μΩ·m at melting is observed. For volume compensated electrical resistivity at the end of melting we obtain a value of 1.39 μΩ·m. Data for the solid phase considering actual sample volume still have to be confirmed by new measurements. The comparison to literature data has been given in [7-9].

[7] marked the first time we succeeded in combining pulse-heating results (resistivity versus enthalpy) with quasistatic DSC (differential scanning calorimetry) measurements (enthalpy versus temperature). Electrical measurements at pulse-heating start from RT but no temperature may be assigned below the pyrometers' signal onset at about 1000 K. By scaling resistivity in values of enthalpy (both available from RT) and then substituting enthalpy by temperature taken from the enthalpy-temperature relationship of our DSC results, we are able to give resistivity versus temperature values starting from the onset-temperature of the DSC (typically 423 K) and not being limited by pyrometer onsets. This approach has yet been tested and used for W, Mo, and Nb only.

Rhenium (Re):

Melting temperature used for data evaluation: 3458 K [10]. Density at RT: 21020 kg·m^{-3} taken from [6] Supplier of our samples: Advent Research Material, Ltd., purity 99.99%.
At the onset of melting we obtain for resistivity with initial geometry, ρ_{IG}, a value of 1.139 μΩ·m and at the end of melting a value of 1.139 μΩ·m, thus no increase of ρ_{IG} at melting is observed. For volume compensated electrical resistivity at the onset of melting we obtain a value of 1.200 μΩ·m and at the end of melting a value of 1.243 μΩ·m. Thus an increase of $\Delta\rho$ = 0.043 μΩ·m at melting is observed.
The data for Rhenium presented here have been remeasured since its first publication [11], which gives comparison to literature values with slightly modified results. For normal spectral emittance obtained at a wavelength of 684.5 nm see [12].

Tantalum (Ta):

Back in 1985, the time of our first investigations on Tantalum, the generally accepted melting temperature was 3270 K [13]. Meanwhile 3280 K are suggested by Bedford et al. [5]. Density at RT: 16654 kg·m^{-3} taken from [6]. Supplier of our samples: Goodfellow Cambridge Ltd., purity 99.95%.
At the onset of melting we obtain for resistivity with initial geometry, ρ_{IG}, a value of 1.114 μΩ·m and at the end of melting a value of 1.195 μΩ·m, thus an increase of $\Delta\rho_{IG}$ = 0.081 μΩ·m at melting is observed. For volume compensated electrical resistivity at the onset of melting we obtain a value of 1.208 μΩ·m and at the end of melting a value of 1.340 μΩ·m. Thus an increase of $\Delta\rho$ = 0.132 μΩ·m at melting is observed. The comparison to literature data has already been given in [13-15].

Molybdenum (Mo):

Melting temperature used for data evaluation: 2895 K [5]. Density at RT 10220 kg·m^{-3} taken from [6]. Supplier of our samples: Goodfellow Cambridge Ltd., purity 99.95%.
At the onset of melting we obtain for resistivity with initial geometry, ρ_{IG}, a value of 0.782 μΩ·m and at the end of melting a value of 0.910 μΩ·m, thus an increase of $\Delta\rho_{IG}$ = 0.128 μΩ·m at melting is observed. For electrical resistivity that is compensated for thermal volume expansion we considered literature values of the thermal expansion for Molybdenum in the

solid state from Goldsmith [16]. For volume compensated electrical resistivity at the onset of melting we thus obtain a value of 0.821 μΩ·m and at the end of melting a value of 0.989 μΩ·m. An increase of $\Delta\rho$ = 0.168 μΩ·m at melting is observed. In the liquid phase our own volume expansion values have been used. The comparison to literature data has been given in [9, 17, 18].

Niobium (Nb):

Melting temperature used for data evaluation: 2745 K [5]. Density at RT 8570 kg·m^{-3} taken from [6]. Supplier of our samples: Goodfellow Cambridge Ltd., purity 99.9%.
At the onset of melting we obtain for resistivity with initial geometry, ρ_{IG}, a value of 0.87 μΩ·m and at the end of melting a value of 0.99 μΩ·m, thus an increase of $\Delta\rho_{IG}$ = 0.12 μΩ·m at melting is observed. For volume compensated electrical resistivity at the end of melting a value of 1.089 μΩ·m is observed. The comparison to literature data has been given in [7, 13, 19].

Iridium (Ir):

Melting temperature used for data evaluation: 2719 K [20]. Density at RT 22560 kg·m^{-3} taken from [20]. Thus Iridium has the highest density of all the herein mentioned refractory metals (and only ranks a close second behind Osmium overall). Supplier of our samples: Alfa Aesar, purity 99.9% . At the time of the iridium measurements our fast camera system was inoperable, therefore literature data for volume correction had to be used instead.
At the onset of melting we obtain for resistivity with initial geometry, ρ_{IG}, a value of 0.645 μΩ·m and at the end of melting a value of 0.849 μΩ·m, thus an increase of $\Delta\rho_{IG}$ = 0.204 μΩ·m at melting is observed. For electrical resistivity that is compensated for thermal volume expansion we considered literature values of the thermal expansion for Iridium from Toulukian [21] and converted density data from Ishikawa [22]. At the onset of melting, we now obtain a value of 0.695 μΩ·m and at the end of melting a value of 0.985 μΩ·m for volume compensated electrical resistivity. Thus an increase of $\Delta\rho$ = 0.290 μΩ·m at melting is observed. The comparison to literature data has been given in [23].

Hafnium (Hf):

Melting temperature used for data evaluation: 2471 K [24]. Density at RT: 13310 kg·m^{-3} taken from [6]. Supplier of our samples: Alfa Aesar, purity 99.95% metal basis excluding Zr, (nominal Zr content: 3%).
At melting ρ_{IG} decreases from 1.581 μΩ·m to 1.564 μΩ m, resulting in a $\Delta\rho_{IG}$ of 0.017 μΩ·m. At melting ρ increases from 1.651 μΩ·m to 1.661μΩ m, resulting in a $\Delta\rho$ of 0.010 μΩ·m. The comparison to literature data has been given in [25].

Table 1. Polynomial least-squares fits (value = a + bT + cT^2 + dT^3). ρ_{IG}: specific electrical resistivity with initial geometry, ρ: specific electrical resistivity, ρ_{IG} and ρ given in μΩ·m.

Metal	Range / K	a	b	c	d
Tungsten:					
ρ_{IG}	423 - 1723	-0.021	2.467×10^{-4}	1.201×10^{-8}	
ρ_{IG}	2390 - 3687	-0.059	3.166×10^{-4}		
ρ_{IG}	3687 - 5400	1.833	-2.573×10^{-4}	2.169×10^{-8}	
ρ	3687 - 5400	2.313	-4.585×10^{-4}	5.650×10^{-8}	
Rhenium					
ρ_{IG}	2000 - 3458	0.354	4.229×10^{-4}	-5.665×10^{-8}	
ρ_{IG}	3458 - 3880	−2.843	2.160×10^{-3}	-2.915×10^{-7}	
ρ_{IG}	3880 - 4500	1.859	-3.001×10^{-4}	3.019×10^{-8}	
ρ	2000 - 3458	0.338	$+4.446 \times 10^{-4}$	-5.650×10^{-8}	
ρ	3458 - 3880	−3.682	$+2.542 \times 10^{-3}$	-3.235×10^{-7}	
ρ	3880 - 4500	1.520	-1.753×10^{-4}	3.150×10^{-8}	
Tantalum:					
ρ_{IG}	2500 – 3270	0.231	2.701×10^{-4}		
ρ_{IG}	3270 - 5000	1.340	-6.243×10^{-5}	5.503×10^{-9}	
ρ	2750 - 3270	0.098	3.394×10^{-4}		
ρ	3270 - 5000	1.196	4.406×10^{-5}		
Molybdenum:					
ρ_{IG}	400 - 2895	-0.038	2.844×10^{-4}	-1.097×10^{-8}	3.662×10^{-12}
ρ_{IG}	2895 - 3600	0.954	-1.150×10^{-5}		
ρ	400 - 2895	-0.034	2.677×10^{-4}	6.774×10^{-9}	9.635×10^{-13}
ρ	2895 - 3600	0.931	3.957×10^{-5}		
Iridium					
ρ_{IG}	2000 - 2719	-0.023	2.453×10^{-4}		
ρ_{IG}	2719 - 3550	0.779	2.515×10^{-5}		
ρ	2000 - 2719	-0.072	2.833×10^{-4}		
ρ	2719 - 3550	0.775	7.553×10^{-5}		
Hafnium					
ρ_{IG}	2200 - 2471	1.389	7.753×10^{-5}		
ρ_{IG}	2471 - 3500	1.642	-3.142×10^{-5}		
ρ	2200 - 2471	1.352	1.212×10^{-4}		
ρ	2471 - 3500	1.606	2.219×10^{-5}		
Niobium:					
ρ_{IG}	473 - 1573	0.023	4.839×10^{-4}	-8.899×10^{-8}	
ρ_{IG}	1790 - 2745	0.199	2.441×10^{-4}		
ρ_{IG}	2745 - 3700	0.972	5.527×10^{-6}		
ρ	2745 - 3700	0.683	1.477×10^{-4}		

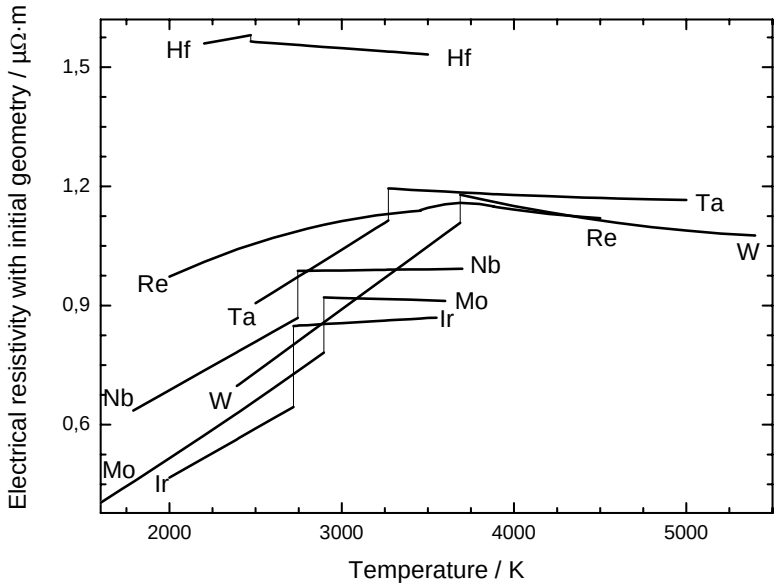

Figure 1. Electrical resistivities with initial geometry, ρ_{IG}, as a function of temperature.

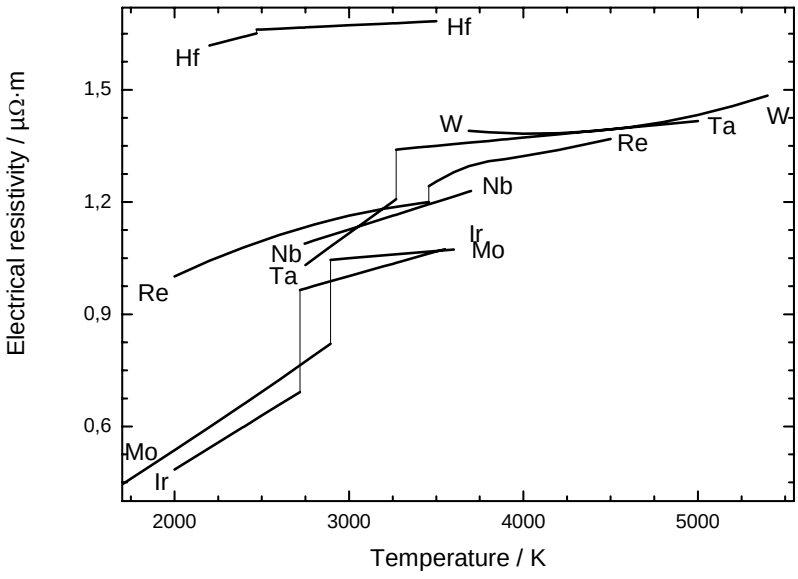

Figure 2. Electrical resistivities, ρ, as a function of temperature.

DISCUSSION

Sometimes newer pulse-heating measurements deliver somewhat different results compared to those performed earlier with the same element. This might result from the nowadays purer samples which are available from different suppliers. We definitely noticed this behaviour for example with Tantalum.

Within this manuscript temperature-dependent resistivities of refractory elements in the temperature regime from mainly 2000 K up to 5000 K are discussed. First, we have to mention that we personally consider values of electrical resistivity with initial geometry to be also important: as volume – or density measurements are not easy to perform in this temperature range, some authors report only electrical resistivity with initial geometry. To be able to compare results with those, we decided to always present two individual sets of data (ρ_{IG} and ρ), which differ only in volume expansion. When thinking about any technological usage such as input–data for numerical modeling only volume compensated resistivities are solely of interest. But there's another experimental reason, why electrical resistivity with initial geometry may become important: Not all materials investigated so far have been available in wire shaped form, as they were so brittle that they could not be drawn into wires, e.g., chromium, a Ti-44Al-8Nb-1B alloy [26], or certain steels [27]. In this case the material has to cut by micro electro-discharge machining (EDM) into samples with rectangular diameter which can also be pulse-heated though without optical expansion measurement. Numerical simulations of the pulse–heating process of rectangular samples [28] did confirm also homogeneous heating of the samples. As can be seen, electrical resistivity data with initial geometry is sometimes the only set of data obtainable when using pulse-heating.

In Fig.1 electrical resistivity with initial geometry versus temperature is plotted for W, Re, Ta, Mo, Nb, Ir, and Hf. At melting generally an increase to higher values can be observed, only Re and Hf are an exception with almost no change at the melting-transition. Resistivities for all materials (ρ_{IG} and ρ) in the solid state increase (with rising temperature) up to the melting point, whereas ρ_{IG} starts to decrease for the W, Re, Ta, Mo, and Hf in the liquid state. Constant resistivity in the liquid is observed for Niobium, and resistivity of Iridium even slightly increases.

Hafnium (with the lowest melting temperature) delivers the highest resistivity values of about 1.5 μΩ m, all other metals range from 0.8 μΩ·m to 1.2 μΩ·m as highest values. Tungsten, Rhenium, and Tantalum reach phase quite similar values in the liquid. Iridium returns the lowest resistivity, followed by Molybdenum and Niobium. Fig.1 clearly indicates no correlation between resistivity and melting temperature.

Fig.2 shows electrical resistivity versus temperature. The ρ values considering the actual volume differ somewhat from Fig.1. Hafnium still has the highest resistivity values, now a maximum of about 1.65 μΩ·m is reached. Generally speaking, the volume compensated resistivity ρ of metals increases both, in the solid and in the liquid phase. Molybdenum is the element with the least effect. It also should be noted; that some dependencies can be fitted with linear least squares fits, whereas other require higher order polynomials. This figure also gives no evidence of a resistivity–melting temperature correlation. Both figures are intended to show general trends and to present an overview of the behaviour of refractory metals.

To obtain the actual values, the reader is referred to Table 1, where all available polynomials are given, both for the solid and the liquid phase and for electrical resistivity with initial geometry and with consideration of thermal expansion. The temperature range of validity for each polynomial is separately indicated. The main goal was to review and summarize the resistivity values obtained up to now with a particular focus on liquid state data.

UNCERTAINTY

According to the guide to the expression of uncertainty in measurements (GUM) a detailed uncertainty budget analysis for our fast pulse-heating system has been performed in [29], which is available online for download from the homepage of the subsecond pulse heating group, see reference [29] for the link.

To briefly summarize the information from [29], the expanded relative uncertainty with a coverage factor of $k = 2$ (equals twice the standard deviation for a normal or Gaussian distribution) for electrical resistivity with initial geometry, ρ_{IG}, yields ± 3%. Considering thermal expansion of the sample will increase the uncertainty for resistivity, ρ, to ± 6%.

CONCLUSION

We present a review of temperature-dependent electrical resistivity measurements of the refractory metals W, Re, Ta, Mo, Nb, Ir, and Hf at the end of the solid phase, at melting, and in the liquid phase performed over the years with a pulse-heating experiment at Graz University of Technology. The comparison to other literature values has been presented in the respective original literature, which is stated for each material, and thus omitted herein. An uncertainty analysis was performed and yields ± 3% for $\rho_{IG}(t)$ and ± 6% for $\rho(t)$, respectively.

ACKNOWLEDGEMENT

The project *Electrical Resistivity Measurement of High Temperature Metallic Melts* is sponsored by the Austrian Space Applications Programme (ASAP) of the FFG, Sensengasse 1, 1090 Wien, Austria.

REFERENCES

[1] E. Nairne, Electrical Experiments, *Phil. Trans. Roy. Soc. London,* **64:** 79-89, 1774.
[2] Chace W. G. and Moore H. K., *Exploding Wires Vol. 1-4*, Plenum Press, Inc., New York, 1959-1968.
[3] C. Cagran, T. Hüpf, R. Dämon, B. Wilthan and G. Pottlacher. „Remodeled Optical Expansion Camera for a Fast Pulse Heating Experiment“ to be submitted to *Rev. Sci. Instruments* 2008.
[4] E. Kaschnitz, G. Pottlacher and H. Jäger, *Int. J. Thermophys*., **13**: 699 – 710, 1992.
[5] R. E. Bedford, G. Bonnier, H. Maas, and F. Pavese. Recommended values of temperature on the international temperature scale of 1990 for a selected set of secondary reference points. *Metrologia*, **33**: 133 – 154, 1996.
[6] D. R. Lide, editor. CRC Handbook of Chemistry and Physics. CRC Press LLC, 2004.
[7] Wilthan B, Cagran C and Pottlacher G., 2005 *Int. J. Thermophys.* **26:** 1017 – 1029
[8] E. Kaschnitz, G. Pottlacher, L. Windholz. High Pressure Research, **4**: 558 – 560, 1990.

[9] C. Cagran, G. Pottlacher, M. Rink and W. Bauer., *Int. J. Thermophys.* **26**: 1001 – 1015, 2005.
[10] C. T. Sims, C. M. Craighead, and R. I. Jaffee. *Journal of Metals,* **7**: 168 – 179, 1955.
[11] G. Pottlacher, T. Neger and H. Jäger., *International Journal of Thermophysics,* **7.1**: 149 – 59, 1986.
[12] C. Cagran, B. Wilthan, and G. Pottlacher Proceedings of Tempmeko 2004, Ed. Davor Zvizdic, ISBN 953-6313-73-1, Zagreb, Croatia, 1313 – 1318, 2005.
[13] R. Gallob, H. Jäger, G. Pottlacher., *High Temperatures - High Pressures* 1985, Vol. 17, p. 207 – 213.
[14] H. Jäger, W. Neff and G. Pottlacher, *Int. J. Thermophys.* **13.1:** 83 – 93, 1992.
[15] G. Pottlacher and A. Seifter, *Int. J. Thermophys.* **23:** 1267 – 1280, 2002.
[16] A. Goldsmith, T. E. Waterman, and H. J. Hirschorn, editors. Handbook of Thermophysical Properties of Solid Metals, Vol. 1 - Elements. Pergamon Press, Oxford, 1961.
[17] G. Pottlacher, E. Kaschnitz, H. Jäger, *J. Phys.: Condens Matter* **3**: 5783 – 5792, 1991.
[18] C. Cagran, B. Wilthan and G. Pottlacher *Int. J. Thermophys.* **25:** 1551 – 1566, 2004.
[19] A. Seifter, F. Sachsenhofer, S. Krishnan, and G. Pottlacher. *Int. J. Thermophys.* **22,5**: 1537 – 1547, 2001.
[20] J. W. Arblaster, *Calphad*, **19(3)**, 365 – 372, 1995.
[21] Y. S. Touloukian, R. K. Kirby, R. E. Taylor, and P. D. Desai, eds., *Thermal Expansion – Metallic Elements and Alloys, (Thermophysical Properties of Matter, Volume 12)*, IFI/ Plenum Publishing, New York, 1975.
[22] T. Ishikawa, P.-F. Paradis, R. Fujii, Y. Saita, and S. Yoda, *Int. J. Thermophys.*, **26.3:** 893 – 904, 2005.
[23] C. Cagran and G. Pottlacher *Int. J. Thermophys.* **28**: 697 – 710, 2007.
[24] Cezairliyan, A. McClure, J. Res. Natl. Bur. Stand., **80A(4)**, 659 – 662, 1976.
[25] C. Cagran, T. Hüpf and G. Pottlacher, *Submitted High.Temp.High.Press*. 2007.
[26] C. Cagran, B. Wilthan, G. Pottlacher, B. Roebuck, M. Wickins and R.A. Harding, Intermetallics, **11:**1327 – 1334, 2003.
[27] B. Wilthan, H. Reschab, R. Tanzer, W. Schützenhöfer, G. Pottlacher *Int. J. Thermophys.,* http://DOI: 10.1007/s10765-007-0300-1.
[28] G. Lohöfer and G. Pottlacher, *Int. J. Thermophys.***26**: 1239 – 1254, 2005.
[29] B. Wilthan, *Phd.-Thesis,* Technical University Graz, Austria, 2005. http://iep.tugraz.at/content/research/subsecondthermophysics/publications/diplomaphd/index_eng.html

7.7 Specific

T. Hüpf, C. Cagran, G. Pottlacher, G. Lohöfer, *Specific*, Poster presented at the 10th Lähnwitzseminar on calorimetry, Warnemünde, Germany, 2008.

The poster shows how the very basics of 'physical thinking' (related values) influence the interpretation of results. This is demonstrated by looking at data obtained by fast pulse-heating.

Comments: The poster was designed by myself with the help of Dr. Claus Cagran and Prof. Pottlacher. Dr. Lohöfer was a partner in the collaboration project which was mentioned in the text.

‚specific‘

T. Hüpf[1], C. Cagran[1], G. Pottlacher[1], G. Lohöfer[2]

[1]Institute of Experimental Physics, TU Graz, Austria
[2]Institut für Materialphysik im Weltraum, DLR, Köln, Germany

thomas.huepf@tugraz.at

During the specification of measured values or quantities we are – for good reason – often not interested in the absolute values, but in some unseful kind of ‚related‘ values.

dt.: „bezogen“: specific, related, referred.

Examples of related values:

gasoline: liter / 100 km 

CO_2: g / km 

car-racing: time / lap

alcohol: volume of alcohol / vol. of liquid 

engine power: J / s (Watt)

health: BMI: kg / m^2 

resistivity: $\rho_{sp}=\rho(r2\pi)/l$

children / inhabitant

sex / week 

…

It even seems as if we hardly use any absolute values to characterise properties. But we do:

Examples of common use:

dress sizes 

money

weight 

temperature

…size does matter.

According to the DIN directives, only values related to mass have to be called *specific*. Referring to the number of atoms gives *molar* values.

The workgroup of Subsecond Thermophysics at Graz University of Technology is investigating the thermophysical properties of metals by means of a fast pulse-heating circuit. In this experiment, wire-shaped specimens (see left figure) are rapidly heated through the passage of a large current pulse. Due to the high heating rates (10^8K/s) the wire maintains its geometry even in the liquid phase.

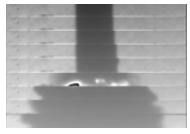

The right figure shows a shadograph picture of the expanding wire obtained with a CCD-camera. The transition to the gas-phase can be seen as wire explosion.

The ***Specific Enthalpy*** (as one of the thermophysical properties) can be found in two common notations: J / kg or J / mol.
But the units are not arbitrary. They will heavily influence the perception of the values:

The ***Specific Enthalpy*** measurements look like this (several materials):

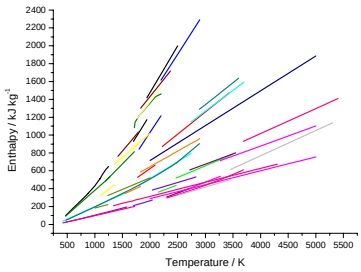

When the Enthalpy is plotted as a molar quantity, the same measurements look like this:

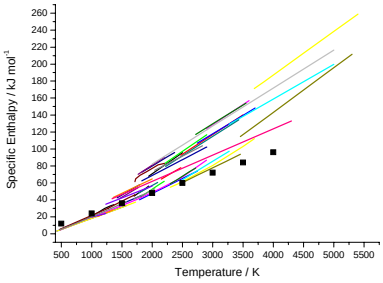

From this behavior one can easily conclude, that the Specific Enthalpy does mainly depend on the number of atoms. This is not a new fact. It is consistent with the rule of Dulong-Petit,

$$c = 3Nk$$

$$c_{mol} = 3N_A k = 24.9 Jmol^{-1}K^{-1}$$

which predicts the heat capacity c (which is the slope of the Enthalpy curves) out of the Boltzman constant k and the number of atoms N. The full squares in the figure are calculated according to this rule.

Developing new theories is often dependent on ideas, which can not be ordered. But to have the appropriate image can give you the crucial impulse. Every scientist has to be aware of this possibility with units and referred values.

In this spirit, there is to tell where this present work is related to: It is the aim of our collaboration project with the DLR in cologne, to compare thermophysical properties of liquid metals measured in very different experiments: Fast pulse-heating (TU Graz) and electromagnetic levitation (DLR). The team members are:




Prof. Gernot Pottlacher, Dr. Claus Cagran, Dipl.-Ing. Thomas Hüpf, Dr. Georg Lohöfer

The project is dedicated to electrical resistivity measurements. Of course we are interested in the ‚specific‘ resistivity:

$$\rho_{sp} = \rho \frac{\pi r^2}{l}$$

r: radius of the wire, l: length. As can be seen in the shadograph picture, the wire radius changes during the heating process. Thus the calculation of the specific resistivity is only correct, if the volume expansion in taken into account.

$$\rho = \rho_{IG} \frac{V(T)}{V_0}$$

V(T): volume at temperature T, ρ_{IG}: resistivity with initial geometry.

A measurement of the volume includes the possibility to quantify densities of liquid metals. The PhD thesis of Thomas Hüpf is dedicated to this topic.

The results of the evaluation of the volume-expansion looks like this:

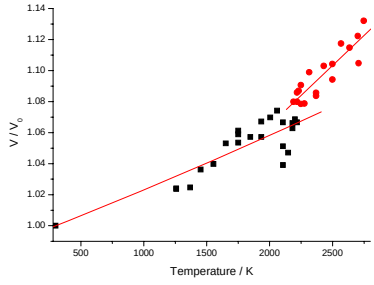

These are the results of vanadium. In case that there is no phase transition in the solid phase (full squares), it is appropriate to draw a linear fit down to room temperature where the ratio has to equal one.

The liquid phase (red dots) is also fitted linearly.

Conclusion:

It is highly human and approved in physics to use related values. Some are so common, that they have names (like specific for the relation on mass).

The choice, where to referre to, is crucial for the interpretation of measured values.

A collaboration project of TU Graz and the DLR in Cologne is focused on electrical resistivity measurements of liquid metals – or more correct:

specific electrical resistivity.

The project: „Electrical Resistivity Measurement of High Temperature Metallic Melts“ is sponsored by the FFG – ASAP programme.

7.8 Thermophysical properties of Ni80Cr20

T. Hüpf, C. Cagran, E. Kaschnitz, G. Pottlacher, *Thermophysical properties of Ni80Cr20*, Thermochimica Acta 494, 2009.

The paper demonstrates that during investigations of alloys quite a lot of approaches are possible. Here, Ni80Cr20 was set in context to its pure ingredients (Ni, Cr) and to the highly alloyed material Inconel 718. The section 'Uncertainty' contains a discussion on how its analysis depends on the type of measurement.

Comments: The paper was written by myself with the help of Dr. Claus Cagran. Dr. Erhard Kaschnitz performed DTA measurements on this alloy and was strongly involved in the reviewing process. Prof. Pottlacher was the supervisor of this work.

Thermochimica Acta 494 (2009) 40–44

Contents lists available at ScienceDirect

Thermochimica Acta

journal homepage: www.elsevier.com/locate/tca

Thermophysical properties of Ni80Cr20

T. Hüpf[a,*], C. Cagran[a], E. Kaschnitz[b], G. Pottlacher[a]

[a] Institut für Experimentalphysik, Technische Universität Graz, Petersgasse 16, 8010 Graz, Austria
[b] Österreichisches Gießerei-Institut, Parkstraße 21, 8700 Leoben, Austria

ARTICLE INFO

Article history:
Received 12 March 2009
Received in revised form 15 April 2009
Accepted 17 April 2009
Available online 24 April 2009

Keywords:
Alloys
Inconel 718
Liquid metals
Nickel
Ni80Cr20
Pulse-heating
Resistivity

ABSTRACT

The fast pulse-heating method provides a possibility to investigate thermophysical properties in the liquid state of electrically conducting materials in terms of a containerless measurement technique. Thereby wire-shaped specimens are rapidly heated by the passage of a large current pulse. This leads to heating rates of 10^8 K/s and an experimental duration of typically 50 μs. In addition to pure elements, multi-component alloys of industrial relevance and more simple alloys like Ni80Cr20 are in our focus of interest. Measured results of specific enthalpy, specific electrical resistivity and density of Ni80Cr20 are presented as a function of temperature as well as the derived quantities heat capacity, heat of fusion, thermal diffusivity and thermal conductivity. The composition of Ni80Cr20 is between pure nickel and highly alloyed materials. Therefore, its properties are compared to pure nickel and to Inconel 718 which has more than ten constituents and approximately 53% nickel and 18% chromium. Resistivity results show not only the intermediate position of the Ni80Cr20 alloy but also that an alloy can be quite different from the average of its constituents.

1. Introduction

The Subsecond Thermophysics Workgroup at TU Graz performed extensive research on pure metals. Currently this experience is extended to alloys. Industrial relevant alloys, such as Inconel 718, are designed by trial and error; the development requires a multitude of know-how in materials science. Therefore it is difficult to establish a relation between the ingredients of a composition and the effective properties. This investigation was performed on the alloy Ni80Cr20[1] (Ni78Cr22 at%) for the following reason: the correlation between a high-alloyed material (Inconel 718), its main pure element (Ni) and a simple alloy with a similar composition of the main constituents (Ni80Cr20) can be studied.

The investigation presented in this work deals mainly with high temperature properties, especially in the liquid state. However, most industrial relevant alloys are designed to meet mechanical properties in the solid state. Consequently, the well-known influence of add-ons in small quantities (e.g. rhodium, rhenium, molybdenum) on these mechanical properties (e.g. ductility) cannot be observed by this investigation technique. Finally, thermal treatments, such as quench hardening, lead to differing qualities, but cannot be quantified.

Nevertheless, small doses of alloying agents, or even impurities, can have a strong influence on the electrical resistivity in the solid state and some influence in the liquid state as well and since this quantity is a dominant parameter in some industrial processes and simulations [1], the present work is intended to provide data not only for basic research but also for the metal working industry.

Ni80Cr20 was chosen for measurement because it bridges the gap between pure nickel and Inconel 718, which consists of about 53% nickel and 18% chromium [2]. Both were studied repeatedly [3,4] and a revision of the measurements performed at TU Graz will be published [5].

2. Experimental

A typical analysis of Ni80Cr20 yields: Al 1000 ppm, Cr 18–20%, Fe 2000 ppm, Mn 2000 ppm, Si 1.5%, rest: Ni + Co [6]. Investigations were made on wire-shaped specimens (diameter nominal 0.5 mm) purchased from Advent Research Materials Ltd. Commercial names of this alloy are Nichrome® and Tophet®. It is used for electric resistance heating elements. The amount of 1.5% Si makes it a ternary alloy. Therefore, the use of a binary Ni-Cr phase diagram is not applicable to obtain solidus and liquidus temperatures. DTA measurements (STA 409 Netzsch, Selb, Germany), used for the following calculations, delivered solidus temperature T_S: 1661 K and liquidus temperature T_l: 1676 K ± 7 K. For the data evaluation, a density at room temperature of 8400 kg m^{-3} was used [7].

* Corresponding author. Tel.: +43 3168738649; fax: +43 3168738655.
E-mail addresses: thomas.huepf@tugraz.at (T. Hüpf), pottlacher@tugraz.at (G. Pottlacher).

[1] The name Ni80Cr20 is used throughout this paper regardless of the fact that the alloy contains 1.5% Si.

0040-6031/$ – see front matter © 2009 Elsevier B.V. All rights reserved.
doi:10.1016/j.tca.2009.04.015

When using this fast pulse-heating technique, wire shaped specimens are clamped in the center of a discharge chamber. During the experiment, a current pulse of about 10^5 A is conducted through the sample for several μs. Due to its ohmic resistivity, it heats rapidly (about 10^8 K/s). This high heating rate is the crucial point of this technique. It provides mechanical stability of the sample, even after the melting transition. The liquid sample with cylindrical geometry keeps its shape while it continues heating. At the boiling point the drastic volume increase leads to the so called 'wire explosion'. In summary this technique provides containerless handling of liquid metals and the short experimental duration (typically 50 μs) prevents chemical reactions.

The apparatus at TU Graz allows for several simultaneous measurements: Temperature is recorded by means of pyrometry under the assumption of a constant emissivity throughout the liquid phase (see [8] for more details on the legitimacy of this assumption). The surface radiation of the samples was detected with a pyrometer working at 1570 nm (FWHM 84 nm). The melting transition with its characteristic plateau in the voltage output of the pyrometer was used as calibration point (1676 K, end of melting). The two phase region of Ni80Cr20 is very narrow. This leads to a flat melting plateau. The current through the sample is recorded with an induction coil and real-time integration (Pearson-probe). Two knife-edge contacts, directly placed on the wire, provide the voltage drop. A fast CCD camera system is used to measure the volume expansion and the change of the sample geometry. To monitor the expanding diameter of the wire, it was backlit with a photoflash and a magnified picture was imaged by a specially designed CCD camera [9], which delivers a shadowgraph picture of a small portion of the wire each 5 μs. The diameter at room temperature is measured prior to the experiment with a digital laser-micrometer (Keyence, LS-7010) and the CCD profiles can be calibrated on the basis of this measurement.

By modifying experimental parameters it is possible to get pictures at different selected temperatures. These parameters are on the one hand the charging voltage of the capacitor bank (which acts as energy storage for the discharge current)—a slight increase leads to a higher heating rate and consequently the temperature is higher at the moment the CCD pictures are taken. On the other hand the framing sequence of the CCD camera can be shifted relatively to the heating process in steps of one microsecond. Thus an expansion picture can be 'directed' to every selected temperature.

From temperature dependent current, voltage and sample geometry, thermophysical properties such as enthalpy, electrical resistivity, density, thermal conductivity and thermal diffusivity as a function of temperature are calculated following the equations in Chapter 3. A detailed description of the experimental setup is given in [10].

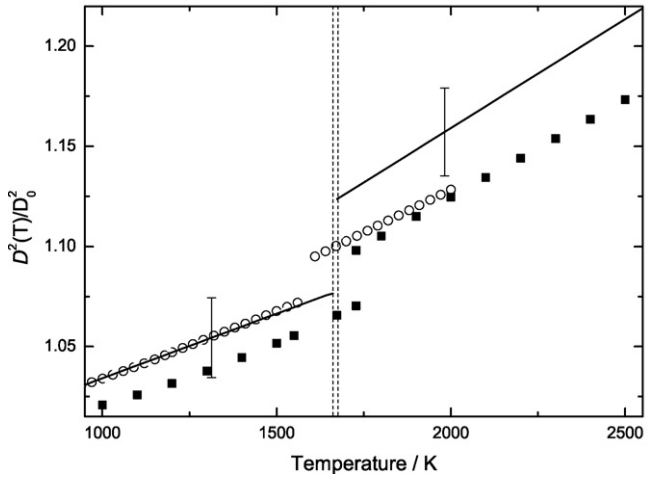

Fig. 1. Volume expansion ($D^2(T)/D_0^2$) of Ni80Cr20, nickel and Inconel 718 as a function of temperature. Solid lines: Ni80Cr20, filled squares: results for nickel [3], open circles: Inconel 718 [5], vertical dashed lines: solidus 1661 K and liquidus 1676 K.

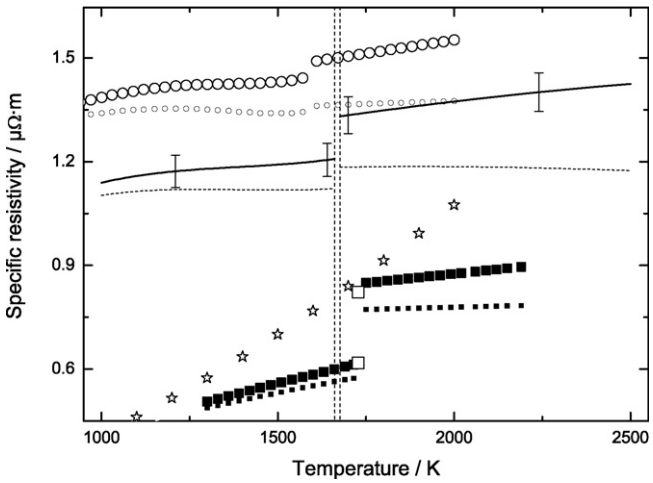

Fig. 2. Specific electrical resistivity of Ni80Cr20, nickel and Inconel 718 as a function of temperature. Solid lines: Ni80Cr20 including thermal expansion, dashed lines: Ni80Cr20 with initial geometry, filled squares: nickel [3] (big: including thermal expansion, small: without thermal expansion), open circles: Inconel 718 [5] (big: including thermal expansion, small: without thermal expansion), open stars: extrapolation of literature values of [11] for pure chromium, open rectangle: recommended value of [12] for Ni at T_m, vertical dashed lines: solidus 1661 K and liquidus 1676 K.

The PC for data recording is placed inside a shielded room because the rapid alteration of electrical current can lead to disturbing electromagnetic fields. Each cable is run inside a copper pipe connected to this faraday-room. Sensitive electronics are placed in boxes of aluminum. Where necessary, TTL signals are converted to optical signals conducted in fiber optics to prevent electrical contact.

3. Results

3.1. Volume expansion

Fig. 1 presents the results of volume expansion obtained from ten independent measurements. The results in the vicinity of melting are excluded from the fits. In order to correspond to the cross section of the wire, the squares of the diameters are used.

The linear least squares fit for the solid phase is

$$D^2(T)/D_0^2 = 0.969 + 6.474 \times 10^{-5} T \quad 1000\,\mathrm{K} < T < 1661\,\mathrm{K} \tag{1}$$

and for the liquid phase

$$D^2(T)/D_0^2 = 0.941 + 1.091 \times 10^{-4} T \quad 1676\,\mathrm{K} < T < 2600\,\mathrm{K} \tag{2}$$

with D_0 being the diameter at room temperature.

3.2. Resistivity

Specific electrical resistivity of Ni80Cr20 as a function of temperature is shown in Fig. 2, together with the results for pure nickel [3] and Inconel 718 [5] (to maintain clearness of the plots, points are displayed regardless of the fact that the cited papers report polynomials). Resistivity with initial geometry ρ_{IG} (without considering thermal expansion) was calculated by the equation

$$\rho_{IG}(T) = \frac{U(T) \cdot \pi \cdot r^2}{I(T) \cdot l} \tag{3}$$

with U: voltage drop, I: current, r: radius at room temperature, l: length.

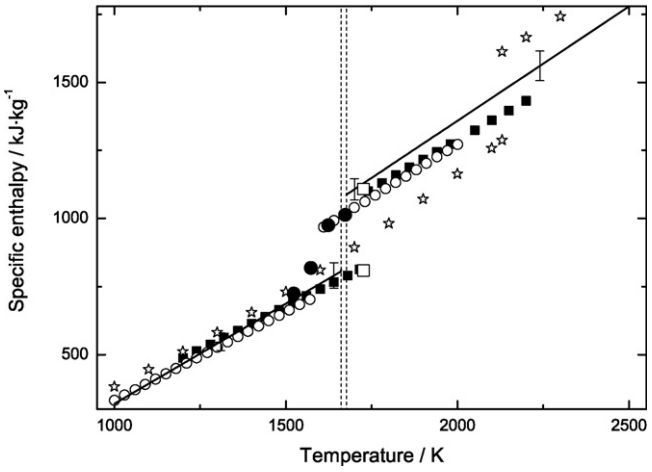

Fig. 3. Specific enthalpy of Ni80Cr20, nickel and Inconel 718 as a function of temperature. Solid lines: Ni80Cr20, filled squares: nickel [3], open circles: Inconel 718 [5], open rectangles: literature values of [13] for Ni, open stars: estimated value of [14] for Cr, full circles: literature values of [15] for Inconel 718, vertical dashed lines: solidus 1661 K and liquidus 1676 K.

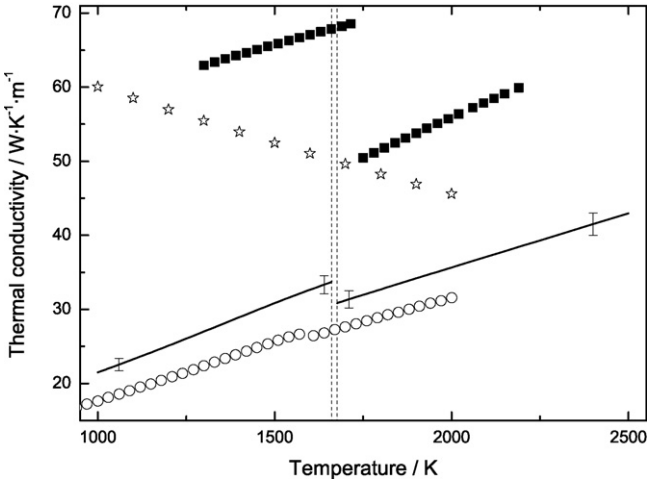

Fig. 4. Thermal conductivity of Ni80Cr20, nickel and Inconel 718 as a function of temperature. Solid lines: Ni80Cr20, filled squares: nickel (converted from [3]), open circles: Inconel 718 [5], open stars: literature values converted from [11], vertical dashed lines: solidus 1661 K and liquidus 1676 K.

The polynomial least squares fits for ρ_{IG} are (in μΩm)

$$\rho_{IG}(T) = 0.121 + 2.186 \times 10^{-3}T - 1.585 \times 10^{-6}T^2 + 3.806 \times 10^{-10}T^3 \quad 1100\,K < T < 1661\,K \tag{4}$$

for the solid phase and

$$\rho_{IG}(T) = 1.071 + 1.210 \times 10^{-4}T - 3.190 \times 10^{-8}T^2 \quad 1676\,K < T < 2500\,K \tag{5}$$

for the liquid phase. During the melting transition $\rho_{IG}(T)$ changes from 1.123 μΩm to 1.184 μΩm, which yields a resistivity change $\Delta\rho$ of 0.061 μΩm.

To account for volume expansion, changing the actual sample diameter, the resistivity with initial geometry $\rho_{IG}(T)$ has to be multiplied by $(D^2(T)/D_0^2)$ to obtain $\rho(T)$. The least squares fits are

$$\rho(T) = 0.022 + 0.240 \times 10^{-2}T - 1.689 \times 10^{-6}T^2 + 4.055 \times 10^{-10}T^3 \quad 1100\,K < T < 1661\,K \tag{6}$$

for the solid phase and

$$\rho(T) = 0.980 + 2.725 \times 10^{-4}T - 3.777 \times 10^{-8}T^2 \quad 1676\,K < T < 2500\,K \tag{7}$$

for the liquid phase. During the melting transition $\rho(T)$ changes from 1.207 μΩm to 1.331 μΩm, which yields a resistivity change $\Delta\rho$ of 0.124 μΩm.

3.3. Enthalpy and isobaric heat capacity

Specific enthalpy H was calculated from the electrical signals current and voltage drop by the equation:

$$H(t) - H(293\,K) = \frac{1}{m}\int I(t)\cdot U(t)dt \tag{8}$$

Herein m represents the mass of the sample obtained from the geometry and the density at RT (8400 kg m^{-3} [7]).

Results of specific enthalpy, $H - H_{RT}$ (starting at room temperature RT), as a function of temperature are shown in Fig. 3. Linear fits representing the measurement results are (in kJ kg^{-1})

$$H(T) = -417.3 + 0.737T \quad 1100\,K < T < 1661\,K \tag{9}$$

for the solid and

$$H(T) = -321.2 + 0.840T \quad 1676\,K < T < 2500\,K \tag{10}$$

for the liquid state, respectively. At the melting transition $H(T_s) = 807$ kJ kg^{-1} and $H(T_l) = 1087$ kJ kg^{-1}; thus a heat of fusion of $\Delta H = 280$ kJ kg^{-1} is obtained.

From its definition as the temperature derivative of enthalpy (under constant pressure), isobaric heat capacity c_p can be obtained from the slope of the linear enthalpy fits. The value for heat capacity in the solid state $c_{p,s}$ should only be regarded as a rough estimate and is limited to a narrow temperature range before the onset of melting, $c_{p,s} = 737$ J kg^{-1} K^{-1}. For the liquid phase $c_{p,l} = 840$ J kg^{-1} K^{-1} is obtained.

3.4. Thermal conductivity and thermal diffusivity

Thermal conductivity λ is calculated using the Wiedemann–Franz law.

$$\lambda(T) = \frac{L\cdot T}{\rho(T)} \tag{11}$$

The theoretical Lorenz-number L of 2.45×10^{-8} V^2 K^{-2} was taken as a first approach, although it may vary for different materials [16].

Results of thermal conductivity λ as a function of temperature are shown in Fig. 4. The linear fits (in W K^{-1} m^{-1}) are given by

$$\lambda(T) = 2.579 + 0.019T \quad 1100\,K < T < 1661\,K \tag{12}$$

for the solid, and by

$$\lambda(T) = 6.177 + 0.015T \quad 1676\,K < T < 2500\,K \tag{13}$$

for the liquid state. Thermal diffusivity a (in 10^{-5} m^2/s), calculated from

$$a(T) = \frac{L\cdot T}{\rho_{IG}\cdot c_p\cdot d} \tag{14}$$

with d: density at RT, is given by

$$a(T) = 1.573 \times 10^{-3} + 3.525 \times 10^{-4}T \quad 1100\,K < T < 1661\,K \tag{15}$$

$$a(T) = -5.178 \times 10^{-3} + 2.958 \times 10^{-4}T \quad 1676\,K < T < 2500\,K \tag{16}$$

More details on the calculations, the actual value of the Lorenz-number and a discussion of its influence on the uncertainty budget are given in [10].

4. Discussion

The phase diagram for Ni80Cr20 shows no phase transition in the solid state. The two phase region is very narrow (1661–1676 K) and subsequently the measured temperature traces show a flat melting plateau. The solidus–liquidus temperatures of the alloy are lower than the melting temperatures of its pure elements. DTA measurements yielded the transition temperatures of the material, which are slightly lower than the temperatures in the phase diagram of the binary Ni80Cr20 that may be expected due to the amount of 1.5% Si.

No measurements can be performed on pure chromium with our technique, because it is too brittle to be drawn as a wire. Therefore, the results for Ni80Cr20 are compared to the respective results for pure nickel and Inconel 718 which are described in detail in [3] and [5]. Although this work is based on a comparison inside a goal-oriented selection of materials measured under the same experimental conditions, the numerical values are of course to be compared with different techniques – that is to say literature values – as well. Thus we have added some to the graphs. A detailed comparison of nickel measurements was performed in [3], for Inconel 718 see [4] and [5].

The volume expansion (Fig. 1) of Ni80Cr20 is somewhat higher than the one of pure nickel. In the solid state Ni80Cr20 almost coincides with Inconel 718, but in the liquid state it is higher. The differences are very small and are not significant.

The electrical resistivity values are depicted in Fig. 2. Nickel has the lowest resistivity values, Inconel 718 the highest. The traces of each material are very similar, but differ in their absolute value. At 1676 K Inconel 718 has a resistivity of 1.502 μΩm, Ni80Cr20 has 1.331 μΩm, nickel: 0.604 μΩm and chromium approximately 0.750 μΩm. Ni80Cr20 is closer to the highly alloyed material Inconel 718 than to pure nickel in respect of resistivity. Additionally some datapoints of Zinovĭyev [11] (average data) for pure chromium are displayed to demonstrate, that the mixture of nickel and chromium does in no way lead to an average or weighted resistivity, but delivers much higher resistivity values. As expected, the (solid) solution has a higher electrical and thermal conductivity. The nickel values at melting agree very well with literature values of [12].

Fig. 3 depicts the results for enthalpy. Ni80Cr20 exhibits a slightly higher increase with increasing temperature than nickel and Inconel 718 and subsequently its heat capacity is higher too. The heat capacities in the liquid state are: Inconel 718: 778 J kg^{-1} K^{-1}, Ni80Cr20: 840.0 J kg^{-1} K^{-1}, nickel: 720.0 J kg^{-1} K^{-1}, chromium: 715.3 J kg^{-1} K^{-1} estimated value of [14]. Literature values for nickel [13] and Inconel 718 [15] at melting almost coincide with our respective measurements. The added literature values for chromium [14] clearly display, that the melting point of chromium is by far the highest out of this material selection (this complicates the interpretation of Fig. 3 and Fig. 2). Enthalpy values of all considered metals are very similar.

As the trends of thermal conductivity and thermal diffusivity are very similar, Fig. 4 depicts thermal conductivity only. It is evident, that the traces calculated according to (11) contain the reciprocal of the electrical resistivity. The strong resistivity increase of chromium with increasing temperature leads to a reversal of the trend in thermal conductivity (decreasing with increasing temperature).

It can be seen in Figs. 2 and 3 that the electrical resistivity as a transport property is much more sensitive to changes in composition. Heat capacities can be assumed similar to the respective pure elements, whereas electrical resistivity undergoes drastic changes. In the case of resistivity and thermal conductivity, Ni80Cr20 falls in the gap between pure nickel and Inconel 718. In the case of volume expansion and enthalpy the differences are alternating and too small to be judged.

5. Uncertainty

During the calculation of uncertainties two approaches are commonly used: the GUM [17] method, which obtains uncertainty by considering the propagation of the respective uncertainty of each input parameter and the (traditional) statistic approach, which obtains uncertainty by looking at the distribution of results.

Depending on the experimental setup and data acquisition the experimentalist chooses in which way uncertainty is calculated. Two examples will show that there can be contradicting results (for more details see [18]): If all experimental points are on a straight line, the statistic standard-deviation for the linear regression will be zero although the measurement devices can be defective. On the other hand, if the input parameters are exact but the results show big scattering, the statistic standard-deviation is exceeding the uncertainty calculated according to GUM (which in this case is zero).

The measurements performed in this work are of type one (statistic standard-deviation would deliver implausible small uncertainties) as the reproducibility is high. Only the thermal expansion measurements lead to considerable scattering. The significance of its fits can be increased by increasing the number of experimental points. Thus the statistic approach is the better choice.

The uncertainty analysis according to GUM [17] yields the following relative uncertainties for the Ni80Cr20 results (coverage factor 2): temperature: T: 2.5% (possible changes of emissivity in the liquid state not considered); enthalpy H: 3.5%; specific heat capacity c_p: 8%; specific electrical resistivity (at initial geometry) ρ_{IG}: 2.6%; electrical resistivity (including expansion) ρ: 3.3%; thermal conductivity (excluding the influence of the Lorenz number) λ: 3.7%; thermal diffusivity a: 8.8%. An elaborate uncertainty analysis of the measurements with the pulse-heating equipment at TU Graz according to GUM is given in [19].

Volume expansion (D^2/D_0^2): standard-deviation σ: 0.011, expressed as relative uncertainty with coverage factor 2: 2% (number of points: 25); diameter at room temperature D_0: ±1 μm (0.2%);

6. Conclusion

Investigations of alloys like Ni80Cr20 are currently in the focus of interest as they bridge the gap between pure elements and highly alloyed materials. The results for Ni80Cr20 are presented in this work and are compared to pure nickel and Inconel 718 measured under the same experimental conditions. They reveal that different types of connections are possible: First, the behaviour of the alloy is different from the average of its main constituents (see electrical resistivity). Regarding the possible applications of this alloy as heating elements, a higher electrical resistivity is wanted. Second, electrical resistivity of Ni80Cr20 is between nickel and Inconel 718 (but closer to Inconel 718). Third, the differences in specific enthalpy (Fig. 3) and volume expansion (Fig. 1) are small.

Acknowledgment

The project *Electrical Resistivity Measurement of High Temperature Metallic Melts* is sponsored by the Austrian Space Applications Programme (ASAP) of the FFG, Sensengasse 1, 1090 Wien.

References

[1] E. Kaschnitz, G. Pottlacher, Thermophysikalische Eigenschaften von Gießwerkstoffen, Giessereipraxis 1 (2002) 23–28.
[2] E.A. Loria (Ed.), Superalloy 718—Metallurgy and Application, The Minerals, Metals & Materials Society, TMS, Warrendale, 1989.
[3] B. Wilthan, C. Cagran, G. Pottlacher, Int. J. Thermophys. 25 (5) (2004) 1519–1534.
[4] G. Pottlacher, H. Hosaeus, E. Kaschnitz, A. Seifter, Scand. J. Metall. 31 (2002) 161–168.

[5] C. Cagran, W. Hohenauer, G. Pottlacher, Inconel 718—A Collection of Thermophysical Data from Quasistatic- and Transient-Measurement Techniques, in press.
[6] http://www.advent-rm.com (2008).
[7] http://www.goodfellow.com (2008).
[8] C. Cagran, C. Brunner, A. Seifter, G. Pottlacher, High Temp.—High Press. 34 (2002) 669–679.
[9] K. Preis, Thermophysikalische Daten von Nimonic 80A in der festen und flüssigen Phase, Diploma Thesis, Graz University of Technology, 2006.
[10] C. Cagran, T. Hüpf, B. Wilthan, G. Pottlacher, High Temp.—High Press. 37 (2008) 205–219.
[11] V. Zinovyev, Metals at High Temperatures—Standard Handbook of Properties, Hemisphere Publishing Corporation, New York, 1990.
[12] Y.S. Touloukian (Ed.), Properties of Selected Ferrous Alloying Elements, CINDAS Data Series on Material Properties III-1, McGraw-Hill Book Company, New York, 1981.
[13] H. Geoffray, A. Ferrier, M. Olette, Compt. Rend. 256 (1963) 139–141;
R. Hultgren, P.D. Desai, D.T. Hawkins, M. Gleiser, K.K. Kelley, D.D. Wagman (Eds.), Selected Values of the Thermodynamic Properties of the Elements, Metals Park, American Society for Metals, 1973.
[14] R. Hultgren, P.D. Desai, D.T. Hawkins, M. Gleiser, K.K. Kelley, D.D. Wagman, Selected Values of the Thermodynamic Properties of the Elements, Metals Park, American Society for Metals, 1973.
[15] C.M. Kenneth, Recommended values of thermophysical properties for selected commercial alloys, Woodhead Publishing Ltd and ASM International, Cambridge England, 2002.
[16] P.G. Klemens, R.K. Williams, Int. Met. Rev. 31 (5) (1986) 197–215.
[17] Leitfaden zur Angabe der Unsicherheit beim Messen, DIN Deutsches Institut für Normung, 1., Beuth Verlag, Berlin, 1995.
[18] M. Matus, Technisches Messen, Oldenbourg Verlag 72 (2005) 584–591.
[19] B. Wilthan, Verhalten des Emissionsgrades und thermophysikalische Daten von Legierungen bis in die flüssige Phase mit einer Unsicherheitsanalyse aller Messgrößen, PhD Thesis, Technische Universität Graz, Austria, 2005.

7.9 Thermophysical properties of five binary copper-nickel alloys

T. Hüpf, C. Cagran, E. Kaschnitz, G. Pottlacher, *Thermophysical properties of five binary copper-nickel alloys*, Int. J. Thermophys., accepted in March 2010.

The paper compares five copper-nickel alloys with the respective results obtained by electromagnetic levitation at the DLR in Cologne. The change of properties at different concentrations in the phase diagram is a famous link between theory and measurement.

Comments: The paper was written by myself in close collaboration with Dr. Erhard Kaschnitz concerning measurements and text. Dr. Cagran was my coworker in this project which was supervised by Prof. Pottlacher.

Int J Thermophys
DOI 10.1007/s10765-010-0732-x

Thermophysical Properties of Five Binary Copper–Nickel Alloys

Thomas Hüpf · Claus Cagran · Erhard Kaschnitz · Gernot Pottlacher

Received: 16 July 2009 / Accepted: 20 March 2010

Abstract Thermophysical properties (e.g., specific enthalpy, heat of fusion, electrical resistivity, thermal volume expansion) are measured in the liquid phase up to very high temperatures by an extreme fast pulse-heating method. Heating rates of about $10^8\,\mathrm{K}\cdot\mathrm{s}^{-1}$ are applied by self-heating of wire-shaped metallic specimens with a current of approximately 10,000 A. Pure elements seem to be still close to thermal equilibrium as the obtained results are in good agreement with those obtained by static methods. However, this situation might be different for alloys. The rapid volume heating can shift diffusion-controlled phase transitions at heating to higher temperatures or even make them not noticeable anymore. The simple binary Cu–Ni system was chosen to test the heating rate dependence; this system is well known and shows complete miscibility in the liquid and solid ranges of interest. This study is a further step to test the performance of the fast pulse-heating method being applied to simple and more complex alloys. Measured results of enthalpy, heat of fusion, heat capacity, and electrical resistivity in the vicinity of the melting range are presented. The results of enthalpy and heat capacity agree with simple mixing rules. The measured electrical resistivity of different compositions is compared to results obtained by electromagnetic levitation measurements.

Keywords Binary alloy · Copper · Electrical resistivity · Heat capacity · Liquid metals · Nickel

T. Hüpf · C. Cagran · G. Pottlacher (✉)
Institut für Experimentalphysik, Technische Universität Graz, Petersgasse 16, 8010 Graz, Austria
e-mail: pottlacher@tugraz.at

T. Hüpf
e-mail: thomas.huepf@tugraz.at

E. Kaschnitz
Österreichisches Gießerei-Institut, Parkstraße 21, 8700 Leoben, Austria

Journal: 10765-IJOT Article No.: 0732 TYPESET DISK LE CP Disp.:2010/3/31 Pages: 9 Layout: Small-X

1 Introduction

Microsecond pulse-heating experiments have been applied to a wide range of electrically conducting elements to obtain thermophysical properties at melting and in the liquid range. Despite the high heating rate (on the order of $10^8\,\mathrm{K}\cdot\mathrm{s}^{-1}$), the measured results agree well with data obtained by static and quasistatic methods. Recently, these methods have been extended to investigate alloys of technical interest. The more complex the alloys are the more non-equilibrium effects might influence the results of measurements with an increasing heating rate [1]. At the transition to the liquid phase and moderate heating rates, mass diffusion in the solid is more or less inhibited; the melting behavior can change dramatically. When the heating rate is further increased, the melting phase transition takes place almost without mass diffusion.

A simple binary alloy system (copper–nickel) with a small melting range and complete miscibility was chosen for this work to investigate different concentrations and to compare the results to properties of both pure elements, which have been extensively investigated by different authors [2–4]. The samples were die-cast and drawn to wires of 0.5 mm in diameter. Each composition (Cu85Ni15, $T_{\mathrm{sol}} = 1417\,\mathrm{K}$, $T_{\mathrm{liq}} = 1447\,\mathrm{K}$; Cu70Ni30, $T_{\mathrm{sol}} = 1472\,\mathrm{K}$, $T_{\mathrm{lig}} = 1520\,\mathrm{K}$; Cu55Ni45, $T_{\mathrm{sol}} = 1528\,\mathrm{K}$, $T_{\mathrm{liq}} = 1576\,\mathrm{K}$; Cu35Ni65, $T_{\mathrm{sol}} = 1599\,\mathrm{K}$, $T_{\mathrm{liq}} = 1638\,\mathrm{K}$; and Cu20Ni80, $T_{\mathrm{sol}} = 1656\,\mathrm{K}$, $T_{\mathrm{liq}} = 1678\,\mathrm{K}$; mass percent) was checked by chemical analysis (ICP spectral analysis, EDX). Solidus and liquidus temperatures close to equilibrium were partially measured by differential thermal analysis and are in very good agreement to literature values [5].

2 Experimental

During fast pulse-heating, wire-shaped specimens (diameter 0.5 mm, length 70 mm) are clamped in the center of a discharge circuit [6]. A capacitor (500 µF) is used as energy storage. The discharge vessel has windows for optical measurements (temperature, thermal expansion), and it provides the attachments for the voltage drop measurement along the wire performed by two knife-edge contacts which are directly touching the sample. The current is measured with an induction coil (Pearson-probe). The surface temperature is recorded with a high-speed pyrometer operated at 1570 nm (bandwidth approximately 85 nm). The melting plateau is used as a reference point, and temperatures are calculated with the assumption of a constant normal spectral emissivity throughout the liquid phase [7,8]. Thermal expansion is recorded by a fast CCD camera. The wire is backlit by a photoflash, and a magnified image is mapped on a multi-channel-plate, which acts as a fast shutter and amplifier [9].

As soon as the current starts, the sample is self-heating rapidly due to its ohmic resistivity. The high heating rate provides geometrical stability of the specimen for several tenths of microseconds even in the liquid phase; this timespan is long enough to perform the entire experiment. Additionally the short experimental time protects the specimen from chemical reactions.

The experimental parameters (e.g., charging voltage, neutral density filters for the pyrometer) were slightly different for each chemical composition of the alloy. An average of typically five individual measurements per composition was taken to calculate

Journal: 10765-IJOT Article No.: 0732 TYPESET DISK LE CP Disp.:2010/3/31 Pages: 9 Layout: Small-X

the specific enthalpy, heat capacity, and electrical resistivity. Independently of that, 12 measurements for each composition were made to obtain thermal volume expansion from optical measurements.

3 Results

3.1 Enthalpy, Heat of Fusion, and Isobaric Heat Capacity

The specific enthalpy H as a function of time t was calculated using the equation,

$$H(t) = \frac{1}{m} \int_0^t I(\tau)\, U(\tau)\, \mathrm{d}\tau, \tag{1}$$

where m is the mass of the sample, I is the current, and U is the voltage drop.

The linear least-squares fits for the liquid phase are shown in Table 1 and Fig. 1. Figure 2 shows enthalpy values at 1750 K (dashed line in Fig. 1) as a function of nickel content. The heat of fusion ΔH was obtained as the difference of H between T_{sol} and

Table 1 Specific enthalpy, heat of fusion, and heat capacity of five Cu–Ni alloys

	H (kJ·kg^{-1})	Range	ΔH (kJ·kg^{-1})	c_{p} (J·kg^{-1}·K)
Cu85Ni15	$-26.1+0.545\,T$	$1447\,\mathrm{K} < T < 2000\,\mathrm{K}$	246.9	545
Cu70Ni30	$-182.9+0.663\,T$	$1520\,\mathrm{K} < T < 2000\,\mathrm{K}$	275.0	663
Cu55Ni45	$-137.5+0.658\,T$	$1576\,\mathrm{K} < T < 2000\,\mathrm{K}$	286.6	658
Cu35Ni65	$-175.6+0.685\,T$	$1638\,\mathrm{K} < T < 2000\,\mathrm{K}$	286.1	685
Cu20Ni80	$-148.7+0.701\,T$	$1678\,\mathrm{K} < T < 2000\,\mathrm{K}$	291.3	701

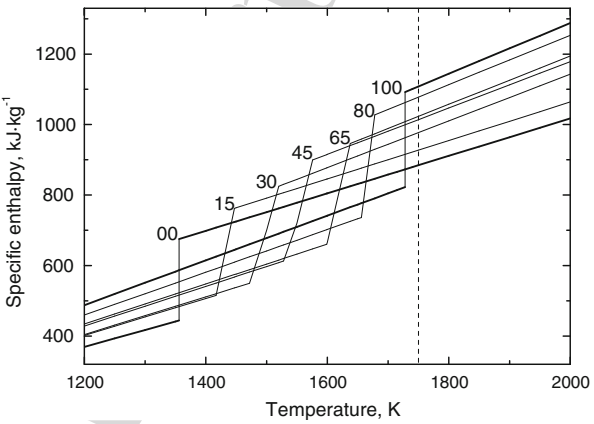

Fig. 1 Specific enthalpy of five Cu–Ni alloys, pure copper [2,3], and pure nickel [4] as a function of temperature; numbers refer to mass % nickel, *dashed line*: 1750 K (see Fig. 2)

Journal: 10765-IJOT Article No.: 0732 TYPESET DISK LE CP Disp.:2010/3/31 Pages: 9 Layout: Small-X

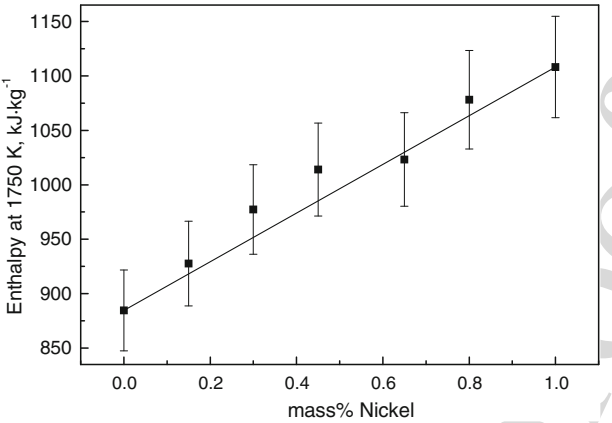

Fig. 2 Specific enthalpy of five Cu–Ni alloys, pure copper [2,3], and pure nickel [4] at 1750 K (as indicated by the *dashed line* in Fig. 1) as a function of nickel content; *solid line*: linear interpolation

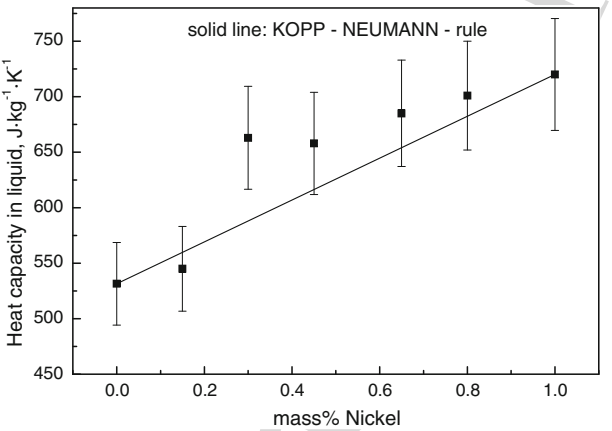

Fig. 3 Specific heat capacity of five Cu–Ni alloys, pure copper [2,3], and pure nickel [4] for the liquid phase as a function of nickel content; *solid line*: linear interpolation according to Kopp–Neumann rule

T_{liq} (subscript sol refers to solidus, liq to liquidus temperature). From its definition as the temperature derivative of enthalpy (under constant pressure), the isobaric heat capacity c_{p} can be obtained from the slope of the linear enthalpy fits (see Table 1). Figure 3 shows isobaric heat capacities for the liquid phase as a function of nickel content.

3.2 Resistivity

The electrical resistivity corresponding to the geometry at room temperature (initial geometry) ρ_{IG} was calculated using the equation,

$$\rho_{\mathrm{IG}}(t) = \frac{U(t)\pi r_0^2}{I(t)l}, \tag{2}$$

Journal: 10765-IJOT Article No.: 0732 TYPESET DISK LE CP Disp.:2010/3/31 Pages: 9 Layout: Small-X

Table 2 Electrical resistivity ρ and $\Delta\rho$ of five Cu–Ni alloys; subindex IG: with initial geometry

	ρ_{IG} ($\mu\Omega \cdot$ m)	ρ ($\mu\Omega \cdot$ m)	Range	$\Delta\rho$ ($\mu\Omega \cdot$ m)
Cu85Ni15	$0.325 - 1.968u \times 10^{-4}T + 1.140 \times 10^{-7}T^2$	$0.358 - 2.599 \times 10^{-4}T + 1.515 \times 10^{-7}T^2$	$1200\,K < T < 1417\,K$	0.150
	$0.276 + 7.763 \times 10^{-5}T$	$0.233 + 1.459 \times 10^{-4}T$	$1447\,K < T < 2000\,K$	
Cu70Ni30	$0.587 - 2.292 \times 10^{-4}T + 1.097 \times 10^{-7}T^2$	$0.673 - 3.609 \times 10^{-4}T + 1.746 \times 10^{-7}T^2$	$1200\,K < T < 1472\,K$	0.161
	$0.560 + 3.211 \times 10^{-5}T$	$0.482 + 1.309 \times 10^{-4}T$	$1520\,K < T < 2100\,K$	
Cu55Ni45	$0.647 - 2.905 \times 10^{-4}T + 1.338 \times 10^{-7}T^2$	$0.808 - 5.290 \times 10^{-4}T + 2.370 \times 10^{-7}T^2$	$1200\,K < T < 1528\,K$	0.188
	$0.625 + 2.702 \times 10^{-5}T$	$0.584 + 9.953 \times 10^{-5}T$	$1576\,K < T < 2100\,K$	
Cu35Ni65	$0.545 - 7.253 \times 10^{-5}T + 6.149 \times 10^{-8}T^2$	$0.528 - 4.267 \times 10^{-5}T + 6.463 \times 10^{-8}T^2$	$1200\,K < T < 1599\,K$	0.221
	$0.688 + 4.538 \times 10^{-5}T$	$0.610 + 1.438 \times 10^{-4}T$	$1638\,K < T < 2100\,K$	
Cu20Ni80	$0.441 + 2.309 \times 10^{-5}T + 4.130 \times 10^{-8}T^2$	$0.425 + 5.167 \times 10^{-5}T + 4.549 \times 10^{-8}T^2$	$1200\,K < T < 1656\,K$	0.234
	$0.751 + 1.919 \times 10^{-5}T$	$0.635 + 1.397 \times 10^{-4}T$	$1678\,K < T < 2100\,K$	

where r_0 is the sample radius at room temperature and l is the length. Due to the thermal volume expansion, the sample radius changes during the heating process. This can be considered by the following equation:

$$\rho(T) = \rho_{IG}(T)\frac{D(T)^2}{D_0^2}, \tag{3}$$

where D_0^2 is the diameter at room temperature squared and D is the diameter at elevated temperature measured by the fast CCD-camera.

The least-squares fits for both ρ_{IG} and ρ are shown in Table 2. Fits are made with polynomials of the appropriate low order. Figure 4 shows the resistivity results corrected for thermal expansion including results obtained by electromagnetic levitation [10].

4 Discussion

4.1 Temperature and Melting Behavior

The traces of the pyrometer output signal exhibit a slightly sloped plateau at the melting transition. Figure 5 shows a single experiment for Cu55Ni45 where the slope is most significant. It should be noted that the temperature of the onset and end of this plateau is not directly correlated to the equilibrium solidus and liquidus temperatures. Slight changes in emissivity as well as the noise influence the signal. The middle of

Journal: 10765-IJOT Article No.: 0732 TYPESET DISK LE CP Disp.:2010/3/31 Pages: 9 Layout: Small-X

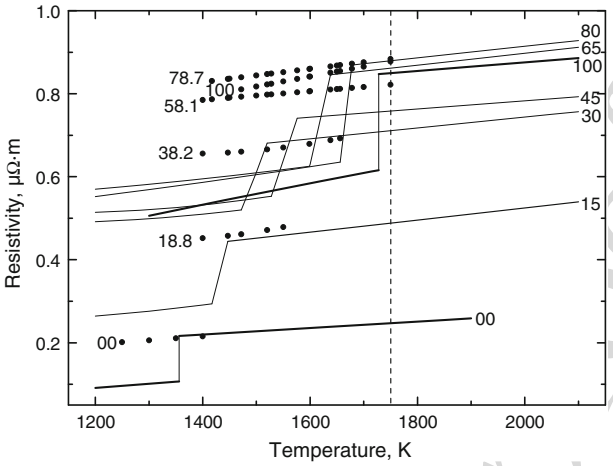

Fig. 4 Electrical resistivity of five Cu–Ni alloys, pure copper [2,3], and pure nickel [4] as a function of temperature; numbers refer to nickel content; *dots*: literature values measured by electromagnetic levitation [10], *open circles*: extrapolation of levitations measurements

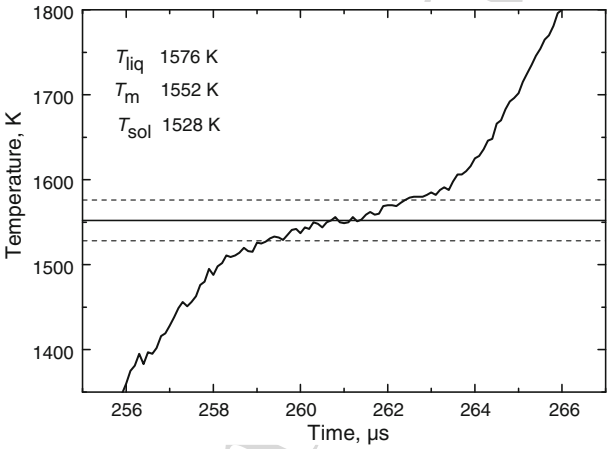

Fig. 5 Close up of the melting range in a temperature curve as a function of experimental time for a single experiment on Cu55Ni45. *Solid horizontal line*: arithmetic mean of solidus and liquidus temperature (*dashed lines*) which was assigned to the middle of the melting plateau

the plateau was used to assign the arithmetic mean of the solidus and liquidus temperatures of the phase diagram as a reference point for the temperature measurement. The temperature is calculated by Planck's law with the assumption of a constant normal spectral emissivity throughout the liquid phase [7]. Basak et al. [1] report for a binary NbTi-alloy that the heating rate (and grain size) can affect the melting behavior. Assuming a local equilibrium at the phase boundary at a moderate heating rate (max. $5 \times 10^3\ \mathrm{K \cdot s^{-1}}$), the melting range tends to be a plateau which converges to the liquidus temperature. For heating rates of approximately $10^8\ \mathrm{K \cdot s^{-1}}$ as used for this work, this approach is not applicable, as full diffusion in the liquid fraction at melting cannot

Journal: 10765-IJOT Article No.: 0732 TYPESET DISK LE CP Disp.:2010/3/31 Pages: 9 Layout: Small-X

take place. For a full understanding of melting at these high speeds, measurements of normal spectral emissivity at melting and a theoretical approach to diffusionless melting have to be included in the future. Since the melting range of copper–nickel alloys is reasonably small, the influence of the uncertainty of the temperature reference point on the temperature measurement is limited.

4.2 Enthalpy and Heat Capacity

Figure 1 compares the traces of the five CuNi alloys with pure copper and pure nickel as a function of temperature. The dashed line (1750 K) represents the vertical section which is displayed in Fig. 2. Both figures show that the variation of enthalpy as a function of composition is more or less a linear function between the two pure elements.

The Kopp–Neumann rule predicts such a linear behavior for the specific heat capacity:

$$c_{p12} = \omega_1 c_{p1} + \omega_2 c_{p2}, \tag{4}$$

where ω_1 and ω_2 are the mass fractions of the constituent elements and c_{p1} and c_{p2} are their respective heat capacities. Figure 3 shows the specific heat capacity as a function of composition; within our uncertainties the results follow more or less the Kopp–Neumann rule. The specific heat capacity value at approximately 30 mass % Ni is higher than expected by the Kopp–Neumann rule. No explanation can be given for this behavior which indicates that the linear function in Fig. 2 is abandoned with increasing temperature.

4.3 Electrical Resistivity

Figure 4 shows the results of the electrical resistivity as a function of temperature for the range of chemical compositions in the copper–nickel binary alloy system. The resistivity of pure copper is significantly lower than an alloyed material. The resistivity increases rapidly with the amount of alloyed nickel and reaches a maximum at approximately 80 mass % nickel. The only results available in the literature with which to compare are obtained with different compositions by a levitation technique [10]. These values are partially gained in the undercooled liquid state. A comparison of the undercooled values to our results can be made by an extension to the regular liquid phase. There is a reasonable agreement between the quasi-static levitation measurement results and the results of this work, obtained by extreme fast heating.

A vertical section of the resistivity function at 1750 K is displayed in Fig. 6. It should be noted that the models for the electrical resistivity, which are discussed subsequently, refer to atoms and hence are described in mole fractions. The figure shows the obtained resistivity measurement results as well as a function obtained by an ideal solution model and the Nordheim rule converted into wt % to be consistent to prior text and images. A literature value for pure nickel [11] was added to the plot. The ideal

Journal: 10765-IJOT Article No.: 0732 TYPESET DISK LE CP Disp.:2010/3/31 Pages: 9 Layout: Small-X

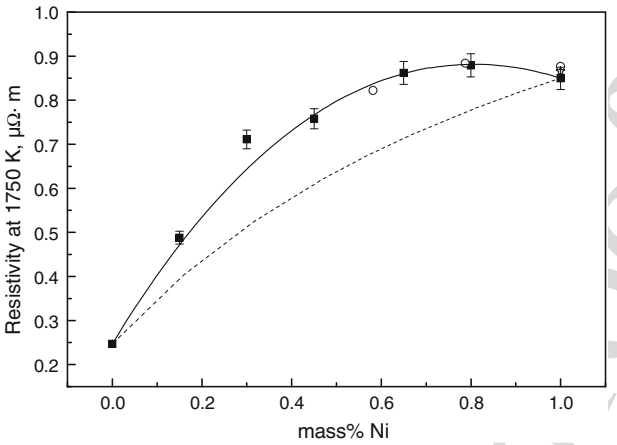

Fig. 6 Electrical resistivity of five Cu–Ni alloys, pure copper [2,3], and pure nickel [4] at 1750 K; *open circles*: literature values measured by electromagnetic levitation [10]; *open star*: literature value converted from [11]; *solid line*: Eq. 5; *dashed line*: Eq. 6

146 solution model calculates the resistivity by,

147 $$\rho = \frac{\sum_i x_i Z_i \rho_i}{\sum_i x_i Z_i}, \tag{5}$$

148 where x_i is the concentration of element i, Z_i is the number of s-band electrons, and
149 ρ_i is the resistivity of the pure component ($Z_{\mathrm{Cu}} = 1$ and $Z_{\mathrm{Ni}} = 2$). The Nordheim
150 rule is calculated by,

151 $$\rho = x_{\mathrm{Ni}}\rho_{\mathrm{Ni}} + (1 - x_{\mathrm{Ni}})\rho_{\mathrm{Cu}} + x_{\mathrm{Ni}}(1 - x_{\mathrm{Ni}})\rho_{\mathrm{Ni,Cu}}, \tag{6}$$

152 where $\rho_{\mathrm{Ni,Cu}}$ is a fit parameter which was found to be $95 \times 10^{-8}\Omega \cdot \mathrm{m}$.
153 Again, the resistivity value at approximately 32 at. % Ni is significantly higher than
154 expected by the Nordheim rule and therefore was excluded from the fit.

155 5 Summary

156 Experimental results of enthalpy, heat capacity, and electrical resistivity of binary cop-
157 per–nickel alloys are presented in this work. It shows that fast pulse-heating can be
158 applied to binary alloys with a small melting range that are miscible in the solid and
159 liquid. The results agree with that obtained by quasi-static measurements. However,
160 for more complex alloys, the behavior of melting in very short time spans needs to be
161 further analyzed.

Journal: 10765-IJOT Article No.: 0732 TYPESET DISK LE CP Disp.:2010/3/31 Pages: 9 Layout: Small-X

6 Uncertainties

A detailed analysis of the estimation of uncertainties is given in [12]. Uncertainties calculated according to GUM [13] are as follows (relative uncertainties with a coverage factor $k = 2$): enthalpy in the solid state: $H_{sol} \pm 6\,\%$; enthalpy in the liquid state: H_{liq}: 4 %; specific heat capacity: $c_{p,sol}$: 7 %; $c_{p,liq}$: 7 %; electrical resistivity with initial geometry: $\rho_{IG,sol}$: 3 %; $\rho_{IG,\ liq}$: 3 %; electrical resistivity: ρ_{sol}: 4 %; ρ_{liq}: 4 %.

A possible change of the normal spectral emissivity throughout the liquid phase is not considered [7].

Acknowledgements This work was supported by the Austrian Space Applications Programme (ASAP), the Basisprogramm of the Österreichische Forschungsförderungsgesellschaft mbH (FFG), and the Steirische Wirtschaftsförderungsgesellschaft mbH (SFG).

References

1. D. Basak, W.J. Boettinger, D. Josell, S.R. Coriell, J.L. McClure, S. Krishnan, A. Cezairliyan, Acta Mater. **47**, 3147 (1999)
2. C. Cagran, A. Seifter, G. Pottlacher, *Thermophysical Properties of Solid and Liquid Copper,* Schriften Des Forschungszentrums, Jülich Ser. Energy Technol. **15**, 763 (2000)
3. G.Nussbaumer, *Weiterentwicklung der zeitaufgelösten Expansions-und Spannungsmessung bei Mikrosekunden-Pulsheizexperimenten–Bestimmung thermophysikalischer Daten von Kupfer und Gold*. Diploma-Thesis, Institute of Experimental Physics, Graz University of Technology (1993)
4. B. Wilthan, C. Cagran, G. Pottlacher, Int. J. Thermophys. **25**, 1519 (2004)
5. S.A. Mey, Calphad **16**, 255 (1992)
6. E. Kaschnitz, G. Pottlacher, H. Jäger, Int. J. Thermophys. **13**, 699 (1992)
7. T. Hüpf, C. Cagran, G. Pottlacher, *Pyrometrische Temperaturmessung – Einfluss des Emissionskoeffizienten auf die Bestimmung thermophysikalischer Daten*. Proceedings: TEMPERATUR2009 (2009)
8. G. Pottlacher, A. Seifter, Int. J. Thermophys. **23**, 1281 (2002)
9. B. Wilthan, H. Reschab, R. Tanzer, W. Schützenhöfer, G. Pottlacher, Int. J. Thermophys. **29**, 434 (2008)
10. G. Lohöfer, J. Brillo, I. Egry, Int. J. Thermophys. **25**, 1535 (2004)
11. E. Kaschnitz, J.L. McClure, A. Cezairliyan, Int. J. Thermophys. **15**, 757 (1994)
12. C. Cagran, T. Hüpf, B. Wilthan, G. Pottlacher, High Temp. High Press. **37**, 205 (2008)
13. *Guide to the expression of uncertainty in measurement* (ISO, Geneva, 1993)

Journal: 10765-IJOT Article No.: 0732 TYPESET DISK LE CP Disp.:2010/3/31 Pages: 9 Layout: Small-X

7.10 Two ways of looking at the intermediate position of binary alloys

T. Hüpf, C. Cagran, G. Pottlacher, *Two ways of looking at the intermediate position of binary alloys*, Poster presented at the ÖPG in Innsbruck, 2009.

The poster analyzes the methodology of investigations on binary alloys.

Comments: The poster was designed by myself with the help of Dr. Cagran and Prof. Pottlacher.

Two ways of looking at the intermediate position of binary alloys

Pulse heating results of Ni80Cr20 and five CuNi alloys

Thomas Hüpf
Claus Cagran
Gernot Pottlacher

Institut für Experimentalphysik
Technische Universität Graz
Austria

thomas.huepf@tugraz.at

Introduction

Plenty of research is done on binary alloys. They contain a lot of ‚physics' and this is why phase diagrams are a big topic in physics lectures as well.

Without going into the details of thermodynamics, one can already think about binary alloys in two different contexts:

Horizontal: By gradually changing the composition, one starts with a pure element and ends up with a second pure element, thus exploring the phase diagram of any property of interest.

Vertical: Starting with a base material (e.g. nickel), one can select additives in different quantities to finally achieve a highly alloyed material with designated properties. The first steps pass through binary and ternary phase diagrams which are still capable for deductive procedures whereas the endmost steps essentially depend on experience (not to say business secrets).

Inconel 718

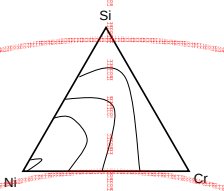

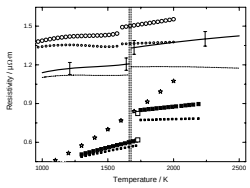

Principles of pulse-heating

Thermophysical properties (e.g. specific enthalpy, heat of fusion, electrical resistivity, thermal volume expansion) can be measured in the liquid phase up to very high temperatures by extreme fast pulse-heating methods as used by the authors. Heating rates of about 10^8 K/s are achievable by resistive self-heating of a metallic specimen with a current of approximately 10 000 A.

The figure shows a wire prepared for experiment. A CCD-camera delivers a picture of the expanding wire each 5 µs. The evaluation thereof gives the graph D^2/D_0^2 vs. temperature (red circles: data from one single experiment).

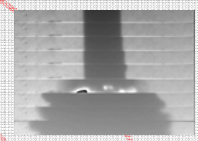

Cu

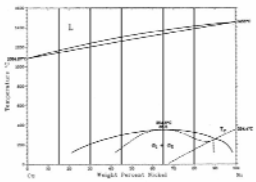

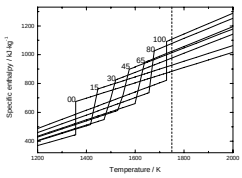

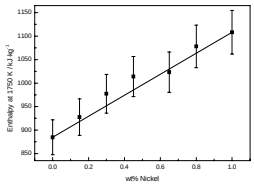

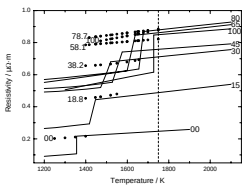

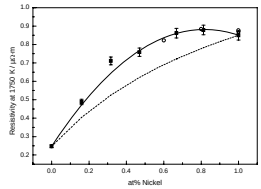

Ni

The samples

Our measurements on five CuNi-alloys and Ni80Cr20 have been interpreted according to these two approaches.

The CuNi samples were die cast at OGI (Österreichisches Gießerei-Institut Leoben). The nominal compositions can be seen in the phase diagram (solid vertical lines). DTA measurements delivered solidus and liquidus temperature used for subsequent calculations.

For the measurement with our pulse-heating apparatus the samples were drawn to wires with 0.5 mm in diameter.

Ni80Cr20 was already achieved in the form of a wire. As this alloy contains 1.5 wt% Si, it was again necessary to perform DTA measurements to get solidus and liquidus. Ni80Cr20 was choosen for experiment because it bridges the gap between nickel and the highly alloyed material Inconel 718, which consistis of about 53% nickel and 18% chromium.

Results 1 (vertical)

The results of Ni80Cr20 [1] for specific electrical resistivity indeed show this intermediate position. Inconel 718 has a higher, nickel and chromium a lower resistivity than Ni80Cr20. Specific enthalpy results are almost an average value of the pure ingredients. This is the expected behavior for bulk-properties, whereas transport-properties can undergo drastic changes during alloying. 1.5% Si make Ni80Cr20 a ternary alloy.

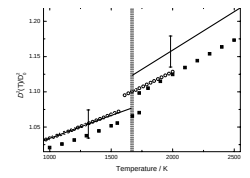

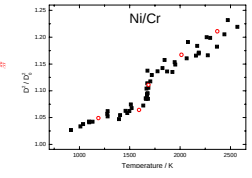

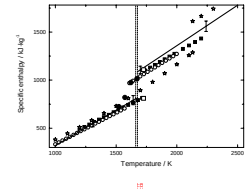

Ni, Cr

Results 2 (horziontal)

The figures display specific enthalpy, heat of fusion, heat capacity, and electrical resistivity (numbers refer to wt% nickel) [2]. Two sections at 1750 K allow a discussion as a function of composition. In the case of resistivity, values of DLR, measured by electromagnetic levitation, are added to the plots (circles).

The dashed line represents the ideal solution model (left)

$$\rho = \frac{\sum_i x_i \cdot Z_i \cdot \rho_i}{\sum_i x_i \cdot Z_i}, \qquad \rho = x_{Ni} \cdot \rho_{Ni} + (1 - x_{Ni}) \cdot \rho_{Cu} + x_{Ni} \cdot (1 - x_{Ni}) \cdot \rho_{Ni,Cu}.$$

The solid line represents the Nordheim rule (right) with fit parameter $\rho_{Ni,Cu} = 95 \times 10^{-8}\ \Omega\cdot m$.

These results show, that pulse-heating can be applied to binary alloys with a small melting range that are miscible in the solid and liquid. They agree with quasi-static measurements.

References:

[1] T. Hüpf, C. Cagran, E. Kaschnitz, G. Pottlacher 2009 *Thermochimica Acta* doi: 10.1016/j.tca.2009.04.015.

[2] T. Hüpf, C. Cagran, E. Kaschnitz, G. Pottlacher 2009 *Thermophysical properties of five binary copper-nickel alloys.*

The project: „Electrical Resistivity Measurement of High Temperature Metallic Melts – Part 2" is sponsored by the FFG – ASAP programme.

7.11 Thermophysical properties of 22 pure metals in the solid and liquid state - The pulse-heating data collection

T. Hüpf. C. Cagran, G. Pottlacher, *Thermophysical properties of 22 pure metals in the solid and liquid state - The pulse-heating data collection*, Lam14, Rome, Italy, July 2010.

The paper focuses on the combination of available data (obtained at the lab) with new measurements, namely available data for resistivity at initial geometry with new expansion measurements. Results of Ir, Pd, Pt, and V are described.

Comments: The paper was written by myself with Prof. Pottlacher as supervisor.

Thermophysical properties of 22 pure metals in the solid and liquid state – The pulse-heating data collection

T. Hüpf[1], C. Cagran[1], and G. Pottlacher[1]

[1]Graz University of Technology, Institute of Experimental Physics, 8010 Graz, Austria

Abstract. The workgroup of subsecond thermophysics in Graz has a long tradition in performing fast pulse-heating experiments on metals and alloys. Thereby, wire-shaped specimens are rapidly heated (10^8 K/s) by a large current-pulse (10^4 A). This method provides thermophysical properties like volume-expansion, enthalpy and electrical resistivity up to the end of the liquid phase. Today, no more experiments on pure metals are to be expected, because almost all elements, which are suitable for pulse-heating so far, have been investigated. The requirements for pulse-heating are: a melting point which is high enough to enable pyrometric temperature measurements and the availability of wire-shaped specimens. These elements are: Co, Cu, Au, Hf, In, Ir, Fe, Pb, Mo, Ni, Nb, Pd, Pt, Re, Rh, Ag, Ta, Ti, W, V, Zn, and Zr. Hence, it is the correct time to present the results in a collected form. We provide data for the above mentioned quantities together with basic information on each material. The uniqueness of this compilation is the high temperature range covered and the homogeneity of the measurement conditions (the same method, the same laboratory, etc.). The latter makes it a good starting point for comparative analyses (e.g. a comparison of all 22 enthalpy traces is in first approximation conform with the rule of Dulong-Petit which states heat capacity – the slope of enthalpy traces – as a function of the number of atoms). The data is useful for input parameters in numerical simulations and it is a major purpose of our ongoing research to provide data for simulations of casting processes for the metal working industry. This work demonstrates some examples of how a data compilation like this can be utilized. Additionally, the latest completive measurement results on Ag, Ni, Ti, and Zr are described.

1 Fast pulse-heating

1.1 Experimental

In the technique of fast pulse-heating electrically conducting samples are heated rapidly by the passage of a large current pulse (approx. 10000 A). The energy is stored in a capacitor which is then discharged over the sample. The resistive heating continues up to the transition to the gas phase. Due to the high heating rate (10^8 K/s) the specimen maintains its position even in the liquid phase. This is the key-feature of pulse-heating. The experimental duration is typically 50 µs; consequently, heat-loss and chemical reactions are strongly inhibited.

During heating, several quantities are measured simultaneously: The temperature T is measured by means of pyrometry. The voltage drop along the specimen is measured by two knife-edge contacts directly touching the surface of the sample. The current I is measured with an induction coil. The thermal expansion is measured with a fast CCD-camera. From these recorded pictures the diameter D can be evaluated in steps of 5 µs or 2.5 µs.

From the raw data, enthalpy H, resistivity at initial geometry ρ_{IG}, and radial expansion D^2/D_0^2 can be calculated as a function of temperature (D_0: diameter at room temperature). Specific resistivity ρ is obtained by multiplying ρ_{IG} with D^2/D_0^2. Due to the clamping the fraction D^2/D_0^2 is equal to the volumetric expansion V/V_0 (V: volume, V_0: volume at room temperature), because the axial component of expansion is deflected in radial direction.

For more details about the experimental setup see [1].

1.2 The situation of today

There are certain requirements concerning the specimens: They must be electrically conducting, the meltingpoint has to be high enough to enable pyrometric temperature measurement, and specimens must be available in the shape of a wire. The latter restriction creates a technological challenge. Some elements, which are too brittle to be drawn as a wire, can be cut into rectangular wires by electro-erosion machining. These wires can be processes by pulse-heating as well, except for the expansion measurement.

Today almost all elements which fulfill the requirements have been investigated at the laboratory in Graz. These elements are: Co, Cu, Au, Hf, In, Ir, Fe, Pb,

Mo, Ni, Nb, Pd, Pt, Re, Rh, Ag, Ta, Ti, W, V, Zn, and Zr (ordered alphabetically by spoken names). The measurements are published in various different journals by different authors, which are – or have been – members of the 'Workgroup of Subsecond Thermophysics' at TU Graz.

Ongoing research is mainly dedicated to binary alloys [2] and alloys with industrial relevance.

2 Creation of a compilation

To summarize all measurements on pure elements and to provide easy access, it was decided to make a compilation. Usually, such data compilations try to assemble such kinds of information about an element, which are appropriate for the user. Hence, different measurement techniques and different workgroups are combined to obtain the best result. In the case of the pulse-heating data collection the situation is different. The measurement technique and the laboratory are identical for every element. This is the central theme of the compilation. On the one hand the homogeneity of results, which is a good starting point for comparative analyses, and on the other hand the large temperature range that can be covered with pulse-heating, make this compilation an exceptional data collection.

2.1. Quantities

It is common to start any investigation with a basic survey. This was implemented in the compilation by including a bachelor-thesis, which is a conglomeration of easy available basic information. Amongst other things the topics 'history', 'common uses', and 'relevance in life' are covered in this thesis in an easy going way, e. g. by text, referring to internet pages.

The stated quantities obtained by pulse-heating are thermal expansion (D^2/D_0^2), enthalpy (H), resistivity with initial geometry (ρ_{IG}), and resistivity (ρ) as a function of temperature. They are displayed graphically and by polynomials, as well. Specific heat capacity c_p and heat of fusion ΔH are calculated from the enthalpy polynomials.

Thermal conductivity λ and thermal diffusivity a can easily be calculated by equations (1) and (2):

$$\lambda(T) = L\ T\ \rho(T)^{-1} \quad (1)$$

$$a(T) = L\ T\ c_p^{-1}\ \rho_{IG}(T)^{-1}\ d_0^{-1} \quad (2)$$

L is the Lorentz-number ($2.45 \cdot 10^{-8}\ V^2K^{-2}$), d_0 is the density at room temperature.

2.2 Completive measurements

To complete the measurement results it was necessary to perform new measurements. The thermal expansion of Ag, Ni, Ti, and Zr belongs to these follow-up measurements.

As ρ has to be calculated from ρ_{IG} combined with thermal expansion, new measurements of thermal expansion can be considered to obtain 'better' values for ρ which prior to that had to be combined with expansion values from the literature.

2.2.1 Silver

The measurements on silver are published in [3]. Follow-up measurements of thermal expansion for the liquid phase (1234 K < T < 2000 K) yield (3):

$$D^2(T)/D_0^2 = 1.002 + 4.736 \cdot 10^{-5}\ T \quad (3)$$

Including these values in the calculation of ρ leads to (1234 K < T < 1950 K) (4):

$$\rho(T) = 4.592 \cdot 10^{-2} + 9.856 \cdot 10^{-5}\ T \quad (4)$$

ρ is given in μΩ m. The resistivity at the onset of melting is $\rho_s = 0.090$ μΩ m (subindex s: solid), the resistivity at the end of melting is $\rho_l = 0.168$ μΩ m (subindex l: liquid). This lead to an increase of resistivity at melting of $\Delta\rho = 0.078$ μΩ m.

2.2.2 Nickel

The measurements on nickel are published in [4]. Follow-up measurements of thermal expansion for the solid phase (300 K < T < 1728 K) yield (5):

$$D^2(T)/D_0^2 = 1.000 - 6.604 \cdot 10^{-6}\ T + 2.738 \cdot 10^{-8}\ T^2 \quad (5)$$

And for the liquid phase (1728 K < T < 2600 K) (6):

$$D^2(T)/D_0^2 = 0.930 + 9.730 \cdot 10^{-5}\ T \quad (6)$$

Including these values in the calculation of ρ leads to (473 K < T < 627 K) (7):

$$\rho(T) = -3.734 \cdot 10^{-2} + 1.857 \cdot 10^{-4}\ T + 5.411 \cdot 10^{-7}\ T^2 \quad (7)$$

In the range 627 K < T < 1270 K (8):

$$\rho(T) = -0.181 + 0.118 \cdot 10^{-2}\ T - 8.145 \cdot 10^{-7}\ T^2 + 2.406 \cdot 10^{-10}\ T^3 \quad (8)$$

In the range 1300 K < T < 1715 K (9)

$$\rho(T) = 0.106 + 3.456 \cdot 10^{-4}\ T - 2.920 \cdot 10^{-8}\ T^2 \quad (9)$$

And for the liquid phase (1750 K < T < 2200 K) (10):

$$\rho(T) = 0.667 + 1.043 \cdot 10^{-4}\ T \quad (10)$$

ρ is given in μΩ m. The resistivity at the onset of melting is $\rho_s = 0.616$ μΩ m, the resistivity at the end of melting is $\rho_l = 0.848$ μΩ m. This lead to an increase of resistivity at melting of $\Delta\rho = 0.232$ μΩ m.

2.2.3 Titanium

The measurements on titanium are published in [5]. Follow-up measurements of thermal expansion for the liquid phase (1943 K < T < 3000 K) yield (11):

$D^2(T)/D_0^2 = 0.938 + 6.108 \cdot 10^{-5}\ T$ (11)

Including these values in the calculation of ρ leads to (1943 K < T < 2500 K) (12):

$\rho(T) = 1.7063 + 1.483 \cdot 10^{-5}\ T$ (12)

ρ is given in µΩ m. The resistivity at the end of melting is $\rho_l = 1.735$ µΩ m.

2.2.4 Zirconium

The measurements on zirconium are published in [6]. Follow-up measurements of thermal expansion for the solid phase (1500 K < T < 2127 K) yield (13):

$D^2(T)/D_0^2 = 0.984 + 2.861 \cdot 10^{-6}\ T$ (13)

And for the liquid phase (2127 K < T < 4000 K) (14):

$D^2(T)/D_0^2 = 0.920 + 5.944 \cdot 10^{-5}\ T$ (14)

Including these values in the calculation of ρ leads to (1660 K < T < 2115 K) (15):

$\rho(T) = 0.830 + 2.592 \cdot 10^{-4}\ T$ (15)

And for the liquid phase (2155 K < T < 3500 K) (16):

$\rho(T) = 1.258 + 8.735 \cdot 10^{-5}\ T$ (16)

ρ is given in µΩ m. The resistivity at the onset of melting is $\rho_s = 1.378$ µΩ m, the resistivity at the end of melting is $\rho_l = 1.446$ µΩ m. This lead to an increase of resistivity at melting of $\Delta\rho = 0.068$ µΩ m.

3 Comparative Analyses

3.1 Enthalpy *H*

Having summarized data is always a motivation for doing comparative analyses. In a first try, one can plot everything into one graph. Figure 1 shows the enthalpy traces of 19 elements as a function of temperature.

Of course, such an illustration is not the best way to present results for every purpose due to difficulties with labeling, but nevertheless, this graph exhibits information about the enthalpy. We can easily identify three bundles of traces, which are correlated to the position of the respective element in the periodic system of the elements (4th, 5th, and 6th period).

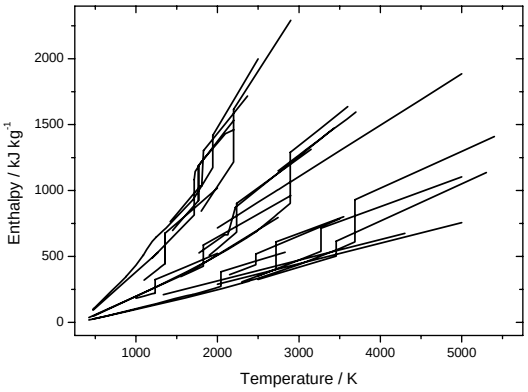

Fig. 1. Enthalpy traces of 19 elements as a function of temperature.

If the same enthalpy traces are plotted in molar units ($J \cdot mol^{-1}$), their relative positions in the graph change remarkably (see figure 2).

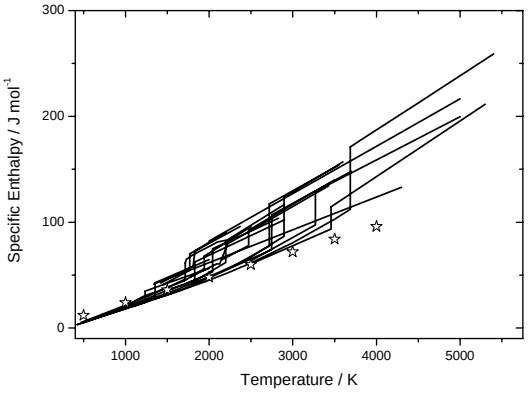

Fig. 2. Enthalpy traces of 19 elements in molar units. Stars: calculation according to equation (18).

The three bundles have contracted into one. This is some kind of experimental indication that the enthalpy mainly depends on the number of atoms. It is consistent with the rule of Dulong-Petit (17):

$c = 3\ N\ k$ (17)

The heat capacity c, which is the slope of the enthalpy traces, depends on the number of atoms N and the Boltzmann-constant k. The calculation for one mole (N_A) yields (18) [7]:

$c_{mol} = 3\ N_A\ k = 24.9\ J \cdot mol^{-1} \cdot K^{-1}$ (18)

The enthalpy calculation thereof yields the stars in figure 2.

3.2 Heat of fusion Δ*H*

The same approach can be applied to the heat of fusion ΔH. Figure 3 displays the heat of fusion as a function of

the respective position of the melting point (x-axis: temperature of melting point, y-axis: heat of fusion). No particular trend can be read out of this graph.

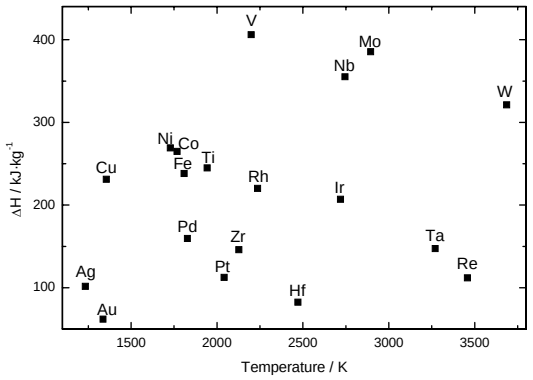

Fig. 3. Heat of fusion as a function of the respective melting-point.

This time we convert the graph by changing the abscissa to enthalpy at melting in the solid H_s instead of temperature. The result can be seen in figure 4.

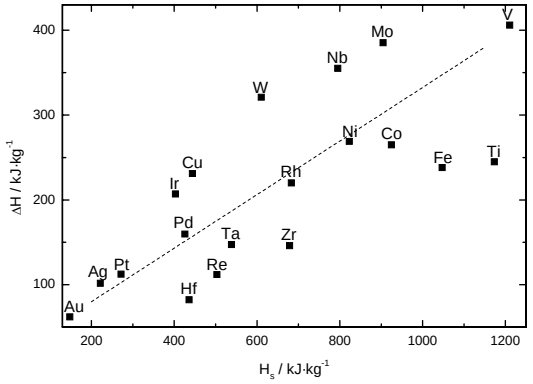

Fig. 4. Heat of fusion as a function of enthalpy at melting in the solid phase H_s. Dashed line: visualization of increasing trend.

In the new graph an increasing trend is recognizable (dashed line). Elements which need more energy input to reach the melting-temperature also need more energy input to be molten.

3.3 Resistivity ρ

To draw all electrical resistivity traces into one graph leads to the result in figure 5.

The traces in figure 5 are hard to compare. Pulse-heating results always cover the temperature-region around the melting-temperature. Only by extrapolation one could make a section at a fixed temperature to compare all resistivities.

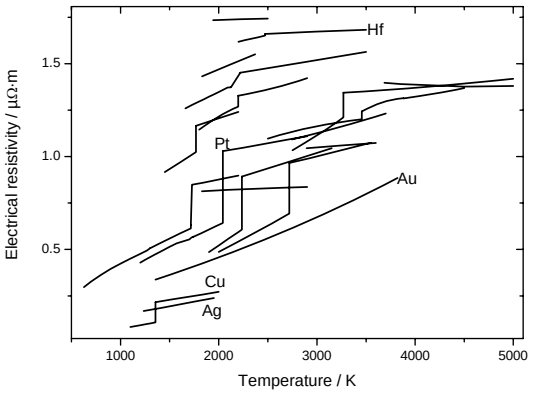

Fig. 5. Electrical resistivity of 19 elements as a function of temperature.

3.4 Expansion

All traces of expansion were drawn into one graph to obtain figure 6.

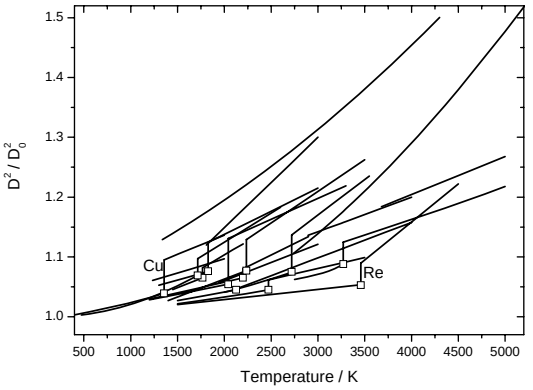

Fig. 6. Relative expansion as a function of temperature. Rectangles: expansion at the onset of melting.

At room temperature the factor of expansion equals unity for every element. Where available, the expansion at the onset of melting is displayed in figure 6. The average value of expansion until melting for these twelve elements is 6.3%.

If this was a general behavior, one would have to conclude, that the expansion coefficient of high melting metals was always low by trend.

3.4 Thermal conductivity and thermal diffusivity

The thermal conductivity traces (see equation (1)) are qualitatively the inverse of the electrical resistivity. Hence no new findings can be expected from a graphical

comparison. Thermal diffusivity *a* is calculated according to equation (2), which includes room temperature density and heat capacity as well. The traces for the liquid phase are displayed in figure 7.

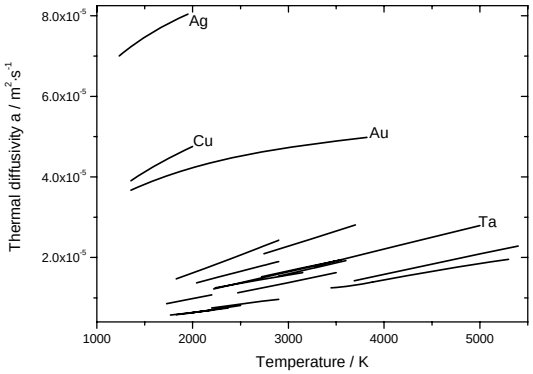

Fig. 7. Thermal diffusivity of 19 elements as a function of temperature.

The interaction of ρ, c_p, and density leads to the difference in distribution between figure 5 and figure 7: Silver has by far the highest thermal diffusivity. Copper and gold are in between silver and the rest of the elements. All other investigated metals are quite similar in their thermal diffusivity.

4 Summary

The 'Workgroup of Subsecond Thermophysics' in Graz has performed a lot of measurements on pure metals with the method of fast pulse-heating. As the focus of ongoing research is no longer on pure elements, but on alloys instead, it was decided to make a compilation of finished measurements. New measurements were performed to complete the data.

The follow up measurements on silver, nickel, titanium, and zirconium are presented in section 'Completive measurements'. New results of thermal expansion give new values for electrical resistivity, which up to this time had to include expansion values from the literature.

We consider this data-collection as a good starting-point for comparative analyses. In this context the unusual – or even unaesthetic – procedure to draw all elements into one graph, seems justified. Some examples are given in section 3: The appearance of the enthalpy traces depends dramatically on the used set of units (compare figure 1 and 2). The heat of fusion is once plotted against melting-temperature (figure 3) and once plotted against enthalpy at melting in the solid (figure 4). All resistivity curves are shown in figure 5. From the thermal expansion traces (figure 6) the average of thermal expansion at the onset of melting was calculated, yielding 6.3%. The behavior of derived quantities like thermal diffusivity depends on the interaction of the input quantities. Consequently, the distribution of thermal diffusivity curves (figure 7) is quite different from the inverse distribution of resistivity curves.

Although for us this data-collection is a summary and somehow the closure of our pure-elements-research, we hope that it will also act as a starting-point for new discussions and collaborations with experimentalists and theoreticians as well.

About the availability of the compilation please contact Prof. Dr. Gernot Pottlacher (pottlacher@tugraz.at).

Acknowledgement

The project *Electrical Resistivity Measurement of High Temperature Metallic Melts* is sponsored by the Austrian Space Applications Programme (ASAP) of the FFG, Sensengasse 1, 1090 Wien.

References

1. T. Hüpf, C. Cagran, B. Wilthan, G. Pottlacher, J. Phys.: Condens Matter **21** (2009)
2. T. Hüpf, C. Cagran, E. Kaschnitz, G. Pottlacher, Thermochimica Acta, **494** (2009)
3. C. Cagran, B. Wilthan, G. Pottlacher, Thermochimica Acta, **445** (2006)
4. B. Wilthan, C. Cagran, G. Pottlacher, Int. J. Thermophys. **25** (2004)
5. B. Wilthan, C. Cagran, G. Pottlacher, Int. J. Thermophys. **26** (2005)
6. C. Brunner, C. Cagran, A. Seifter, G. Pottlacher, *Temperature: Its measurement and control in science and industry*, volume 7 (American Institute of Physics, 2003)
7. N.W. Ashcroft, N.D. Mermin, *Festkörperphysik*, p. 540 (Oldenbourg, Wien, 2001)

7.12 Thermal expansion in pulse-heating - a status report

T. Hüpf, C. Cagran, G. Pottlacher, *Thermal expansion in pulse-heating - a status report*, ITCC, Pittsburgh, USA, September 2009.

This paper treats some very detailed aspects of expansion measurements performed in Graz. A specific problem is approached by scientifically taking into account existing results, literature data and new experimental results.

Comments: The paper was written by myself with the help of Dr. Claus Cagran and Prof. Pottlacher as supervisor.

Cover sheet

Title: *Thermal expansion in pulse-heating – a status report*

Authors: Thomas Hüpf
Claus Cagran
Gernot Pottlacher

Affiliation: Graz University of Technology
Institute of Experimental Physics
Petersgasse 16
8010 Graz
Austria

ABSTRACT

A fast pulse-heating method enables simultaneous measurements of several thermophysical properties like enthalpy, electrical resistivity, and thermal (volume) expansion. The latter is in the focus of this work. The high temperatures achievable (typically 1000 K into the liquid phase) are the special feature of this technique.

Different measurement setups turned out to deliver different results: Experiments with water as ambient medium at 100 MPa exhibit more expansion than experiments performed in nitrogen at 0.23 MPa. Due to the optical measurement devices (shadowgraph-technique with fast CCD-camera image recording) different explanations of this behavior are possible. They are discussed on the basis of the results of Ni80Cr20 and niobium.

The consideration of former measurement results of expansion (e.g.: obtained by conventional photography) as well as literature values of density provide arguments for conclusions and suggest a direction for further investigations.

INTRODUCTION

Fast pulse-heating is an approved method to investigate thermophysical properties of metals and alloys. Especially the liquid phase can easily be explored (see section ‘Experimental’). The ‘Workgroup of Subsecond Thermophysics’ at TU Graz exists since 1980 and our pulse-heating facility has improved continuously. Properties like electrical resistivity, enthalpy, and normal spectral emissivity at 684.5 nm have been studied extensively [1, 2].

Although measurements of thermal (volume) expansion existed from the very beginning (see section ‘Developments in expansion measurement’) this property was mainly used to consider the actual geometry of the samples in the calculation of their electrical resistivity. This approach does not require high precision in thermal expansion due to the small index (approx. 30%) in the uncertainty budget following GUM [3]. But when talking about expansion as main issue its uncertainty impact is 100%. Thus efforts have been undertaken to improve the expansion measurement setup.

Recent developments have revitalized this situation. Additionally, they revealed that there was a discontinuity between ‘old’ and ‘new’ devices of expansion measurements. These recent developments concern the optical measurement of thermal expansion via a specially designed CCD-camera (see section ‘Experimental’). The ambition to reach further refinement has stimulated increased cross-checking of results. Unfortunately, literature values for liquid phase thermal expansion are inconclusive and the very ‘old’ measurements delivered significantly higher values compared to newer ones. It turned out that during the conversion to the new system (CCD-camera), which took quite some time due to necessary replacement of components, the pulse-heating apparatus was changed in a second way: from high pressure experiments in water to ambient pressure experiments in nitrogen atmosphere (see section high pressure setup). It was not confirmed if this second change might misleadingly influence the results of thermal expansion.

For this reason, the high pressure setup was put into operation again to compare thermal expansions at high pressure and at low pressure obtained by the same optical detection system (the CCD-camera). And in fact the difference could be reproduced. Figure 1 displays the results of Ni80Cr20. This material was chosen, because these were the latest measurements at that time. On one hand this is a satisfactory result – all the phenomena can be investigated on the basis of the new optical device – but on the other hand this result claims for further investigations. What is the reason for this difference and which result is more to the point?

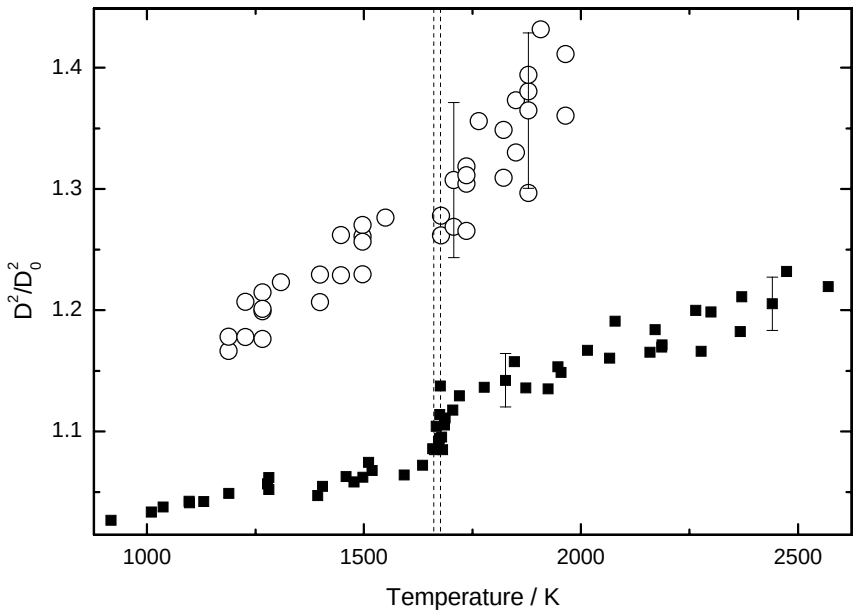

Figure 1. Thermal Expansion of Ni80Cr20 as a function of temperature.
Circles: high pressure (water) results, rectangles: low pressure (nitrogen) results;
dashed lines: solidus 1661 K and liquidus 1676 K temperature.

EXPERIMENTAL

Fast Pulse-Heating

Wire shaped specimens are clamped in the middle of a discharge vessel. The heating is achieved by discharging a capacitor bank (500 µF) over the sample. With charging voltages of up to 10 kV the resulting high heating rate (10^8 K/s) leads to a rapid increase of the temperature (ohmic heating) of the sample. Heating continues until the end of the liquid phase where, at the transition to the gas phase, the so called wire explosion takes place. The short experimental duration (about 50 µs) prevents mechanical (and gravitational) disturbances and chemical reactions. The contact-free temperature measurement is performed by means of pyrometry. The ambient atmosphere is usually nitrogen with 0.23 MPa (2.3 bar) [4].

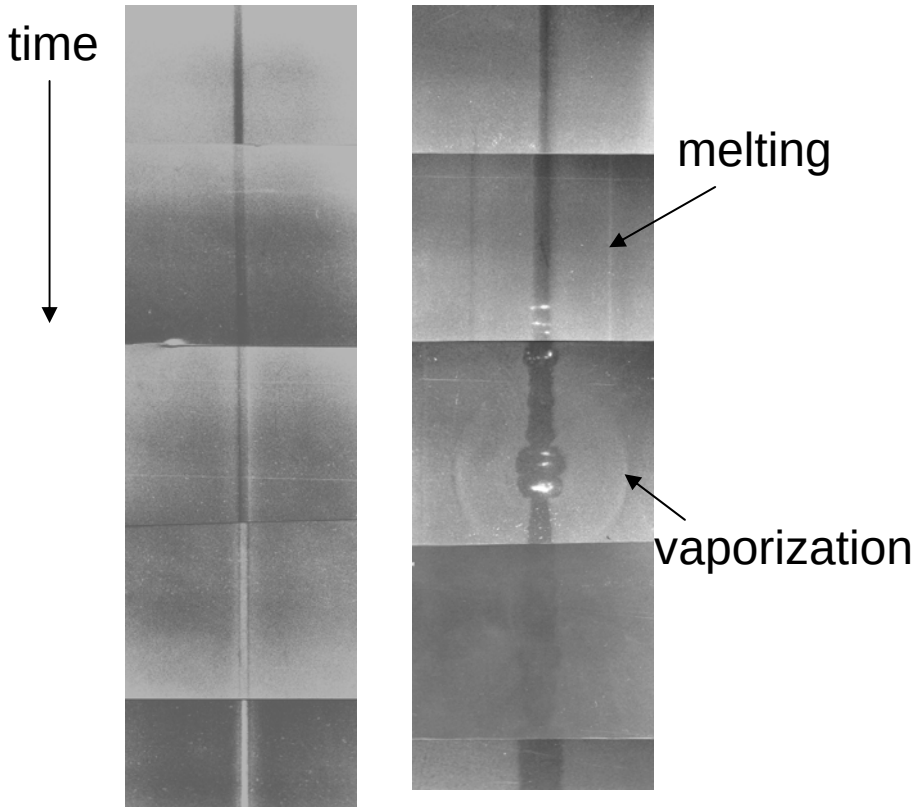

Figure 2. Photographs of the expanding wires from several independent experiments lined up according to experimental time. Left: Ta at 300 MPa (proper result); right: Pb at 0.1 MPa (with irregularities caused by inhomogeneities in the starting material).

Developments in Expansion Measurement

The very first measurements were done with a shadowgraph method. The expanding wire led to a shielding of the detector. Proper calibration allowed estimations of the wire diameter from the detector output traces on a memory oscilloscope.

Later, the wire was imaged on a photographic film with a Kerr-cell used as a fast shutter. The wire is backlit by a photoflash (which is still used today). This method delivers one image per experiment. Metering the wire-diameter is possible directly from the film. Figure 2 shows such photographs from several independent measurements ordered by the temperature.

Finally a CCD-camera was used instead of the photographic film. A Multi-Channel-Plate (MCP) acts as shutter and amplifier. The picture of the phosphor is imaged on the chip (magnification 1). In order to obtain a high frame rate which should enable more than one picture per experiment, only a small part of the chip is exposed to light. The masked rest is used as memory. The content of the exposed lines is shifted into the memory area. This is much faster than to read out the entire chip. The number of lines was decreased stepwise to 8 which gives a resulting frame rate of 400 000 pictures per second (one picture each 2.5 µs). It is now possible to take several pictures per experiment. The evaluation of the wire-diameter is done with the recorded intensity profiles.

High Pressure Setup

In order to investigate critical data of metals pulse-heating experiments were performed in a high pressure vessel. For safety reasons the pressurized ambient medium in these experiments is water. Pressures of 500 MPa can be applied. The minimum pressure to ensure proper sealing is 50 MPa. The vessel is made of stainless steel (85 mm thick). Sapphire windows permit optical measurements [5].

RESULTS

The first measurements available at both high pressure and low pressure are Ni80Cr20 as shown in figure 1. Each data point represents one picture that was used for diameter evaluation.

Figure 3 displays the results of pure niobium. Again, the water (high pressure) experiments deliver significantly more expansion. Only these two materials can be presented up to now.

DISCUSSION

During the interpretation of the expansion measurements one faces a tricky situation, because there are always two parameters that are different: water together with high pressure and nitrogen together with low pressure. The experiments in water have to be performed at high pressures (higher than the critical point of water) to prevent a possible steam layer that might surround the

heated sample. In the intensity profiles steam and water would not be distinguishable. In contrast, the nitrogen experiments can not be processed at these high pressures in the used apparatus.

Hence, it can be either pressure or the ambient medium that causes the difference in results. The assumption that higher pressures would lead to higher expansion is at least an unexpected behavior and hence is not pursued.

Water is very different from nitrogen in terms of density. Its density is higher and closer to the density of metals. One could imagine, that some kind of energy transfer process like pulse transmission in elastic collision is supported by this fact which probably also forwards high speed thermal expansion. Up to now, no experiments were performed that would identify such an effect. It is even possible that there is no physical background of the difference in expansion at all but rather an optical effect, because water is also very different from nitrogen in terms of optical properties.

However, imaging defects or a different optical path can not be the reason for the obtained difference due to the procedure the pictures are evaluated: Each picture in the framing sequence is ratioed with its accordant picture taken prior to the heating process. Simple imaging effects would cancel out.

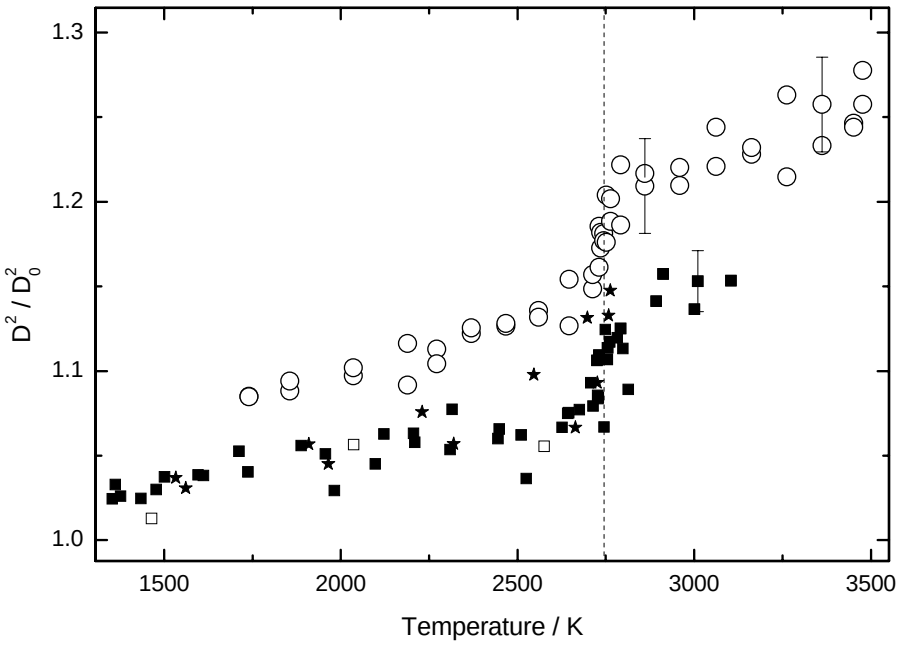

Figure 3. Thermal Expansion of niobium as a function of temperature. Circles: high pressure (water) results, full rectangles: low pressure (nitrogen) results, stars: low pressure results obtained with ‘8-line-setup’, open rectangles: low pressure results backlit with laser, dashed line: melting temperature 2745 K [6].

Nevertheless, there is evidence of more complex optical effects that only occur during heating and thus can influence the ratio. One of them is the propagation of shock-waves. The medial pictures in Figure 2 demonstrate the appearance of diverse shock-waves propagating with even different speeds. They could act as a lens (or cylindrical lens) and thus lead to measurement artifacts. But there is a chance to get behind this impact on the results: shock-waves are acoustic waves which have their certain speed of sound. Changing the heating rate would change the physical expansion but not the speed of sound. Hence the formation of lenses should be different and one would observe a heating-rate dependency of the results. Additionally, changing the pressure while leaving the heating rate unchanged is an alternative approach.

The ‘optical homogeneity’ of the ambient medium could be studied with a probe-light beam. If the transmitted light spot changed its position during the heating process it would indicate fluctuations.

A second effect that might occur during heating solely could be related to movements of the wire. Radial oscillations, be it translatory or in the mode of compression and elongation, which have a shorter periodicity than the exposure time (0.6 µs), would simulate widened edges of the profile and these movements could be dependent on the ambient medium. This could be studied by shortening the exposure time which was kept constant so far. As a preparation for this it was tested to use a laser instead of the photoflash to provide enough intensity. Figure 3 shows one experiment (with three analyzable pictures) at low pressure parameters indicating that there is no dependence on the light source.

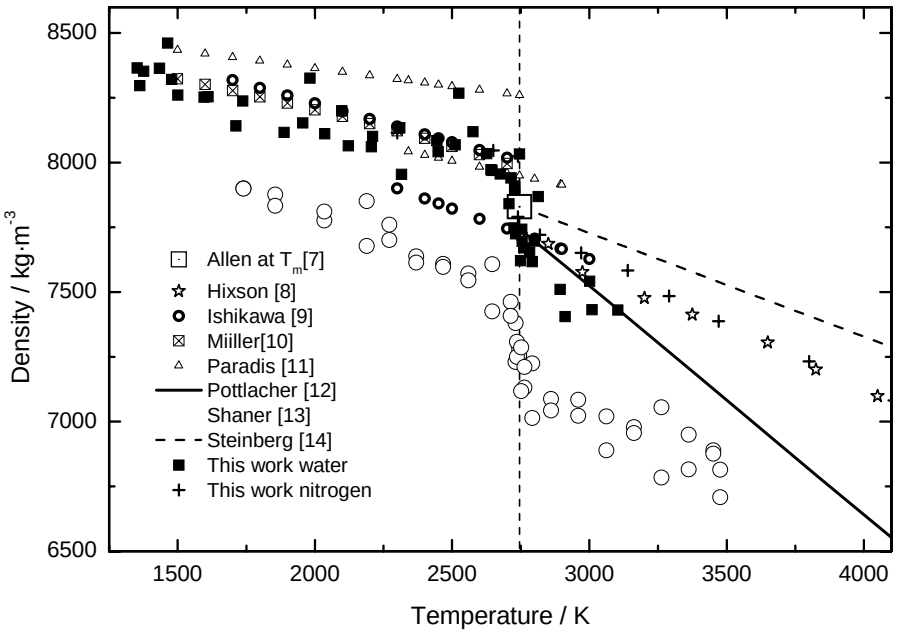

Figure 4. Density of niobium as a function of temperature, dashed line: melting temperature 2745 K [6].

Thirdly: The self-radiation of the heated wire has increasing influence on the profile with increasing temperature, as the shadowgraph of the wire (low intensity) becomes a self-emitting light source with high intensity. This is the limiting factor for the processability of the pictures. However, this effect influences both, water and nitrogen atmosphere experiments similarly, but it could lead to an increasing deviation to literature values at higher temperatures. The remark brings back the second question raised in the introduction section: which result is more to the point?

A general statement is not permissible based on just two finished datasets but the literature values of niobium (though inconclusive in themselves) are in much better agreement with the low pressure measurements performed in nitrogen atmosphere than the high pressure water experiments. Figure 4 depicts the results for niobium converted into density by dividing the room temperature density (8570 kg/m^3 [15]) by the measured thermal volume expansion. The expansion values from figure 3 obtained in high pressure experiments lead to implausible low density values. Although this selection of literature values in this large temperature range illustration appears sufficient to answer the questions, it has to be mentioned that the consistence is questionable.

At the melting point the results obtained with the very first generation of expansion measurements (wire occluding detector) [12] are located at the center of the scattered literature values. As they were performed in water at ambient pressure, the sharp decline with increasing temperature could be related to the formation of a steam layer surrounding the heated wire. For the criterion of self-radiation the temperature range of the new measurements is too small to comment on a possible increasing deviation with increasing temperature.

Uncertainty

As there is considerable scatter of the results the statistic standard deviation σ seems to be the proper approach [16]. 2σ is displayed as uncertainty-bars in the figures (liquid phase only): Ni80Cr20: low pressure (rectangles): 0.022; high pressure (circles): 0.064; niobium: low pressure: 0.018; high pressure: 0.028.

Again figure 2 contains useful information: If the wire does not heat up uniformly (e.g. because of contaminations) its diameter will not be uniform as well. As the ‘line-pictures’ of the CCD-camera can only record the diameter at one fixed point, distortions like the bubbles in photograph number three will only be realized as heavy scattering.

SUMMARY

The constant aim for further improvements of expansion measurements in the pulse-heating apparatus has revealed a discrepancy between different methods to measure thermal expansion which needs further attention. The experiments performed in water as ambient medium deliver larger thermal expansions than the experiments performed in nitrogen. As the difference between water and nitrogen atmosphere is always coupled with the difference between high pressure and low pressure the experimental results need systematic treatment to obtain a complete chain of evidence.

Formerly established methods, like conventional photography, turn out to contain valuable information. The developments in the expansion measurement are described in a separate chapter.

Up to now only Ni80Cr20 [16] and pure niobium have been investigated in this regard. For niobium the low pressure (nitrogen) experiments are much more consistent with literature values. Some effects that could cause the differences are described. Not all of them are accessible by this kind of experiments. Necessary further steps include: other materials to compare, investigations of pressure dependency and heating-rate dependency, the decrease of exposure time, and the installation of a probe-light.

Acknowledgement

This work was supported by the Austrian Space Applications Programme (ASAP) by the FFG, Vienna, Austria.

REFERENCES

1. Hüpf, T., C. Cagran, G. Lohöfer, and G. Pottlacher. 2008. "Electrical Resistivity Measurement of High Melting Metals up into the Liquid Phase (V, Nb, Ta, Mo, W)," *J. Phys. Conf. Series*, 98.
2. Cagran, C., Ch. Brunner, A. Seifter, and G. Pottlacher. 2002. "Liquid-phase Behaviour of Normal Spectral Emissivity at 684.5 nm of some Selected Metals," *High Temp. – High Pres*., 34: 669-679.
3. GUM: *Guide to the Expression of Uncertainty in Measurement* 1993 (Geneva: ISO)
4. Cagran, C., T. Hüpf, B. Wilthan, and G. Pottlacher. 2008. "Selected Thermophysical Properties of Hf-3%Zr from 2200 K to 3500 K obtained by a Fast Pulse-heating Technique," *High Temp. – High Pres*., 37: 205-210.
5. Gallob, R., H. Jäger, and G. Pottlacher. 1996. "A Submicrosecond Pulse Heating System for the Investigation of Thermophysical Properties of Metals at High Temperatures," Int. J. Thermophys., 7(1): 139-147.
6. Bedford: Bedford, R. E., G. Bonnier, H. Maas, and F. Pavese. 1996. "Recommended Values of the Temperature on the International Temperature Scale of 1990 for a Selected Set of Secondary Reference Points," *Metrologia*, 33: 133-154.
7. Allen, B. C. 1963. *Trans. AIME,* 227: 1175.
8. Hixson, R. S., and M. A. Winkler. "Thermophysical Properties of Liquid Niobium," Los Alamos National Laboratory, Los Alamos, New Mexico, USA 87545.
9. Ishikawa, T., P.-F. Paradis, and S. Yoda. 2001. "Thermophysical Property Measurement of Refractory Metals using a Ground-based Electrostatic Levitations Furnace," 2nd Pan Pacific Basin Workshop on Microgravity Sciences, 2001.
10. Miiler, A. P., and A. Cezqirliyan. 1988. "Thermal Expansion of Niobium in the Range 1500-2700 K by a Transient Interferometric Technique," *Int. J. Thermophys.* 9(2): 195-203.

11. Paradis, P.-F., T. Ishikawa, and S. Yoda. 2001. “Non-contact Measurements of Thermophysical Properties of Niobium at High Temperatures,” *J. Mat. Sci.*, 36: 5125-5130.
12. Gallob R., H. Jäger, and G. Pottlacher. 1985. “Recent Results on Thermophysical Data of Liquid Niobium and Tantalum,” *High Temp. – High Pres.* 17: 207-213.
13. Shaner, J. W., G. R. Gathers, and W. M. Hodgson. 1977. “Thermophysical Measurements on Liquid Metals Above 4000 K,” in Proc. *7th Symposium on Thermophysical Properties*, A. Cecairliyan, ed. American Society of Mechanical Engineers, New York, pp. 896-903.
14. Steinberg, D. J. 1974. “A Simple Relationship Between the Temperature Dependence of the Density of Liquid Metals and Their Boiling Temperatures,” *Metall. Trans.* 5: 1341-1343.
15. CRC, Lide Handbook: Lide, D. R. 2004. *CRC Handbook of Chemistry and Physics*. CRC Press LLC, 4: pp. 21.
16. Hüpf, T., C. Cagran, E. Kaschnitz, and G. Pottlacher. 2009. “Thermophysical Properties of Ni80Cr20,” *Thermochimica Acta*, doi:10.1016/j.tca.2009.04.015.